ORNL/CON-63

ornl

OAK
RIDGE
NATIONAL
LABORATORY

UNION
CARBIDE

# Design Optimization and the Limits of Steady-State Heating Efficiency for Conventional Single-Speed Air-Source Heat Pumps

C. K. Rice
S. K. Fischer
W. L. Jackson
R. D. Ellison

OPERATED BY
UNION CARBIDE CORPORATION
FOR THE UNITED STATES
DEPARTMENT OF ENERGY

Printed in the United States of America. Available from
National Technical Information Service
U.S. Department of Commerce
5285 Port Royal Road, Springfield, Virginia 22161
NTIS price codes—Printed Copy: A06 Microfiche A01

ORNL/CON-63

Contract No. W-7405-eng-26

Energy Division

# DESIGN OPTIMIZATION AND THE LIMITS OF STEADY-STATE HEATING EFFICIENCY FOR CONVENTIONAL SINGLE-SPEED AIR-SOURCE HEAT PUMPS

C. K. Rice
S. K. Fischer
W. L. Jackson*
R. D. Ellison

Date Published: October 1981

Department of Energy
Division of Buildings and Community Systems

---

*On loan from the Computer Sciences Division, Oak Ridge National Laboratory.

OAK RIDGE NATIONAL LABORATORY
Oak Ridge, Tennessee 37830
operated by
UNION CARBIDE CORPORATION
for the
DEPARTMENT OF ENERGY

TABLE OF CONTENTS

LIST OF FIGURES

LIST OF TABLES

# DESIGN OPTIMIZATION AND THE LIMITS OF STEADY-STATE HEATING EFFICIENCY FOR CONVENTIONAL SINGLE-SPEED AIR-SOURCE HEAT PUMPS

C. K. Rice
W. L. Jackson
S. K. Fischer
R. D. Ellison

## ABSTRACT

The ORNL Heat Pump Model* and an optimizing program were used to explore the limits of steady-state heating efficiency for conventional air-source heat pumps. The method used allows for the simultaneous optimization of ten selected design variables, taking proper account of their interactions, while constraining other parameters to chosen limits or fixed values. Designs were optimized for a fixed heating capacity, but the results may be scaled to other capacities.

Substantial performance improvement is predicted compared to today's state of the art heat pump. With increased component efficiencies that are expected in the near future and with modest increases in heat exchanger area, a 28% increase in heating efficiency is predicted; for long-term improvements with considerably larger heat exchangers, a 56% increase is possible. The improved efficiencies are accompanied by substantial reductions in the requirements for compressor and motor size. The predicted performance improvements are attributed not only to improved components and larger heat exchangers but also to the use of an optimizing design procedure.

Deviations from the optimized design may be necessary to make use of available component sizes and to maintain good cooling-mode performance while improving the heating efficiency. Sensitivity plots (i.e., COP as a function of one or more design parameters) were developed to explore design flexibilities and to evaluate their consequences. The performance of the optimized designs was compared to that of modified ideal cycles to assess the factors that limit further improvement.

It is hoped that the design methods developed will be useful to designers in the heat pump industry.

---

*The ORNL Heat Pump Model was developed by Oak Ridge National Laboratory.

# 1. INTRODUCTION

Modern heat pumps are energy conserving and economically competitive when compared to alternate space conditioning systems other than those using natural gas for heating. There are, however, further opportunities to improve the efficiency and thus the energy conservation potential of conventional air-source heat pumps. The purpose of this study was to develop a design technique to optimize efficiency and best exploit further advances in technology. This design method was also used to estimate the practical limits of heating efficiency for conventional heat pumps at various levels of component efficiency and heat exchanger size.

The ORNL Heat Pump Model*[1] and an optimizing program were used to calculate the maximum heating coefficient of performance (COP) that can be attained, both with components that are presently available and with improved ones, for a range of heat exchanger sizes. The program allows the simultaneous optimization of all the selected design variables while constraining other parameters to chosen limits or constant values. With this technique, the complex interactions between design parameters are properly taken into account. If the constraints are properly formulated, the results are independent of the heating capacity at which the heat pump design was optimized. The above procedure is in contrast to traditional design methods that have been characterized as ". . . an intuitive design approach searching for a few optimum parameters at a time in a sequence dependent on customary and comfortable patterns of old."[2]

The heat pump configuration selected by an optimizing procedure may not be unique for the calculated COP. "Trade-offs" between some of the design parameters are usually possible. Thus there is no "best" design, but rather a family of configurations clustered about the calculated optimum. Plots of the sensitivity of COP to changes in these variables were developed to explore the trade-offs and other design flexibilities.

---

*The ORNL Heat Pump Model was developed by Oak Ridge National Laboratory.

Finally, suitably modified, ideal cycle calculations were used to assess the extent to which improved design may close the gap between presently achieved performance and that which is theoretically possible.

The numerical results of this study are of interest in setting the goals and priorities of the Department of Energy National Heat Pump R&D Program, which is managed by ORNL. It is hoped that the design methods developed will be interesting and useful to designers in the heat pump industry.

# 2. SUMMARY AND CONCLUSIONS

The ORNL Heat Pump Model and an optimizing program were used to explore the limits of steady-state heating efficiency for conventional air-source heat pumps. The predicted improvements in performance are attributed to three factors:

- an optimizing design procedure,
- larger heat exchangers, and
- more efficient components.

No radical design changes or exotic components were considered.

## 2.1 Optimization Procedure

Ten design parameters were simultaneously optimized *while the heating capacity was held constant*. They are

- compressor displacement,
- refrigerant subcooling at condenser exit,

and separately for each heat exchanger (condenser and evaporator),

- frontal area,
- volumetric air flow rate,
- number of tube rows, and
- number of parallel refrigerant circuits.

Although the frontal areas and number of tube rows were varied separately for each heat exchanger, the sum of the products of frontal area times number of tube rows (proportional to the total available heat exchanger area) was constrained to preselected values:

- 0.21 $m^2/kW$ (8 $ft^2/ton$) of nominal capacity to represent a "base case" typical of middle-of-the-line units,
- 0.42 $m^2/kW$ (16 $ft^2/ton$) to represent a 30% increase compared to the largest presently available, and

— 0.84 $m^2/kW$ (32 $ft^2/ton$) to represent long-range possibilities.

Similarly, three discrete levels of maximum overall compressor efficiency (combined compressor and compressor-motor efficiency) were considered: 48, 56, and 64%. Two levels of overall fan efficiency (combined fan and fan-motor efficiencies) were considered for the indoor and outdoor fans:

Overall fan efficiencies (%)

| | Indoor | Outdoor |
|---|---|---|
| Level 1 | 17 | 14 |
| Level 2 | 34 | 28 |

Typical values were chosen for other geometric parameters such as

— indoor duct size,
— fin spacing (wavy fin and tube construction),
— tube spacing,
— refrigerant line diameters and lengths, and
— compressor clearance volume.

*All systems were optimized for an ambient temperature of 8.3°C (47°F), ambient relative humidity of 70%, and an indoor temperature of 21.1°C (70°F), that is, the Air Conditioning and Refrigeration Institute (ARI) high-temperature rating point for heating application.*[3]

The optimizer calculates values for the design parameters that will yield a maximum COP consistent with the specified constraints on heating capacity and total heat exchanger area. However, as found by subsequent sensitivity analysis, trade-offs are possible that do not significantly alter the COP. Thus, there is no unique "best" design for a particular set of constraints, but rather a family of designs clustered about the calculated optimum. These trends and flexibilities are discussed below.

## 2.2 Calculated Efficiency Limits

Representative results of the optimized heat pump efficiency calculations are shown in Fig. 2.1, where heating COPs for the 8.3°C (47°F)

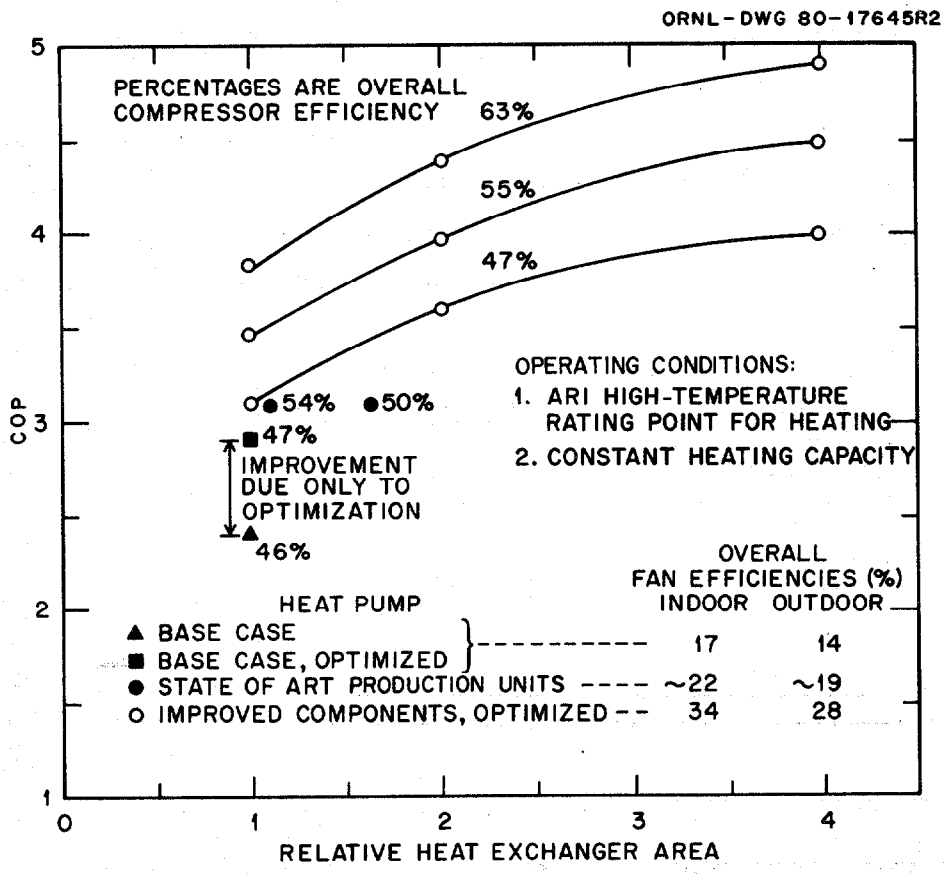


Fig. 2.1. Effects of compressor efficiency, heat exchanger area, and design optimization on heat pump COP.

ambient are plotted as functions of available heat exchanger area for the three levels of overall compressor efficiency. As reference points, the COPs of our base case, base case optimized, and two state of the art (SOA) heat pumps are shown. The results shown are for a 11.7-kW (40,000-Btu/h) heat pump; with consistent scaling, they may be applied for other capacities. Overall compressor and fan efficiencies are noted on the graph (Fig. 2.1). All values of overall compressor efficiency are actual rather than maximum values. The actual values of compressor efficiency (except those for the SOA systems) correspond to within 1 to 2 percentage points of the assumed maximum values of 48, 56, and 64%. The reductions from the assumed values are caused by the effects of suction gas superheating within the compressor shell; the effects vary slightly with the amount of compressor power input required.

As may be seen from the curves, substantial performance improvement is predicted, compared to today's SOA heat pumps. For near-term improvements [55% overall compressor efficiency and 0.42 $m^2/kW$ (16 $ft^2/ton$) heat exchanger area], an increase of 28% in heating efficiency is possible; for long-range improvements [63% compressor and motor efficiency and 0.84 $m^2/kW$ (32 $ft^2/ton$) heat exchanger area], a 56% increase from the SOA is predicted. The efficiency levels shown by the curves represent the combined result of component improvements and optimized system design. Increases in overall compressor efficiency are seen to be uniformly beneficial for all heat exchanger areas considered. However, for a given compressor efficiency, increases in heat exchanger area show eventually diminishing returns.

For the sake of clarity, the variations of compressor displacement and motor size are not shown in Fig. 2.1. It should be noted, however, that for a given compressor efficiency and heating capacity, increases in heat exchanger area allow reductions in compressor displacement and motor size; these effects tend to offset the increased cost of the larger heat exchangers. Increases in compressor efficiency alone call for accompanying increases in displacement but further decreases in motor size. This is shown in the tables in Sect. 4. Performance and configuration values for four selected systems of Fig. 2.1 are shown in Table 2.1.

## 2.3 Benefits of the Optimizing Procedure

The importance of the optimizing design procedure may be seen from its application to the base case heat pump which is typical of today's middle-of-the-line product. As shown in Fig. 2.1 and Table 2.1, a 22% improvement in COP from the base case (from 2.4 to 2.9) was obtained by optimizing the ten design variables (20%) and reducing evaporator superheat (2%); no increases in component efficiency level or heat exchanger area were required. The use of more efficient fans with this optimized design improves the COP another 8% for a net gain of 30% over the base case, giving the heat pump a COP of 3.1, equivalent to the state of the art but with smaller heat exchangers and a lower efficiency compressor typical of the less-expensive middle-of-the-line products.

Table 2.1. Performance and configuration of the base case and three optimized systems

| | System | | | |
|---|---|---|---|---|
| | Base case | Optimized base case | Short-term improved | Long-term improved |
| **Performance** | | | | |
| At 8.3°C (47°F) ambient | | | | |
| COP | 2.40 | 2.92 | 3.96 | 4.90 |
| Heating capacity, kW ($10^3$ Btu/h) | 11.8 (40.4) | 11.7 (40.1) | 11.7 (40.0) | 11.7 (39.9) |
| At -8.3°C (17°F) ambient | | | | |
| COP | 2.11 | 2.36 | 3.13 | 3.55 |
| Heating capacity, kW ($10^3$ Btu/h) | 7.71 (26.3) | 7.44 (25.4) | 7.32 (25.0) | 6.97 (23.8) |
| **Constraints** | | | | |
| Maximum overall compressor efficiency, % | 48 | 48 | 56 | 64 |
| Overall fan efficiency, % | | | | |
| Indoor | 17 | 17 | 34 | 34 |
| Outdoor | 14 | 14 | 28 | 28 |
| Relative heat exchanger area | 1 | 1 | 2 | 4 |
| **Design parameters** | | | | |
| Condenser (indoor coil) | | | | |
| Air flow rate, L/s (cfm) | 566 (1200) | 732 (1550) | 708 (1500) | 755 (1600) |
| Frontal area, $m^2$ ($ft^2$) | 0.31 (3.35) | 0.41 (4.40) | 0.65 (6.94) | 1.42 (15.3) |
| Number of tube rows | 3 | 3 | 4 | 4 |
| Number of circuits | 3 | 2 | 4 | 6 |
| Subcooling, C° (F°) | 28 (50)[a]<br>17 (30)[b] | 8.9 (16) | 7.2 (13) | 9.4 (17) |
| Evaporator (outdoor coil) | | | | |
| Air-flow rate, L/s (cfm) | 1090 (2300) | 1580 (3350) | 2270 (4800) | 3300 (7000) |
| Frontal area, $m^2$ ($ft^2$) | 0.5 (5.55) | 1.25 (13.5) | 2.25 (24.2) | 4.21 (45.3) |
| Number of tube rows | 3 | 1 | 1 | 1 |
| Number of circuits | 4 | 6 | 7 | 8 |
| Superheat, C° (F°) | 11 (19)[a]<br>1.7 (3)[b] | 1.7 (3.0) | 1.7 (3.0) | 1.7 (3.0) |
| **Compressor** | | | | |
| Displacement, mL ($in.^3$) | 68.9 (4.20) | 58.5 (3.57) | 56.0 (3.42) | 50.8 (3.10) |
| Motor shaft power,[a] kW (hp) | 3.35 (4.49) | 2.58 (3.46) | 2.23 (2.99) | 1.72 (2.30) |

[a] Value at 8.3°C (47°F) ambient condition.

[b] Value at -8.3°C (17°F) ambient condition.

The use of the optimizing procedure in conjunction with larger heat exchangers and more efficient compressors and motors has led to designs with significantly improved efficiency accompanied by substantial reductions in the requirements for compressor displacement and motor size. For example, the most efficient heat pump shown in Fig. 2.1 (COP = 4.9) may use a compressor displacement 26% smaller than that for the base case (COP = 2.4) and a 49% smaller motor.

## 2.4 Sensitivity of COP to Design Parameters

The optimizing procedure calculates a single set of the "best" design parameters consistent with a given set of constraints; it gives no information about the sensitivity of efficiency to departures from this optimum design. Sensitivity plots (i.e., COP as a function of one or more design parameters) were used to evaluate design flexibility about the optimum configuration.

Conclusions of these analyses are as follows:

- The optimum air flows found at the 8.3°C (47°F) ambient condition are near optimum for the ambient temperature range of -8.3 to 8.3°C (17 to 47°F) when the effects of supplemental resistance heat are considered. Thus single-speed fans are adequate for the heating mode operation of conventional heat pumps.
- The optimum amount of condenser subcooling is between 5 and 11°C (10 and 20°F) for the ambient temperature range of -8.3 to 8.3°C.
- A critical minimum number of parallel refrigerant circuits is necessary for good performance; this minimum increases with increases in heat exchanger size.
- With simplified outdoor fan models, a one-row evaporator (outdoor) coil resulted in optimum performance for all cases considered. The implications of such large face area, one-row coils with regard to fan requirements are discussed in Appendix B. The optimum COP is, in contrast, rather insensitive to the number of condenser (indoor) rows. This insensitivity would allow the use of more condenser rows and a proportionally smaller frontal area to accommodate more indoor-coil surface area within the size restrictions of the indoor cabinet.
- Significant trade-offs are possible between compressor displacement and air flow rates while keeping the ratio of condenser to evaporator size constant. Within limits, smaller compressors combined with appropriately increased air flow rates perform as well as larger compressors with reduced air flow rates.

— For fixed compressor displacement, the ratio of condenser (indoor) area to the total heat exchanger area may range from 0.4 to 0.7, provided the air flow rates are properly adjusted.

Thus there are a number of system configurations that give near-optimum performance but allow considerable design flexibility while maintaining a constant value for heating capacity. In particular, trade-offs between

— compressor displacement,
— air flow rates, and the
— ratio of condenser to total heat exchanger area

allow the COP to remain nearly constant over a range of condensing and evaporating temperatures, a flexibility that is important in designing a heat pump that provides good cooling performance and humidity control as well as enhanced heating efficiency. The possible range of compressor displacements is also of interest because a designer may be limited to choices of discrete compressor displacement values.

## 2.5 Compressor Motor Sizing

For all of the heat pump simulations, compressor motor sizes were chosen such that the motor would operate at 100% of rated load in the heating mode at the 8.3°C (47°F) ambient condition. To check the validity of this sizing technique, the heat pump model was run for a range of heating and cooling conditions. Results from the cooling-mode analysis indicate that motors selected for 100% rated load operation at the 8.3°C ambient condition will be slightly undersized to meet the load at maximum operating conditions in the cooling mode. However, the undersizing is not large enough to significantly affect the values of heating COP calculated for light-load operation at the -8.3°C ambient.

## 2.6 Comparison with Ideal Cycle Efficiencies

The wide gap between the efficiency achieved by currently available heat pumps and that calculated for the Carnot cycle is only partially narrowed by the improvements suggested in this study. To assess the

factors that limit further improvement, modified ideal cycle efficiencies were calculated. The Carnot efficiency was modified to reflect the following:

- inefficiencies inherent in the vapor compression cycle,
- compressor, fan, and motor inefficiencies,
- heat losses from the compressor shell,
- the necessity for finite heat exchanger sizes and air flow rates, and
- the effects due to the variation of capacity with changing ambient temperatures.

Comparison of the efficiencies of the optimized-design heat pumps with those thus predicted was used to analyze possible routes to further improvement. It is concluded that substantial further improvement will most readily be achieved by new design approaches. Three promising alternatives are

- variable capacity systems,
- the use of nonazeotropic refrigerant mixtures, and
- two-stage cycles.

A future report is planned that will evaluate the limits of steady-state heating efficiency for continuously modulating, variable-capacity heat pumps.

## 2.7 Recommendations

Information gained concerning heat pump efficiencies, improvement trends, and design trade-offs constitute one major result of this study. The optimizing design technique, the other major result, is an efficient and reliable method for finding a design that yields maximum COP for a particular set of constraints. Further, sensitivity analyses about the optimum are useful in evaluating the flexibility available in implementing that design. Accordingly, we plan to use these methods in future work and recommend their use for achieving heat pump designs for high efficiency.

The present study was confined to steady-state heating efficiency. A similar analysis of the steady-state cooling efficiency of heat pumps, combined with the results of this study on heating efficiency, will provide the basis for evaluation of design compromises required for a machine that provides both heating and cooling at high efficiency. The combination will also give better understanding of the appropriate procedures, variables, and constraints needed to optimize the annual performance of heat pumps in varied locations.

The methods of optimization on a yearly basis will depend also on the design philosophy chosen. Optimum performance could be defined simply as that which minimizes life-cycle costs.[4,5] Alternatively, constraints that lead to maximum energy conservation could be introduced first (as was done in this study), and cost considerations applied for a range of optimum configurations. Because an optimizing process leads to a single "best" design but does not search for others that are equally good, premature introduction of cost equations in the process could obscure designs that are equally cost-effective but more energy conserving. It is anticipated that cost-effectiveness calculations based on the latter approach will be the subject of a later report by the authors.

# 3. MODELING AND OPTIMIZATION APPROACH FOR CONVENTIONAL VAPOR COMPRESSION CYCLES

## 3.1 The ORNL Heat Pump Model

### 3.1.1 General characteristics

The heat pump computer model used in this study is an improved version of the model reported by Ellison and Creswick.[1] This discussion provides an overview of the basic features reported previously and concentrates on subsequent improvements that relate to this study. Further information about the version used in this study may be obtained from the authors. A comprehensive report on the model is planned after further improvements have been completed.

The current version of the program is well suited for the purpose of exploring realistic efficiency limits. The model is based, to the extent possible, on underlying physical principles rather than on empirical equations derived from performance data for existing heat pumps. A physically based model is generally more flexible and provides more explicit detail of the interactions of the system components. Such flexibility and detail are important for a study such as this in which the performance trade-offs of the various design and operating parameters are to be studied in regions beyond present-day practice.

### 3.1.2 Input parameters and organization of the model

Input quantities required by the computer program are similar to those described in detail in the preliminary report[1] of the model. They include:

- dimensions of the tubing and geometry of the heat exchangers,
- indoor and outdoor air temperatures and flow rates,
- compressor parameters as described below, and
- desired values of condenser subcooling and evaporator superheat.

Refrigerant 22 is the assumed working fluid.

The flow chart in Fig. 3.1 outlines the calculational scheme used in this study. The model is organized in three principal sections — the compressor, condenser, and evaporator models. A fourth section — a refrigerant flow control device model — is required if a specific flow control device such as a capillary tube, thermostatic expansion valve, or fixed orifice is to be modeled. The choice of a subcooling control device (i.e., specified value of subcooling) is more appropriate for the present work. A fifth section — a refrigerant charge inventory model — would be required to correctly model certain types of systems. We have assumed, however, that the heat pump system being modeled contains a suction line accumulator which remains partially filled with liquid refrigerant; thus a charge inventory model is not needed since a low value of refrigerant superheat is maintained at the compressor shell entry. This assumption is appropriate for our present purposes because maximum performance is achieved with low superheat values.

### 3.1.3 Compressor model

The compressor model is based on performance and efficiency parameters. This approach is in contrast to the use of design parameters and affords much simplification while retaining sufficient detail of the underlying physical principles. The model is compatible with the intended use in that predictions can be made of how changes in compressor efficiency affect the heat pump system. The model cannot, however, be used to determine what specific changes in compressor design might lead to the improved efficiency.

The basic compressor model requires seven input parameters:

1. compressor isentropic efficiency from suction port to discharge port — $\eta_{isen}$,
2. compressor mechanical efficiency — $\eta_{mech}$,
3. maximum value of the compressor motor efficiency — $\eta_{motor(max)}$,
4. shaft power of compressor motor at nominal load,
5. synchronous motor speed,
6. compressor piston displacement, and
7. effective clearance volume ratio.

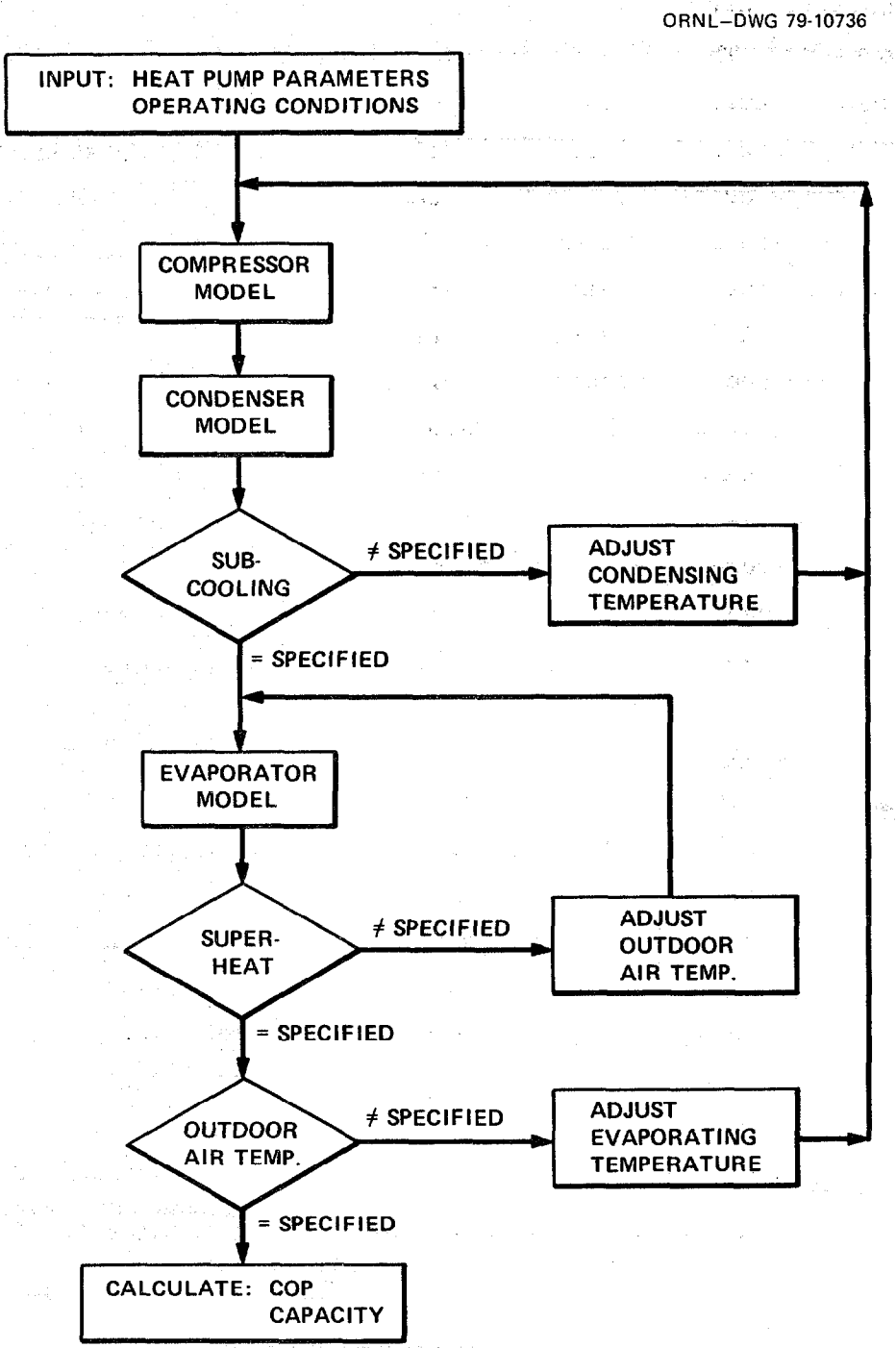


Fig. 3.1. Flow diagram of the version of the ORNL heat pump model used for design optimization.

Using input parameters 3, 4, and 5, the actual motor efficiency ($\eta_{motor}$) and motor speed at part-load conditions can be calculated from typical load performance curves.

The most common efficiency parameters used in discussing compressor performance are overall compressor efficiency and volumetric efficiency.

Overall compressor efficiency is defined as

$$\eta_{cm} = \frac{\dot{m}_r \Delta h_{r,isen,shell\ inlet}}{\dot{W}_{cm}} , \tag{3.1}$$

where

$\dot{m}_r$ = refrigerant mass flow rate,

$\Delta h_{r,isen,shell\ inlet}$ = specific enthalpy change for an isentropic compression from shell inlet conditions to shell outlet pressure,

$\dot{W}_{cm}$ = compressor motor power input.

The overall compressor efficiency is related to the input data for the compressor model by[6]

$$\eta_{cm} = \eta_{isen} \cdot \eta_{mech} \cdot \eta_{motor} \cdot \eta_{super} , \tag{3.2}$$

where $\eta_{super}$ is the suction gas heating efficiency given by

$$\eta_{super} = \frac{\Delta h_{r,isen,shell\ inlet}}{\Delta h_{r,isen,suction\ port}} , \tag{3.3}$$

where

$\Delta h_{r,isen,suction\ port}$ = specific enthalpy change for an isentropic compression from suction port conditions to shell outlet pressure.

The parameter $\eta_{super}$ is calculated from the results of an internal energy balance on the compressor which accounts for internal heat transfer to the suction gas as it travels from the compressor shell inlet to the suction port. The suction gas heat transfer, $\dot{Q}_{suction}$, is calculated from the assumed relation

$$\dot{Q}_{suction} = [0.1(1 - \eta_{motor} \cdot \eta_{mech}) + 0.03] \cdot \dot{W}_{cm} . \tag{3.4}$$

The term $0.1(1-\eta_{motor} \cdot \eta_{mech})\dot{W}_{cm}$ represents an assumed amount of heat transfer from the compressor motor and mechanical heat losses; the term $0.03\dot{W}_{cm}$ represents the assumed heat transfer from the discharge line inside the compressor.

For high-efficiency compressors, Eqs. (3.3) and (3.4) yield $\eta_{super}$ values above 0.96.

In Sect. 3.2.4, various levels of $\eta_{cm(max)}$ will be assumed by choosing specific combinations for the internal efficiency parameters; that is,

$$\eta_{cm(max)} = \eta_{isen} \cdot \eta_{motor(max)} \cdot \eta_{mech} \cdot \tag{3.5}$$

Thus $\eta_{cm(max)}$ is related to the *actual* $\eta_{cm}$ [Eq. (3.2)] by

$$\eta_{cm} = \eta_{cm(max)} \cdot \frac{\eta_{motor}}{\eta_{motor(max)}} \cdot \eta_{super} \cdot \tag{3.6}$$

Volumetric efficiency is calculated using the effective clearance volume ratio and the standard methods given by McQuiston and Parker.[7]

The final quantity needed to characterize a given compressor is the compressor shell heat loss. The assumed equation is

$$\dot{Q}_{shell} = 0.9(1 - \eta_{motor} \cdot \eta_{mech}) \cdot \dot{W}_{cm} \cdot \tag{3.7}$$

Note that all the compressor motor and mechanical heat losses are accounted for in the formulations for $\dot{Q}_{shell}$ and $\dot{Q}_{suction}$ in Eqs. (3.7) and (3.4).

### 3.1.4 Heat exchanger models

The heat exchanger models, adapted from Hiller and Glicksman,[8] are predicated on the conventional crossflow configuration and staggered tube and sheet fin construction. The heat exchanger performance analysis uses equations for the effectiveness ($\varepsilon$) as a function of the number of transfer units (NTU) for a crossflow heat exchanger with both fluids unmixed. The correlations for heat transfer and pressure drop are described in detail in refs. 1, 8, and 9. The air-side heat transfer correlations have been modified for use with wavy fin geometry rather than the smooth fin geometry assumed by Hiller and Glicksman. The assumed air-side heat transfer equation is

$$St = 0.317(Pr)^{0.667}(Re)^{-0.385} , \qquad (3.8)$$

where St, Pr, and Re are the Stanton, Prandtl, and Reynolds numbers, respectively. The Reynolds number is based on outside tube diameter and minimum free-flow area. The condenser analysis is performed separately for the regions in which the refrigerant is superheated, two-phase, or subcooled. The evaporator analysis is broken into two-phase and superheating regions and *accounts for dehumidification of air.*

### 3.1.5 Fan and indoor duct models

Air-side pressure drops across the heat exchangers are calculated using empirical correlations given by Kirschbaum and Veyo.[10] Values of combined fan and fan motor efficiencies for each heat exchanger are inputs to the program. The computed values of fan power consumption are in close agreement with experimental results from our laboratory. The indoor air duct system is modeled by equations also from ref. 10. This model calculates the pressure losses due to six equivalent parallel duct lines each with an equivalent length of 30.5 m (100 ft) and also includes filter and cabinet pressure drops.

### 3.1.6 Other improvements

The major improvement from the previous model[1] is that which allows the user to specify the outdoor air temperature (as well as the indoor) as an input parameter for the computer program. The outermost iteration loop shown in Fig. 3.1 was added to implement this feature. A number of calculational changes were made to improve the speed and the accuracy of the calculations for use with an optimization routine. Such changes include (1) provisions for accommodating incomplete evaporation and condensation, (2) quadratic interpolation schemes to assure rapid convergence in the condenser and evaporator iteration loops, (3) iteration loops on the refrigerant pressure drop calculations in each heat exchanger, (4) more accurate calculation of the condensation heat transfer coefficient, (5) better psychrometric routines, and (6) tightened convergence tolerances.

### 3.1.7 Model validation

Earlier versions of the heat pump model had been tested against laboratory data to evaluate the accuracy of the calculations.[9] Because the computer programs were modified for this study, it was judged necessary to repeat the validation calculations. The program was executed using the geometric descriptions of a unit in our laboratory, compressor calibration parameters derived from laboratory tests reported by Domingorena,[11] and the operating conditions of run 10 described in that report. The computed performance parameters are compared to observed values from the laboratory test in Table 3.1. Inspection of the table reveals that agreement is good. The calculated mass flow rates, power consumption, heat exchange rates, and COP fall within 3.5% of the observed values. The largest difference between calculated and observed temperatures, 1.6°C (2.9°F), is for the air temperature at the condenser exit. This difference exists mainly because the measured air-side capacity was higher than the refrigerant-side capacity.

## 3.2 Choice of Fixed Parameters, Optimization Variables, Constraints, and Component Efficiencies

### 3.2.1 Fixed geometric parameters

To keep the number of optimization variables to a manageable level, a number of parameters were fixed at values considered typical of present practice. These parameters were judged to have only minor effects on system efficiency. For each heat exchanger, the following parameters were fixed:

- tube spacing in the longitudinal and transverse directions of 25.4 mm (1 in.) and 22.2 mm (0.875 in.), respectively,
- inside and outside tube diameters of 8.5 mm (0.33 in.) and 10 mm (0.39 in.), respectively,
- fin spacing of 0.55 fins/mm (14 fins/in.),
- fin thickness of 0.16 mm (0.0064 in.),
- suction line length of 2.4 m (8 ft), and
- discharge and liquid line length of 9.1 m (30 ft).

Table 3.1. Comparison of calculated and observed heating-mode performance

| | Observed | Calculated |
|---|---|---|
| **Compressor model** | | |
| Refrigerant mass flow rate, kg/h (lbm/h) | 149 (329) | 150 (330)[a] |
| Compressor-motor power input, kW | 4.09 | 3.95[a] |
| Refrigerant temperature at compressor exit, °C (°F) | 107 (224) | 106 (223)[a] |
| Saturation temperature at compressor inlet, °C (°F) | -4.4 (24.0) | -4.3 (24.2) |
| Refrigerant temperature at compressor inlet, °C (°F) | 6.0 (42.8) | 6.4 (43.5) |
| Saturation temperature at condenser entry, °C (°F) | 51.3 (124.3) | 51.6 (124.9) |
| Refrigerant pressure at capillary tube entry, kPa (psia) | 1895 (275) | 1909 (277) |
| **Condenser model** | | |
| Air temperature, entry, °C (°F) | 22.5 (72.5) | 22.5 (72.5)[b] |
| Air temperature, exit, °C (°F) | 38.4 (101.2) | 36.8 (98.3) |
| Refrigerant temperature, entry, °C (°F) | 94.3 (201.7) | 93.3 (200.0) |
| Refrigerant temperature, exit, °C (°F) | 26.6 (79.8) | 26.6 (79.8) |
| Refrigerant subcooling, C° (F°) | 24.8 (44.7) | 24.8 (44.7)[c] |
| Heat rejection rate, kW (Btu/h) | 9.397 (32,064) | 9.367 (31,961) |
| Fan-motor power consumption, kW | 0.608 | 0.608[b] |
| **Evaporator model** | | |
| Air temperature, entry, °C (°F) | 5.39 (41.7) | 5.39 (41.7)[c] |
| Air temperature, exit, °C (°F) | 0.83 (33.5) | 2.06 (35.7) |
| Refrigerant temperature, exit, °C (°F) | 6.0 (42.8) | 6.39 (43.5) |
| Saturation temperature, exit, °C (°F) | -4.44 (24.0) | -4.17 (24.5) |
| Refrigerant superheat, C° (F°) | 10.5 (18.9) | 10.5 (18.9)[c] |
| Heat absorption rate, kW (Btu/h) | 7.52 (25,659) | 7.43 (25,354) |
| Fan-motor power consumption, kW | 0.511 | 0.516 |
| **System performance** | | |
| COP | 1.92 | 1.96 |

[a] Calibration parameters.

[b] Fixed input values. Condenser (indoor) fan power was fixed because the observation was made with atypical duct size.

[c] Convergence check points, required to agree with observations.

The effective clearance volume ratio of the compressor was fixed at 0.12.

### 3.2.2 Optimization variables

Ten variables were chosen for optimization with regard to steady-state heating efficiency. For each heat exchanger, the variables are

- volumetric air flow rates,
- frontal area,
- number of tube rows, and
- number of refrigerant circuits;

the two remaining variables are

- compressor displacement and
- refrigerant subcooling at condenser exit.

Four of the ten optimization variables (i.e., the number of circuits and tube rows in each heat exchanger) should, of course, be represented by integers. They were treated, however, as being continuously variable; upon completion of the optimization, sensitivity plots were used to determine the most appropriate integer values.

### 3.2.3 Capacity-related constraints

*Nominal capacity.* For a consistent comparison of the relative steady-state heating efficiency of various heat pump configurations, the nominal heating capacity must be held constant. The nominal capacity size chosen for the optimizations was 11.7 kW (40,000 Btu/h or 3.33 tons) at the 8.3°C (47°F) ambient condition. The optimum configuration found for one capacity can, however, be linearly scaled to any other capacity size as explained in Appendix A.

The ability to scale the optimum configuration to capacity sizes other than the one for which the calculations were made means that the value of the COP can be maintained constant (i.e., it is capacity independent). Such scaling is facilitated if the capacity-related

constraints are appropriately formulated. Thus, for generalized COP results subject to the approximations noted in Appendix A, the following constraints are discussed as values *per unit of nominal heating capacity*:

- total heat exchanger area,
- number of return bends,
- indoor duct cross-sectional areas, and
- cross-sectional area of suction, discharge, and liquid lines.

*Heat exchanger area.* Because the internal geometry of the heat exchangers has been fixed, total heat exchanger area for both coils is directly proportional to the sum of the products of frontal area times the number of tube rows for each coil. This sum, denoted by $A_{tot}$, was used to constrain the total available heat exchanger area to physically realizable sizes. Note that the constraint on the *sum* of areas allows some flexibility in that the optimum ratio of indoor to outdoor coil size can be found while constraining the total available heat exchanger material.

Three values of $A_{tot}$ are considered in the analysis:

- 0.21 $m^2$/kW (8 $ft^2$/ton),
- 0.42 $m^2$/kW (16 $ft^2$/ton), and
- 0.84 $m^2$/kW (32 $ft^2$/ton).

The value of 0.21 $m^2$/kW is typical of middle-of-the-line units presently marketed. One top-of-the-line model currently sold has an $A_{tot}$ of 0.36 $m^2$/kW (13.6 $ft^2$/ton). Thus the 0.42 and 0.84 $m^2$/kW cases represent short-term and long-term possibilities, respectively. The larger areas may be considered surrogates for the combined effect of larger and more efficient heat exchangers provided that air-side pressure drops remain the same.

*Number of return bends.* The number of return bends for each heat exchanger was constrained to 41/$m^2$ (3.8/$ft^2$) for the outdoor coil and 78/$m^2$ (7.21/$ft^2$) for the indoor coil; the reference areas are the individual products of frontal area times the number of tube rows for each heat exchanger. The number of return bends is therefore related to the nominal capacity size through the constraint on $A_{tot}$.

*Indoor duct size.* Based on the chosen nominal capacity of 11.7 kW (40,000 Btu/h), the diameter of each of the six equivalent circular air ducts was set at 0.2 m (8 in.), that is, a cross-sectional area of $2.7 \times 10^{-3}$ $m^2/kW_{nom}$ (15 $in.^2/ton_{nom}$). Under this assumption, for an air flow rate of 0.66 L/s (1400 cfm), the duct pressure drop is 0.025 kPa (0.1 in. $H_2O$) and the combined cabinet and filter pressure drop is 0.075 kPa (0.3 in. $H_2O$). Thus at the indicated flow rate, the indoor air loop of the heat pump system modeled here would have approximately 0.125 kPa (0.5 in. $H_2O$) total pressure drop when the pressure drop across the indoor coil is included.

*Interconnecting pipe sizes.* The cross-sectional areas of the suction, discharge, and liquid lines were fixed at values typical of today's practice: 20 $mm^2/kW$ (0.11 $in.^2/ton$) for the suction line; 13 $mm^2/kW$ (0.073 $in.^2/ton$) for the discharge line; and 15 $mm^2/kW$ (0.0084 $in.^2/ton$) for the liquid line. For the chosen capacity, the corresponding inside diameters are 17, 14, and 4.8 mm (0.68, 0.55, and 0.19 in.), respectively.

### 3.2.4 Component efficiency assumptions

*Compressors.* Three levels of *maximum* overall compressor efficiency, $\eta_{cm(max)}$, were considered for single-speed compressors: 48, 56, and 64%. As defined earlier in Eq. (3.5), $\eta_{cm(max)}$ is the product of three compressor model parameters: $\eta_{motor(max)}$, $\eta_{mech}$, and $\eta_{isen}$. The specific combinations of compressor efficiency parameters assumed for chosen levels of $\eta_{cm(max)}$ are given in Table 3.2. The particular combination chosen for each value of $\eta_{cm(max)}$ can be varied somewhat with minimal effect on the resultant COP and capacity.

When discussing compressor efficiency, compressor manufacturers quote values of compressor-only COP (or EER) at specified rating conditions rather than overall compressor efficiency values as defined here. Overall compressor efficiency is a more basic compressor performance index and as such is less dependent on the chosen rating conditions than is the value of COP (or EER). The correspondence between the overall compressor efficiency and compressor-only COP (or EER) for

Table 3.2. Compressor efficiency assumptions

| $\eta_{cm(max)}$ (%) | $\eta_{motor(max)}$ (%) | $\eta_{mech}$ (%) | $\eta_{isen}$ (%) |
|---|---|---|---|
| 64 | 84 | 95 | 80 |
| 56 | 84 | 95 | 70 |
| 48 | 79 | 95 | 64 |

heat pump and air conditioning rating conditions as specified in ARI Standard 520-78[12] is given in Table 3.3. Note that, for the heat pump ratings in Table 3.3, the COPs are calculated on the basis of cooling capacity rather than heating capacity.

As noted in Sect. 3.1.3, $\eta_{cm}$ differs from $\eta_{cm(max)}$ by the factors $\eta_{motor}/\eta_{motor(max)}$ and $\eta_{super}$. For the optimizations at the 8.3°C (47°F) ambient condition, it is assumed that the compressor motor is operating at 100% of rated load; under this condition $\eta_{motor} = \eta_{motor(max)}$ for the assumed motor performance curve as a function of load (given in Appendix D). The value of $\eta_{super}$ at the 8.3°C ambient condition ranges between 0.97 and 0.98. Thus, from Eq. (3.6), the actual values of $\eta_{cm}$ at the 8.3°C condition are 1 to 1.5 percentage points lower than the assumed $\eta_{cm(max)}$ values.

Table 3.3. Correspondence between overall compressor efficiency and compressor-only COP (or EER)

| | ARI 520-78 rating conditions | |
|---|---|---|
| Overall compressor efficiency (%) | Heat pump COP (EER) | Air-conditioning EER |
| 64 | 3.3 (11.2) | 10.5 |
| 56 | 2.9 (9.8) | 9.2 |
| 48 | 2.5 (8.4) | 7.9 |

Actual values of $\eta_{cm}$ for typical heat pumps range from 42 to 54%. Therefore, the 48% case represents an average of present compressor performance. Some current single-speed compressors used in air conditioners have $\eta_{cm}$ values of 56 to 60%. Thus the 56 and 64% cases represent short-term and long-term compressor performance possibilities, respectively, for heat pump application.

*Fans.* Two levels of overall fan efficiency (combined fan and fan-motor efficiencies) were selected. Based on the overall efficiencies measured on a heat pump unit tested in our laboratory, base case values of 14% were chosen for the outdoor (evaporator) and 17% for the indoor (condenser) units. For the second level of efficiencies, the base case values were doubled (28 and 34%); such improved efficiencies represent an assumed average between short- and long-term improvement possibilities.

## 3.3 Optimization Code and Procedure

All but two of the constraints discussed in Sect. 3.2.3 are applied by fixed input parameters or through calculations built into the model. The remaining two constraints, capacity and total available area ($A_{tot}$), are handled by the use of a constrained optimization program.

### 3.3.1 Optimization code

The constrained optimization code chosen for this task is a routine prepared by the Numerical Analysis Group at the Atomic Energy Research Establishment, Harwell, England.[13] The routine is capable of *minimizing* a function subject to equality and/or inequality constraints. To *maximize* the COP subject to the chosen constraints, the function minimized was the negative of the COP plus penalty functions designed to force conformance with the selected constraints.

### 3.3.2 Optimization procedure

The procedure used was to specify the desired indoor and outdoor air conditions and initial estimates of the heat pump design parameters, calculate the COP and other performance parameters using the heat pump model, and then let the optimization routine test the results against the

constraints. The optimizer then calculated changes in the design parameters to increase the COP while ensuring compliance with the constraints. These new design parameters were sent to the heat pump model for the iterative calculation of the COP. The procedure was fully automated on the computer; changes to the design parameters continued until successive improvements to the COP were smaller than the convergence limits of the heat pump model (within 1%).

The constraints, fixed parameters, and lists of the parameters that were varied for each computer run are shown in Table 3.4. The nominal heating capacity of 11.7 kW (40,000 Btu/h) was maintained for all calculations referenced to an ambient temperature of 8.3°C (47°F). At this ambient, all ten variables were optimized (except for systems in which the heat exchanger configurations of the base case were used) for maximum COP within the specified constraints.

Limited optimizations were performed for some of the systems with an ambient temperature of -8.3°C (17°F), allowing only the refrigerant subcooling at condenser exit and the condenser and evaporator air flow rates to vary. Subsequent analysis of the sensitivity of COP to these design parameters revealed that the values of air flow rates and subcooling found in the optimizations at +8.3°C were reasonably optimum at the -8.3°C ambient as well when the effects of supplemental resistance heat are considered at the lower ambient (these effects are discussed in Sects. 5.2.1 and 5.2.2). Accordingly, the computer runs and results reported here are for system configurations optimized for +8.3°C ambient temperature. The efficiencies reported for the -8.3°C ambient condition result from runs of the heat pump model (without the optimizer) using the configuration determined at +8.3°C and allowing the heat pump to assume its "natural" capacity at the -8.3°C ambient. Since the compressor motor size was chosen so that the motor would operate at its rated load at ambients of +8.3°C, curves of motor efficiency and speed at part-load conditions were used for the runs at -8.3°C.

As shown in Table 3.3, the heat pump systems were optimized for various combinations of overall compressor and fan efficiencies and total available heat exchanger area. The results for each run are discussed and compared in the next section of this report.

Table 3.4. Schedule of system optimizations and single heat pump model runs[a,b]

| System No. | Run type | $T_{amb}$ [°C (°F)] | General constraints: $\dot{Q}_{H_{nom}}$ [kW (kBtu/h)] | General constraints: $A_{tot}$ [$m^2/kW_{nom}$ ($ft^2/ton_{nom}$)] | Component efficiencies: Maximum overall compressor efficiency, $\eta_{cm(max)}$ (%) | Component efficiencies: Overall fan efficiencies: Cond. (%) | Component efficiencies: Overall fan efficiencies: Evap. (%) | Compressor motor specifications: Calculation of part-load performance of compressor motor | Compressor motor specifications: Specification of compressor rated load | Independent variable choice: Compressor: Piston displacement [mL (in.$^3$)] | Compressor: Motor speed (rpm) | Air flow rates [L/s (cfm)]: Cond. | Air flow rates [L/s (cfm)]: Evap. | Heat exchangers: Condenser: Frontal area [$m^2$ ($ft^2$)] | Condenser: Number of tube rows | Condenser: Number of circuits | Evaporator: Frontal area [$m^2$ ($ft^2$)] | Evaporator: Number of tube rows | Evaporator: Number of circuits | Cond. subcooling [C° (F°)] | Evap. superheat [C° (F°)] |
|---|---|---|---|---|---|---|---|---|---|---|---|---|---|---|---|---|---|---|---|---|---|
| | | | | | | | | | | Base case | | | | | | | | | | | |
| 1 | SR | 8.3 (47) | 11.7 (40) | 0.2 (8) | 48 | 17 | 14 | No | C | 68.9 (4.20) | 3450 | 566 (1200) | 1085 (2300) | 3.11 (3.35) | 3 | 3 | 5.16 (5.55) | 3 | 4 | 28 (50) | 11(19) |
| | SR | -8.3 (17) | NA | NA | 48 | 17 | 14 | Yes | – | 68.9 (4.20) | C | 566 (1200) | 1085 (2300) | 3.11 (3.35) | 3 | 3 | 5.16 (5.55) | 3 | 4 | 17 (30) | 2(3) |
| | | | | | | | | | | Limited optimizations with base case heat exchangers | | | | | | | | | | | |
| 2,3 | OP | 8.3 (47) | 11.7 (40) | 0.2 (8) | 48 | 17,34 | 14,28 | No | C | V | 3450 | V | V | 3.11 (3.35) | 3 | 3 | 5.16 (5.55) | 3 | 4 | V | 2(3) |
| | SR | -8.3 (17) | NA | NA | 48 | 17,34 | 14,28 | Yes | – | – | C | – | – | 3.11 (3.35) | 3 | 3 | 5.16 (5.55) | 3 | 4 | – | 2(3) |
| | | | | | | | | | | Full optimizations | | | | | | | | | | | |
| 4-7 | OP | 8.3 (47) | 11.7 (40) | 0.2 (8) | 48,56 | 17,34 | 14,28 | No | C | V | 3450 | V | V | V | V | V | V | V | V | V | 2(3) |
| | SR | -8.3 (17) | NA | NA | 48,56 | 17,34 | 14,28 | Yes | – | – | C | – | – | – | – | – | – | – | – | – | 2(3) |
| 8 | OP | 8.3 (47) | 11.7 (40) | 0.2 (8) | 64 | 34 | 28 | No | C | V | 3450 | V | V | V | V | V | V | V | V | V | 2(3) |
| | SR | -8.3 (17) | NA | NA | 64 | 34 | 28 | Yes | – | – | C | – | – | – | – | – | – | – | – | – | 2(3) |
| 9-11 | OP | 8.3 (47) | 11.7 (40) | 0.4 (16) | 48,56,64 | 34 | 28 | No | C | V | 3450 | V | V | V | V | V | V | V | V | V | 2(3) |
| | SR | -8.3 (17) | NA | NA | 48,56,64 | 34 | 28 | Yes | – | – | C | – | – | – | – | – | – | – | – | – | 2(3) |
| 12-14 | OP | 8.3 (47) | 11.7 (40) | 0.8 (32) | 48,56,64 | 34 | 28 | No | C | V | 3450 | V | V | V | V | V | V | V | V | V | 2(3) |
| | SR | -8.3 (17) | NA | NA | 48,56,64 | 34 | 28 | Yes | – | – | C | – | – | – | – | – | – | – | – | – | 2(3) |

[a] OP = optimization, SR = single heat pump model run, NA = not applicable, C = calculated by heat pump model, V = optimization variable, – = parameter fixed at the value found in the corresponding system at $T_{amb}$ = 8.3°C (47°F).

[b] $T_{indoor}$ = 21°C (70°F) and ambient relative humidity = 70%.

# 4. RESULTS: OPTIMIZED HEAT PUMP PERFORMANCE AND ASSOCIATED SYSTEM CONFIGURATIONS

## 4.1 Tabular Results

Table 4.1 contains the results of the optimization calculations as outlined in the schedule given in Table 3.4. *The system parameters entered in script and underscored in the table are values which were held fixed for that particular computer run.* Additional system operating conditions, heat exchanger performance data, and component power consumption values are given in Appendix B.

As an aid to the interpretation of the results, the parameter values tabulated are those calculated for the chosen nominal capacity rather than after conversion to values per unit of nominal capacity. To convert a given configuration to that for another desired capacity, all the system parameters except tube rows, condenser subcooling, evaporator superheat, and motor speed must be multiplied by the ratio of the new capacity to the given capacity.

As previously discussed in Sect. 3.3.2, no changes in the design parameters were required to give near-optimum performance at -8.3°C (17°F) for heat pumps that were optimized at +8.3°C (47°F). Accordingly, the COP and capacity values given in Table 4.1 for operation at -8.3°C were calculated using the heat pump model alone, that is, without the optimizer. The compressor motor efficiency was adjusted at the -8.3°C ambient as necessary by use of typical part-load efficiency curves with the assumption of nominal (rated) load at the +8.3°C ambient condition. The validity of this motor "sizing" assumption is examined in Appendix C, in which the assumed sizing procedure is found to underestimate slightly the required rated load. However, the undersizing is not large enough to affect significantly the values of heating COP calculated for ambients -8.3°C and higher.

## 4.2 Base Case and State of the Art (SOA) Systems

System 1 in Table 4.1 represents an assumed base case configuration. This system has air flow, compressor, and heat exchanger parameters that are fairly representative of a low- to middle-of-the-line heat pump with refrigerant flow control by means of capillary tubes. The resultant COPs of 2.4 at 8.3°C (47°F) and 2.1 at -8.3°C (17°F) are used to establish a baseline from which to gauge improvement.

As a further point of reference, note that state of the art heat pumps have

- available heat exchanger areas ($A_{tot}$) of 0.23 to 0.34 $m^2/kW_{nom}$ (9 to 13 $ft^2/ton_{nom}$),
- $\eta_{cm}$ values of 50 to 54%, and
- overall fan efficiencies of 20 to 24% indoor, 17 to 21% outdoor.

The corresponding steady-state COPs are

- 3.0 to 3.1 at +8.3°C (47°F) ambient and
- 2.1 to 2.3 at -8.3°C (17°F) ambient.

## 4.3 Improvements with Heat Exchanger Hardware Fixed at Base Case Configurations

In systems 2 and 3 (Table 4.1), the heat exchanger frontal areas, tube rows, and circuits were held fixed at values given for the base case; evaporator superheat was fixed at 17C° (3F°); and the remaining system parameters (air flow rates and condenser subcooling) were optimized. System 3 has improved fans which are twice as efficient as those of systems 1 and 2. When compared to system 1, the limited optimizations in systems 2 and 3 result in

- higher condenser air flow rates,
- lower evaporator air flow rates,

Table 4.1A. Results of system optimizations and single heat pump model runs[a]

| System No. | Area constraint, $A_{tot}$ ($ft^2/ton_{nom}$) | Component efficiencies (%) | | | System parameter results | | | | | | | | | | | | Performance results | | | | |
|---|---|---|---|---|---|---|---|---|---|---|---|---|---|---|---|---|---|---|---|---|---|
| | | | | | Air flow rates (cfm) | | Compressor | | Condenser | | | Evaporator | | | R-22 conditions (F°) | | | | | | |
| | | $\eta_{cm}$ (max) | Overall fan η's | | | | | | | | | | | | | | | | | | |
| | | | Cond. | Evap. | Cond. | Evap. | Displacement ($in.^3$) | Required shaft power at 47°F (hp) | Frontal area ($ft^2$) | No. of tube rows | No. of circuits | Frontal area ($ft^2$) | No. of tube rows | No. of circuits | Cond. sub-cooling | Evap. superheat | Supply air temp. at 47°F ambient (°F) | $\dot{Q}_H$ at 47°F (kBtu/h) | $\dot{Q}_H$ at 17°F (kBtu/h) | COP at 47°F | COP at 17°F |
| **Base case** | | | | | | | | | | | | | | | | | | | | | |
| 1 | 8 | 48 | 17 | 14 | 1200 | 2300 | 4.20 | 4.49 | 3.35 | 3 | 3 | 5.55 | 3 | 4 | at 47°F 50 at 17°F 30 | 19 3 | 101.2 | 40.4 | 26.3 | 2.40 | 2.11 |
| **Limited optimizations with base case heat exchangers** | | | | | | | | | | | | | | | | | | | | | |
| 2 | 8 | 48 | 17 | 14 | 1600 | 1750 | 3.75 | 3.66 | 3.35 | 3 | 3 | 5.55 | 3 | 4 | 9 | 3 | 93.2 | 40.1 | 25.7 | 2.66 | 2.16 |
| 3 | 8 | 48 | 34 | 28 | 1750 | 2000 | 3.75 | 3.64 | 3.35 | 3 | 3 | 5.55 | 3 | 4 | 9 | 3 | 91.1 | 39.9 | 25.2 | 2.86 | 2.33 |
| **Full optimizations** | | | | | | | | | | | | | | | | | | | | | |
| 4 | 8 | 48 | 17 | 14 | 1550 | 3350 | 3.57 | 3.46 | 4.40 | 3 | 2 | 13.5 | 1 | 6 | 16 | 3 | 94.0 | 40.1 | 25.4 | 2.92 | 2.36 |
| 5 | 8 | 48 | 34 | 28 | 1725 | 3550 | 3.57 | 3.44 | 4.40 | 3 | 2 | 13.5 | 1 | 6 | 18 | 3 | 91.4 | 39.8 | 25.0 | 3.11 | 2.51 |
| 6 | 8 | 56 | 17 | 14 | 1450 | 3100 | 3.75 | 3.33 | 4.40 | 3 | 2 | 13.5 | 1 | 6 | 18 | 3 | 95.4 | 39.8 | 24.9 | 3.27 | 2.66 |
| 7 | 8 | 56 | 34 | 28 | 1650 | 3750 | 3.75 | 3.29 | 4.40 | 3 | 2 | 13.5 | 1 | 6 | 14 | 3 | 92.5 | 40.0 | 25.0 | 3.48 | 2.82 |
| 8 | 8 | 64 | 34 | 28 | 1550 | 3800 | 3.95 | 2.96 | 4.49 | 3 | 2 | 13.4 | 1 | 6 | 19 | 3 | 92.9 | 40.1 | 24.5 | 3.77 | 3.09 |
| 9 | 16 | 48 | 34 | 28 | 1700 | 5600 | 3.10 | 2.94 | 6.62 | 4 | 3 | 26.0 | 1 | 7 | 15 | 3 | 91.6 | 39.6 | 24.7 | 3.59 | 2.75 |
| 10 | 16 | 56 | 34 | 28 | 1500 | 4800 | 3.42 | 2.99 | 6.94 | 4 | 4 | 24.2 | 1 | 7 | 13 | 3 | 94.7 | 40.0 | 25.0 | 3.96 | 3.13 |
| 11 | 16 | 64 | 34 | 28 | 1550 | 4400 | 3.55 | 2.65 | 6.76 | 4 | 4 | 26.1 | 1 | 7 | 11 | 3 | 93.9 | 40.0 | 24.7 | 4.37 | 3.41 |
| 12 | 32 | 48 | 34 | 28 | 1800 | 9000 | 2.86 | 2.62 | 14.0 | 4 | 5 | 50.4 | 1 | 8 | 15 | 3 | 90.8 | 40.4 | 24.6 | 3.99 | 2.85 |
| 13 | 32 | 56 | 34 | 28 | 1600 | 7400 | 2.96 | 2.52 | 13.9 | 4 | 5 | 48.1 | 1 | 8 | 13 | 3 | 92.9 | 39.4 | 24.0 | 4.49 | 3.32 |
| 14 | 32 | 64 | 34 | 28 | 1600 | 7000 | 3.10 | 2.30 | 15.3 | 4 | 6 | 45.3 | 1 | 8 | 17 | 3 | 93.1 | 39.9 | 23.8 | 4.90 | 3.55 |

[a] $\dot{Q}_{H_{nom}}$ = 40,000 Btu/h (3.33 tons); $T_{indoor}$ = 70°F; outdoor relative humidity = 70%.

Table 4.1B. Results of system optimization and single heat pump model runs[a]

| Area constraint, $A_{tot}$ ($m^2/kW_{nom}$) | Component efficiencies (%) | | | System parameter results: Air flow rates (L/s) | | Compressor | | Condenser | | | Evaporator | | | R-22 conditions (C°) | | Performance results | | | | |
|---|---|---|---|---|---|---|---|---|---|---|---|---|---|---|---|---|---|---|---|---|
| | $\eta_{cm}$ (max) | Overall fan η's | | | | Displacement (mL) | Required shaft power at 8.3°C (kW) | Frontal area ($m^2$) | No. of tube rows | No. of circuits | Frontal area ($m^2$) | No. of tube rows | No. of circuits | Cond. subcooling | Evap. superheat | Supply air temp. at 8.3°C ambient (°C) | $\dot{Q}_H$ at 8.3°C (kW) | $\dot{Q}_H$ at -8.3°C (kW) | COP at 8.3°C | COP at -8.3°C |
| | | Cond. | Evap. | Cond. | Evap. | | | | | | | | | | | | | | | |
| **Base case** | | | | | | | | | | | | | | | | | | | | |
| 0.2 | 48 | 17 | 14 | 566 | 1085 | 68.9 | 73.6 | 0.31 | 3 | 3 | 0.51 | 3 | 4 | at 8.3°C: 28<br>at -8.3°C: 17 | 11<br>2 | 38.4 | 11.8 | 7.7 | 2.40 | 2.11 |
| **Limited optimizations with base case heat exchangers** | | | | | | | | | | | | | | | | | | | | |
| 0.2 | 48 | 17 | 14 | 755 | 826 | 61.5 | 60.0 | 0.31 | 3 | 3 | 0.51 | 3 | 4 | 5 | 2 | 34.0 | 11.7 | 7.5 | 2.66 | 2.16 |
| 0.2 | 48 | 34 | 28 | 826 | 944 | 61.5 | 59.7 | 0.31 | 3 | 3 | 0.51 | 3 | 4 | 5 | 2 | 32.8 | 11.7 | 7.4 | 2.86 | 2.33 |
| **Full optimizations** | | | | | | | | | | | | | | | | | | | | |
| 0.2 | 48 | 17 | 14 | 732 | 1581 | 58.5 | 56.7 | 0.41 | 3 | 2 | 1.25 | 1 | 6 | 9 | 2 | 34.4 | 11.7 | 7.4 | 2.92 | 2.36 |
| 0.2 | 48 | 34 | 28 | 814 | 1581 | 58.5 | 56.4 | 0.41 | 3 | 2 | 1.25 | 1 | 6 | 10 | 2 | 33 | 11.7 | 7.3 | 3.11 | 2.51 |
| 0.2 | 56 | 17 | 14 | 684 | 1463 | 61.5 | 54.6 | 0.41 | 3 | 2 | 1.25 | 1 | 6 | 10 | 2 | 35.2 | 11.7 | 7.3 | 3.27 | 2.66 |
| 0.2 | 56 | 34 | 28 | 779 | 1770 | 61.5 | 54.0 | 0.41 | 3 | 2 | 1.25 | 1 | 6 | 8 | 2 | 33.6 | 11.7 | 7.3 | 3.48 | 2.82 |
| 0.2 | 64 | 34 | 28 | 732 | 1794 | 64.8 | 48.5 | 0.42 | 3 | 2 | 1.24 | 1 | 6 | 11 | 2 | 33.8 | 11.7 | 7.2 | 3.77 | 3.09 |
| 0.4 | 48 | 34 | 28 | 802 | 2643 | 50.8 | 48.2 | 0.61 | 4 | 3 | 2.42 | 1 | 7 | 8 | 2 | 33.1 | 11.6 | 7.2 | 3.59 | 2.75 |
| 0.4 | 56 | 34 | 28 | 708 | 2266 | 56.1 | 49.0 | 0.64 | 4 | 4 | 2.25 | 1 | 7 | 7 | 2 | 34.8 | 11.7 | 7.3 | 3.96 | 3.13 |
| 0.4 | 64 | 34 | 28 | 732 | 2077 | 58.2 | 43.5 | 0.63 | 4 | 4 | 2.42 | 1 | 7 | 6 | 2 | 34.4 | 11.7 | 7.2 | 4.37 | 3.41 |
| 0.8 | 48 | 34 | 28 | 850 | 4248 | 46.9 | 43.0 | 1.30 | 4 | 5 | 4.68 | 1 | 8 | 8 | 2 | 32.7 | 11.8 | 7.2 | 3.99 | 2.85 |
| 0.8 | 56 | 34 | 28 | 755 | 3493 | 48.5 | 41.3 | 1.29 | 4 | 5 | 4.47 | 1 | 8 | 7 | 2 | 33.8 | 11.5 | 7.0 | 4.49 | 3.32 |
| 0.8 | 64 | 34 | 28 | 755 | 3304 | 50.8 | 37.7 | 1.42 | 4 | 6 | 4.21 | 1 | 8 | 9 | 2 | 33.9 | 11.7 | 7.0 | 4.90 | 3.55 |

≈ 11.7 kW; $T_{indoor}$ = 21°C; outdoor relative humidity = 70%.

om

— substantially smaller values of subcooling, and

— smaller compressor requirements.

Systems 2 and 3 have 11 and 19% improvements, respectively, in COP from the base case.

## 4.4 Fully Optimized Systems

For systems 4 through 15, all ten variables were optimized for the 8.3°C (47°F) ambient.

### 4.4.1 $A_{tot}$ constrained to base case value

Systems 4 through 8 represent optimized cases for various levels of compressor and fan efficiencies with the common constraint of available heat exchanger area ($A_{tot}$) equal to 0.21 $m^2/kW_{nom}$ (8 $ft^2/ton_{nom}$).

*Performance levels.* The COP of 2.92 found for system 4 represents an improvement from the base case of 21.7%. This improvement was achieved solely by system optimization (20%) and a reduction in evaporator superheat (1.7%); no increases in component efficiency or total heat exchanger area were required.

The COP of 3.11 found for system 5 is comparable to the performance of SOA systems. System 5 has better fans than the SOA heat pumps but lower compressor efficiency and smaller heat exchangers.

In systems 6 through 8, the calculated COPs range from 3.27 to 3.77. These results show the significant impact of improved compressors and fans on performance when both improvements are made simultaneously and the other parameters are optimized for these new component efficiencies.

*System configurations.* The optimum evaporator air flow rates [1460 to 1790 L/s (3100 to 3800 cfm)] in systems 4 through 8 are approximately 1.5 times the values found for systems 1 through 3. The main reason for the increase is that the number of evaporator rows was reduced from 3 to 1 and the evaporator frontal area was increased by nearly the

inverse ratio. This result is not particularly surprising since SOA systems typically have 1- or 2-row evaporator coils and evaporator air flow rates ranging from 1320 to 1700 L/s (2800 to 3600 cfm).

### 4.4.2 $A_{tot}$ constrained to twice base case values

Systems 9 through 11 represent fully optimized cases for three levels of compressor efficiency, fans twice as efficient as the base case, and a constraint on $A_{tot}$ of 0.42 $m^2/kW_{nom}$ (16 $ft^2/ton_{nom}$).

Comparison of systems 9, 10, and 11 with systems 5, 7, and 8, respectively, shows the effects of doubling the heat exchanger area.

*Performance levels.* For each of the three levels of compressor efficiency, a 100% increase in heat exchanger area from the base case results in a 15% improvement in COP.

*System configurations.* Configuration changes accompanying the system with larger heat exchangers include

- larger evaporator air flow rates,
- an increase in the number of refrigerant circuits,
- smaller compressor displacement, and
- smaller motor size requirements for the compressor and the fans.

The latter effects would tend to offset somewhat the increased cost of larger coils.

### 4.4.3 $A_{tot}$ constrained to four times base case values

Systems 12 through 14 represent fully optimized cases for the three compressor efficiency levels, the improved fans, and a constraint on $A_{tot}$ of 0.84 $m^2/kW_{nom}$ (32 $ft^2/ton_{nom}$).

*Performance levels.* Comparison of systems 12, 13, and 14 with systems that have the base case heat exchanger area, that is, systems 5, 7, and 8 respectively, shows performance improvements of 29% for a 400% increase in heat exchanger area. It was previously noted that the

first 100% increase in heat exchanger area resulted in a 15% increase in performance; the next 300% was required for an equivalent further improvement in COP.

*System configurations.* The system parameter changes noted in Sect. 4.4.2 also apply here.

### 4.4.4 Effects of improved compressor efficiency

Within each group of systems with the same area constraints, the effects of compressor efficiency improvements can be studied. Three such groups are systems [5, 7, 8], [9, 10, 11], and [12, 13, 14]. The general effects due to improved compressor efficiency are

(1) COP improvements of
   - about 11% resulting from a 17% increase in compressor efficiency and
   - about 22% resulting from a 33% increase in compressor efficiency;
(2) reduced air flow requirements, coupled with
(3) increased compressor displacement, but
(4) decreased motor size.

### 4.4.5 Effects of improved fan efficiency

Comparison of systems within the groups [2, 3], [4, 5], and [6, 7] shows that a 100% increase in combined fan and fan-motor efficiencies results in

(1) a COP improvement of 6 to 7.5%,
(2) higher optimal air flow rates, and
(3) smaller fan motors.

### 4.4.6 Indoor air supply temperature

The indoor air flow rates found optimum for all the improved systems are near, or in some cases above, the upper limits of indoor air flow rates selected by ARI[3] for rating purposes. The maximum ARI value for

indoor air flow rate is 60.4 L $s^{-1}$ $kW_{nom}^{-1}$ (450 cfm/$ton_{nom}$); this converts to 708 L/s (1500 cfm) for the nominal capacity chosen for this study. The indoor air supply temperature corresponding to this indoor air flow rate is 35°C (95°F) when the indoor air return temperature is 21.1°C (70°F).

The related indoor air supply temperatures for the optimized systems in Table 4.1 range from 33 to 35°C (91 to 95°F). With fixed air flow rates, the supply air temperatures decrease along with the heating capacity as the ambient air temperature decreases. Values of 29 to 31°C (85 to 88°F) would result at an ambient of -1°C (30°F), which is near the usual system balance point. Below this point, resistance heaters would be used to supplement the heat pump and boost the indoor air supply temperatures. The indoor air supply temperatures mentioned above are on the lower border of tolerable comfort conditions. In Sect. 5, design trade-offs are addressed which would allow higher indoor air temperatures, if required, without significant degradation of system performance.

# 5. DESIGN SENSITIVITY ANALYSIS

Use of the optimizing routine results in a single set of the "best" design parameters consistent with a given set of constraints; it gives no information about the sensitivity of efficiency to departures from this optimum design. As a practical matter, it is desirable to consider heat pump designs that approximate but do not fully achieve optimum performance. Once the optimum COP levels have been found, sensitivity analysis can be used to find the regions of design flexibility.

## 5.1 General Description of Sensitivity Plots

Plots were generated which show contours of constant values of COP as pairs of design parameters are varied about their optimum values. For each plot the remaining system parameters are held fixed (except for special cases noted below). When appropriate, the plots also contain contours of constant value of the heating capacity. These are used to illustrate the effects of the capacity constraint on achievable efficiency levels. The "x" marked on each plot locates the values of the two variables about which the plot was generated. It also denotes, except as noted in the text, the constrained optimum COP.

The plots shown in this section were chosen to illustrate the usefulness of sensitivity analysis as a design tool as well as to examine some specific design "trade-offs."

## 5.2 Sensitivity Analysis for a Sample Case

System 10, as given in Table 4.1, was chosen as a sample for illustration of the sensitivity analysis. This system represents improvement possibilities that may be achieved in the near future.

### 5.2.1 Sensitivity to evaporator and condenser air flow rates

*At 8.3°C ambient conditions.* Figure 5.1 shows the sensitivity of COP to changes in air flow rates about the optimum configuration for system 10. The "concentric" solid and dashed curves are lines of constant

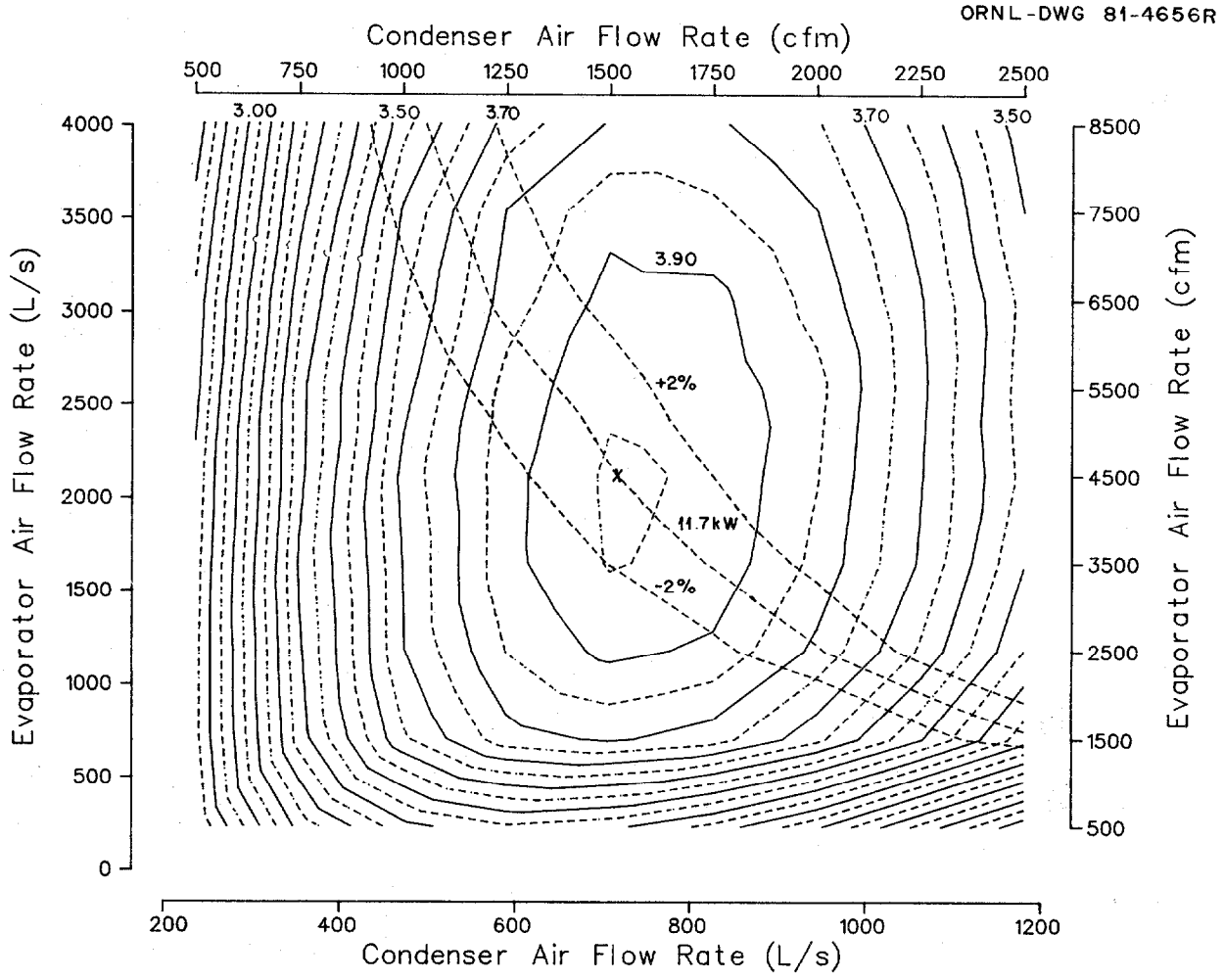


Fig. 5.1. Sensitivity of COP and heating capacity to air flow rates at $T_{amb}$ = 8.3°C (47°F) — system 10.

COP and the "diagonal" dashed lines show the combinations of condenser and evaporator air flows that give capacities of 11.7 kW (40,000 Btu/h) and ±2% variations from that value.

In general, the configuration that produces the maximum COP (as a function of air flow rates) and also provides the required heating capacity will be achieved where the required capacity line is tangent to a surface of constant COP.[14] In Fig. 5.1, this point of tangency occurs at the maximum unconstrained COP value. This particular situation is the best obtainable, but it will not be achieved for all possible sets of variables. As is shown in Appendix D, for a different system, the point of tangency may be away from the unconstrained COP maximum for air flow vs air flow plots as well.

The optimum combination of air flow rates shown in Fig. 5.1 is the result of trade-offs between compressor power and fan powers. As the air flows are increased beyond their optimum values, the power consumed by the fans is increased. The compressor power, on the other hand, is reduced because the larger air flows reduce the refrigerant to air temperature differences and thus the pressure ratio. However, the increase in fan power dominates, and the net effect is a decrease in COP. Conversely, if the air flow rates are decreased from the optimum, the compressor power consumption increases faster than fan power decreases; again there is a net decrease in COP.

*At -8.3°C ambient conditions, no supplemental resistance heat.* Figure 5.1 was generated for ambient air conditions of +8.3°C (47°F). A similar curve can be generated at lower ambient temperatures to study how the optimum air flow rates are affected by outdoor air temperatures. Such a plot is shown in Fig. 5.2 for an ambient temperature of -8.3°C (17°F). No capacity constraint lines are shown on this plot because the heating capacity is allowed to assume its natural value. The optimum COP in Fig. 5.2 occurs at lower values of air flow rates than those indicated by the "x." This "x" denotes the optimum values for the +8.3°C (47°F) condition as shown in Fig. 5.1. Figure 5.2 indicates that, at lower ambient temperatures, a reduction in air flow rates is slightly beneficial to the *heat pump* COP. However, since the heating capacity of the heat pump at the -8.3°C (17°F) ambient condition is not sufficient to supply the house demand for the typical application, supplementary resistance heat will be required. Air flow rates that are more nearly optimum for the combined system (heat pump plus resistance heaters) should instead be considered.

*At -8.3°C ambient conditions, supplemental resistance heat.* In Fig. 5.3 the effect of resistance heat requirements on the system (heat pump plus resistance heaters) optimum COP is shown. The combined COP was calculated from the equation

$$COP_{sys} = \frac{\dot{Q}_{h(sys)}}{\dot{W}_{sys}} = \frac{COP_{hp}}{F_{hp} + (1 - F_{hp})COP_{hp}}, \qquad (5.1)$$

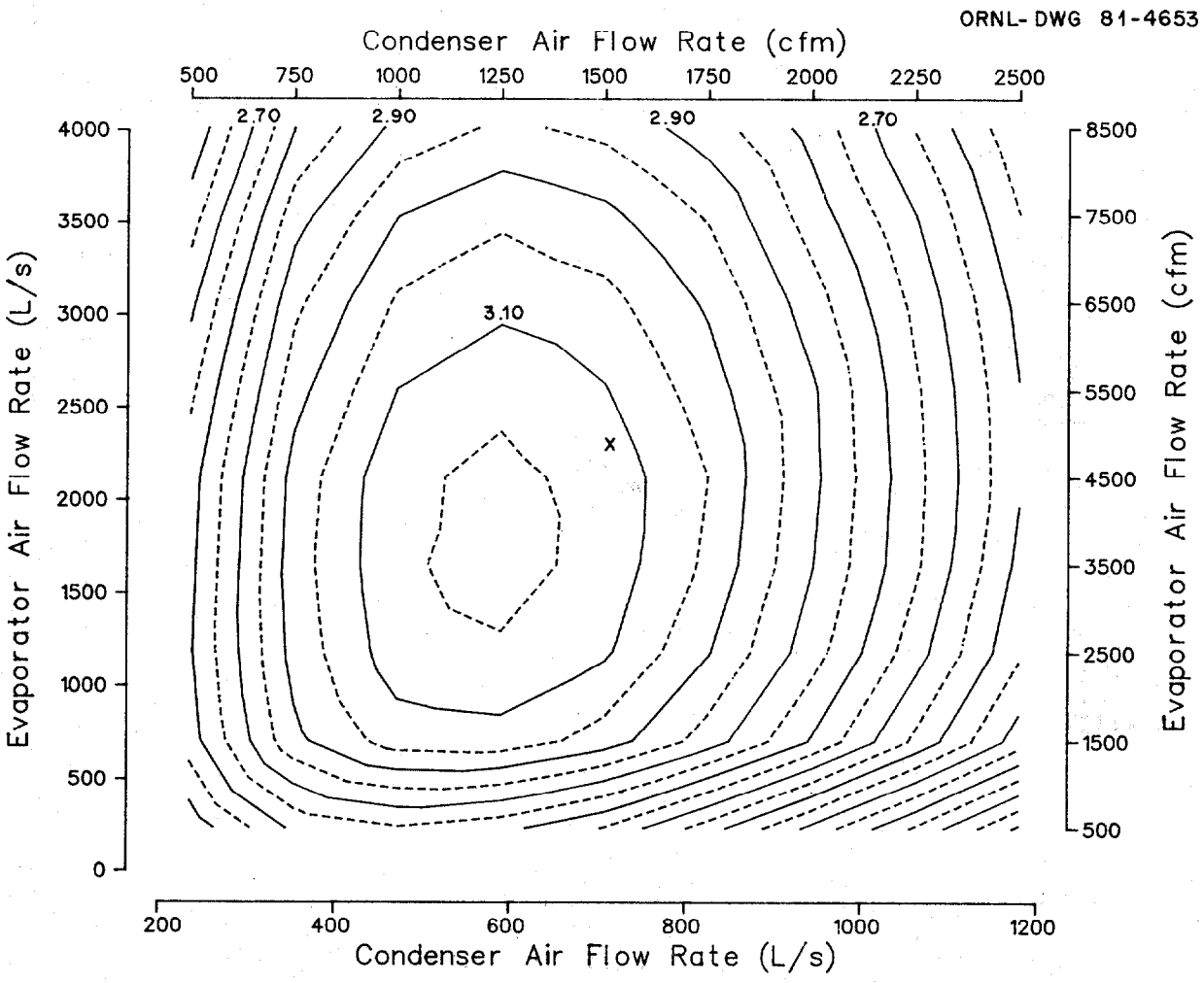


Fig. 5.2. Sensitivity of COP (with no supplemental resistance heat) to air flow rates at $T_{amb}$ = -8.3°C (17°F) — system 10.

where the subscripts "sys" and "hp" refer to system and heat pump and $F_{hp}$ is the fraction of the house load supplied by the heat pump; that is,

$$F_{hp} = \frac{\dot{Q}_{h(hp)}}{\dot{Q}_{h(sys)}} . \qquad (5.2)$$

For Fig. 5.3, $\dot{Q}_{h(sys)}$ was assumed to be 11.7 kW (40,000 Btu/h). Examination of Fig. 5.3 shows that, at the -8.3°C ambient, an optimum system COP of 1.80 (or higher) occurs at condenser and evaporator air flow rates nearly twice the values found optimum at the +8.3°C (47°F) ambient condition (denoted by the "x" in Fig. 5.3). Thus, the lower air flows

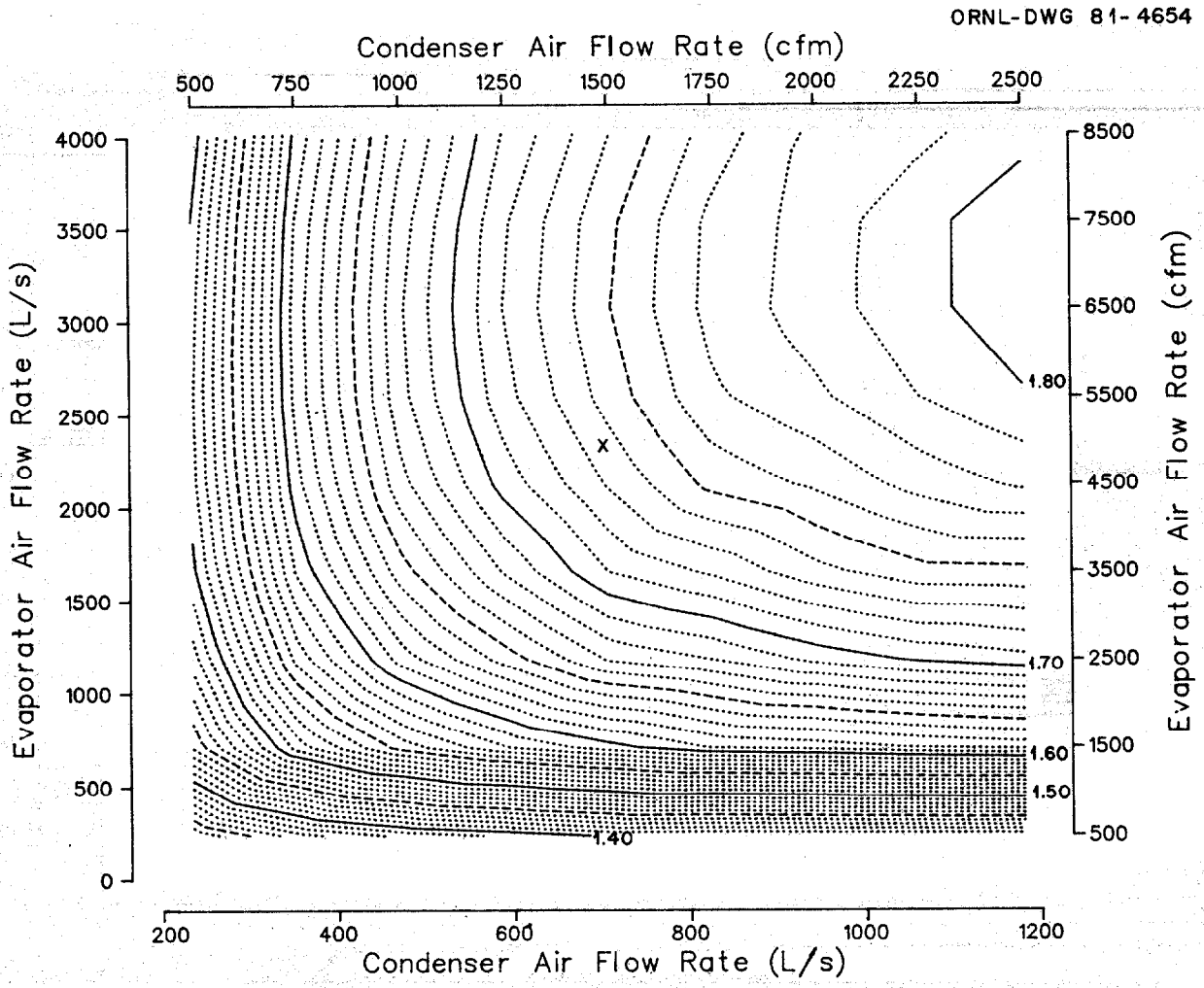


Fig. 5.3. Sensitivity of COP (with supplemental resistance heat) to air flow rates at $T_{amb}$ = -8.3°C (17°F) — system 10.

found (in Fig. 5.2) to be optimum for the heat pump at -8.3°C (17°F) are farther away from the total system optimum than the values found to be optimum for the +8.3°C (47°F) ambient condition. Thus the optimum values of air flow for the +8.3°C (47°F) ambient condition give reasonably optimum system performance at the -8.3°C (17°F) ambient. For ambient temperatures at and slightly above the system balance point where supplemental resistance heat is not needed [typically between -2 and 0°C (28 and 32°F)], the results of Fig. 5.2 indicate that a slight reduction in air flows would be beneficial; conversely, above +8.3°C (47°F), a further

increase in air flows would be more nearly optimum. However, because conventional variable-speed fans are more expensive and less efficient at the lower speeds, such fine tuning does not appear worthwhile for the heating mode in single-capacity systems.

### 5.2.2 Condenser subcooling and condenser air flow rate

In Figs. 5.4, 5.5, and 5.6, the effects of nonoptimal condenser subcooling are examined at +8.3°C (47°F) and at -8.3°C (17°F) without and with supplemental resistance heat added. The choice and sizing of

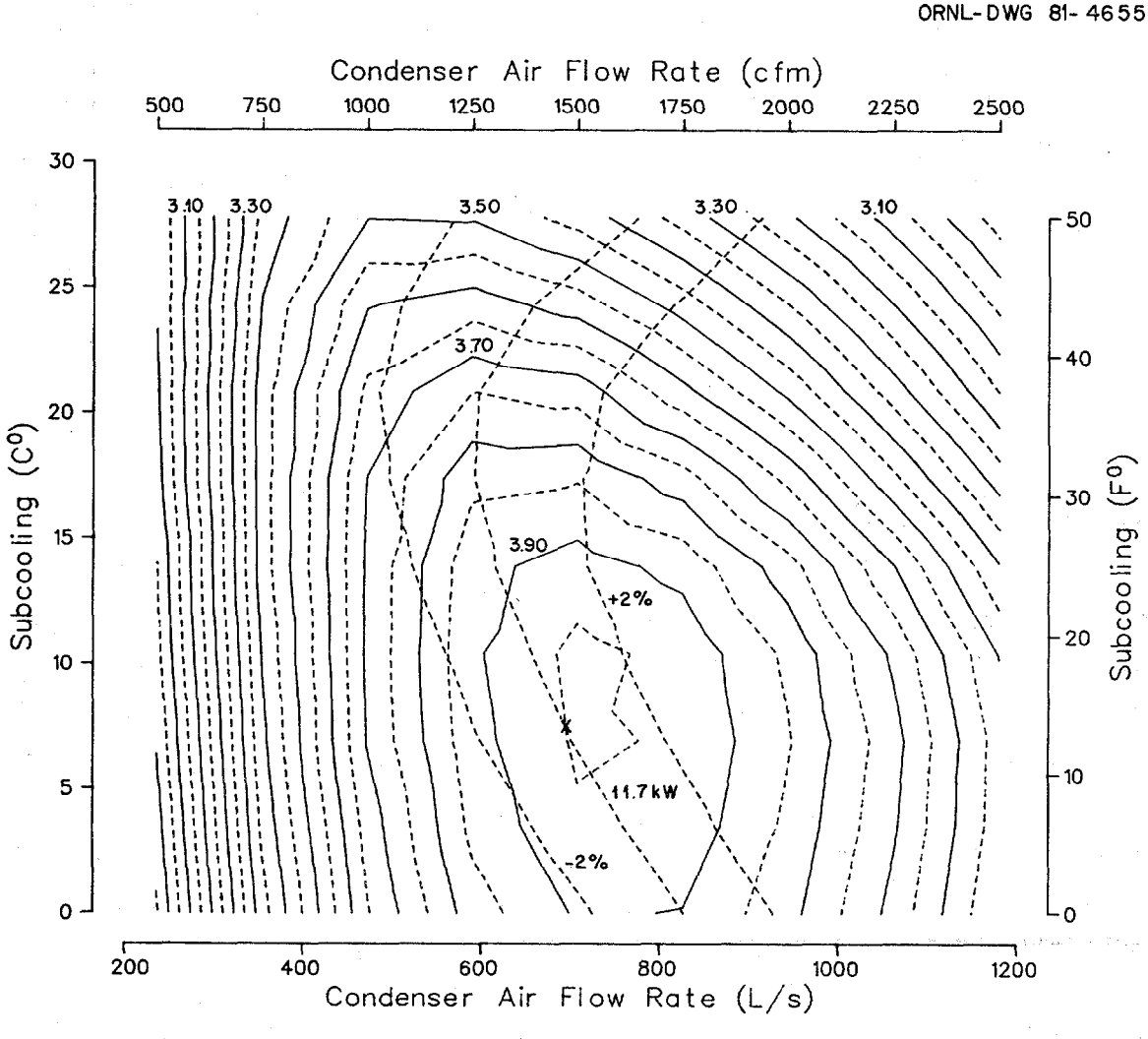


Fig. 5.4. Sensitivity of COP and heating capacity to condenser subcooling and air flow rate at $T_{amb}$ = 8.3°C (47°F) — system 10.

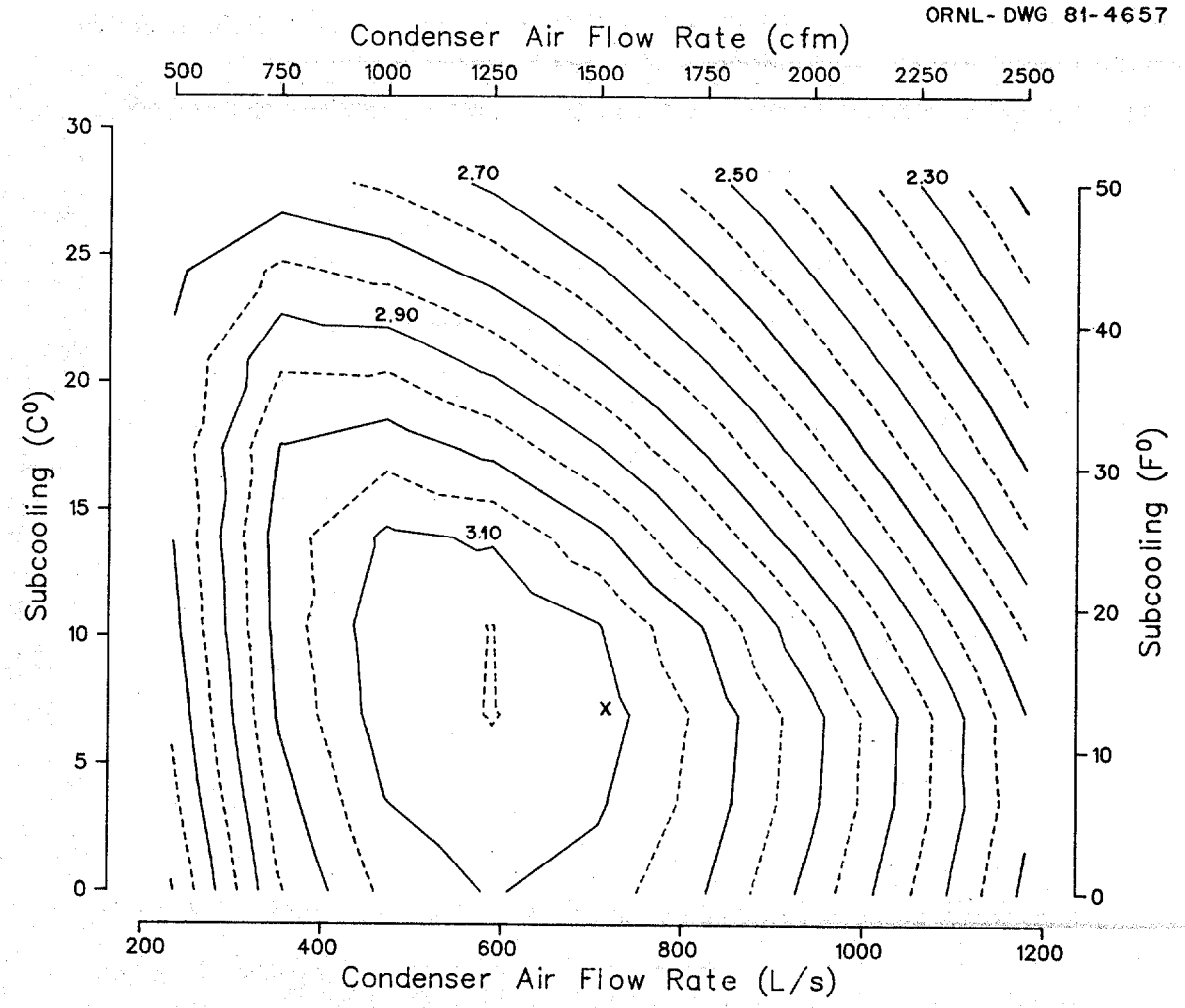


Fig. 5.5. Sensitivity of COP (with no supplemental resistance heat) to condenser subcooling and air flow rate at $T_{amb}$ = -8.3°C (17°F) — system 10.

the refrigerant control device governs this parameter. For both ambient temperatures, a condenser subcooling value between 5.6 and 11.2C° (10 and 20F°) is near optimum. Plots such as Figs. 5.4 through 5.6 would be useful in evaluating how much performance is affected by refrigerant control devices that do not maintain optimum subcooling over a range of ambient conditions.

These results differ from those of Kirschbaum and Veyo[15] who found a subcooling value of 15.6C° (28F°) to be optimum at an ambient temperature of 0°C (32°F). They also found higher values to be optimum at higher ambients and lower values to be optimum at lower ambients. The difference in results is caused, we feel, by the differences in condenser

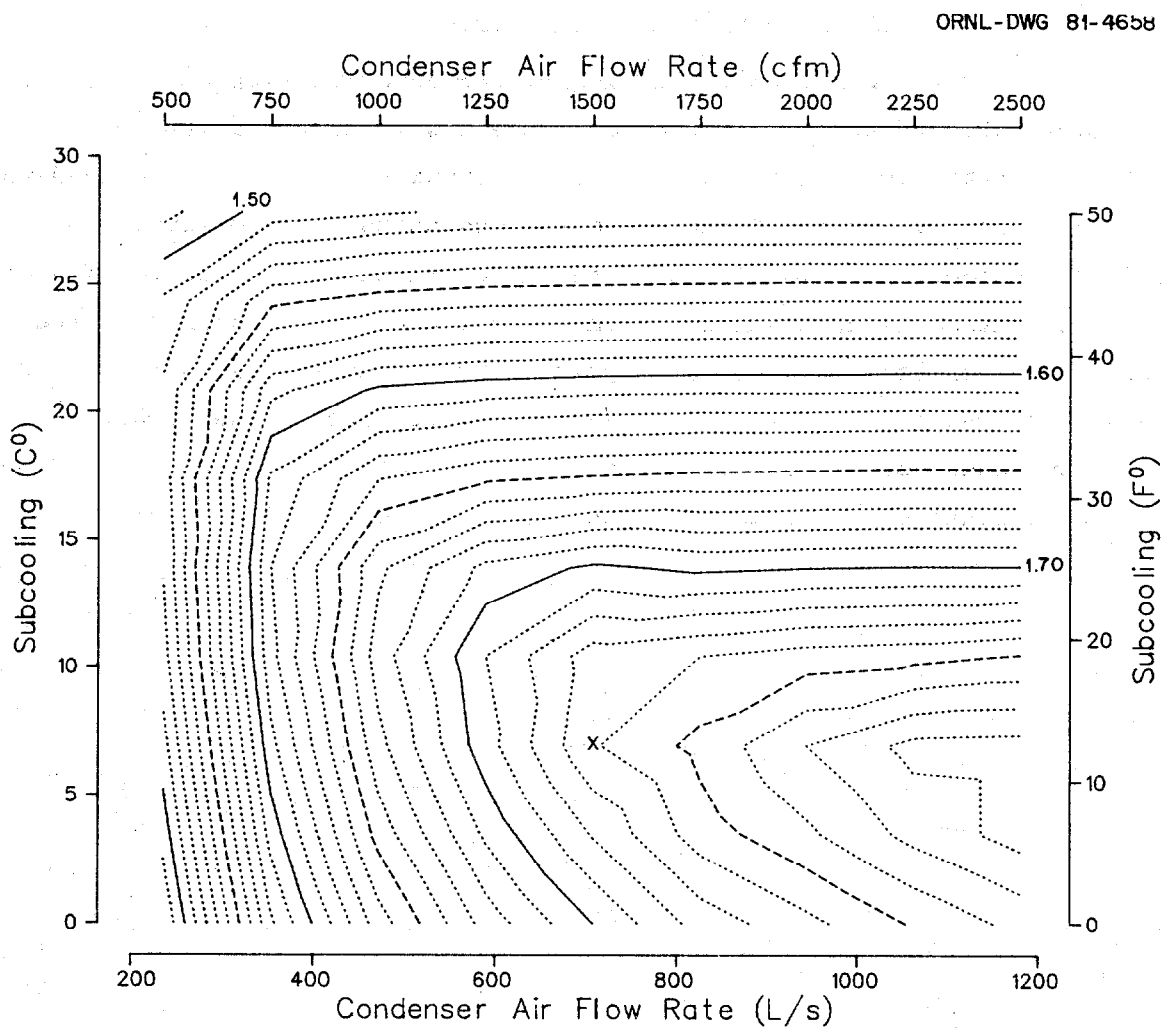


Fig. 5.6. Sensitivity of COP (with supplemental resistance heat) to condenser subcooling and air flow rate at $T_{amb}$ = -8.3°C (17°F) — system 10.

configurations. In ref. 15, the subcooling section of the condenser was modeled as being before the two-phase region (with respect to the air flow direction); in the ORNL model the subcooling section of the condenser is modeled as being in parallel with the two-phase section. The latter case is, in our experience, the more usual situation. However, the configuration used by Kirschbaum and Veyo may offer efficiency advantages not considered here. The differences in optimum subcooling values emphasize that, for each new heat exchanger configuration, the system parameters should be reoptimized.

For all the plots which follow, only +8.3°C (47°F) ambients are considered.

### 5.2.3 Air flow rates and number of tube rows

*Condenser.* In Fig. 5.7, COP is plotted as a function of condenser air flow rate and number of condenser tube rows. As the number of condenser tube rows was varied from the optimum number of 4, the condenser frontal area (given in the tabular data) was adjusted to maintain a constant product of rows times frontal area; in this way, the total heat exchanger area was constrained to the same limit for all points on the plot. The results show that the optimum COP is rather insensitive to the number of tube rows. For the condenser, a reduction in the number of coil rows does not significantly reduce the total air-side pressure drop of the combined coil and indoor duct systems; the drop in air-side heat

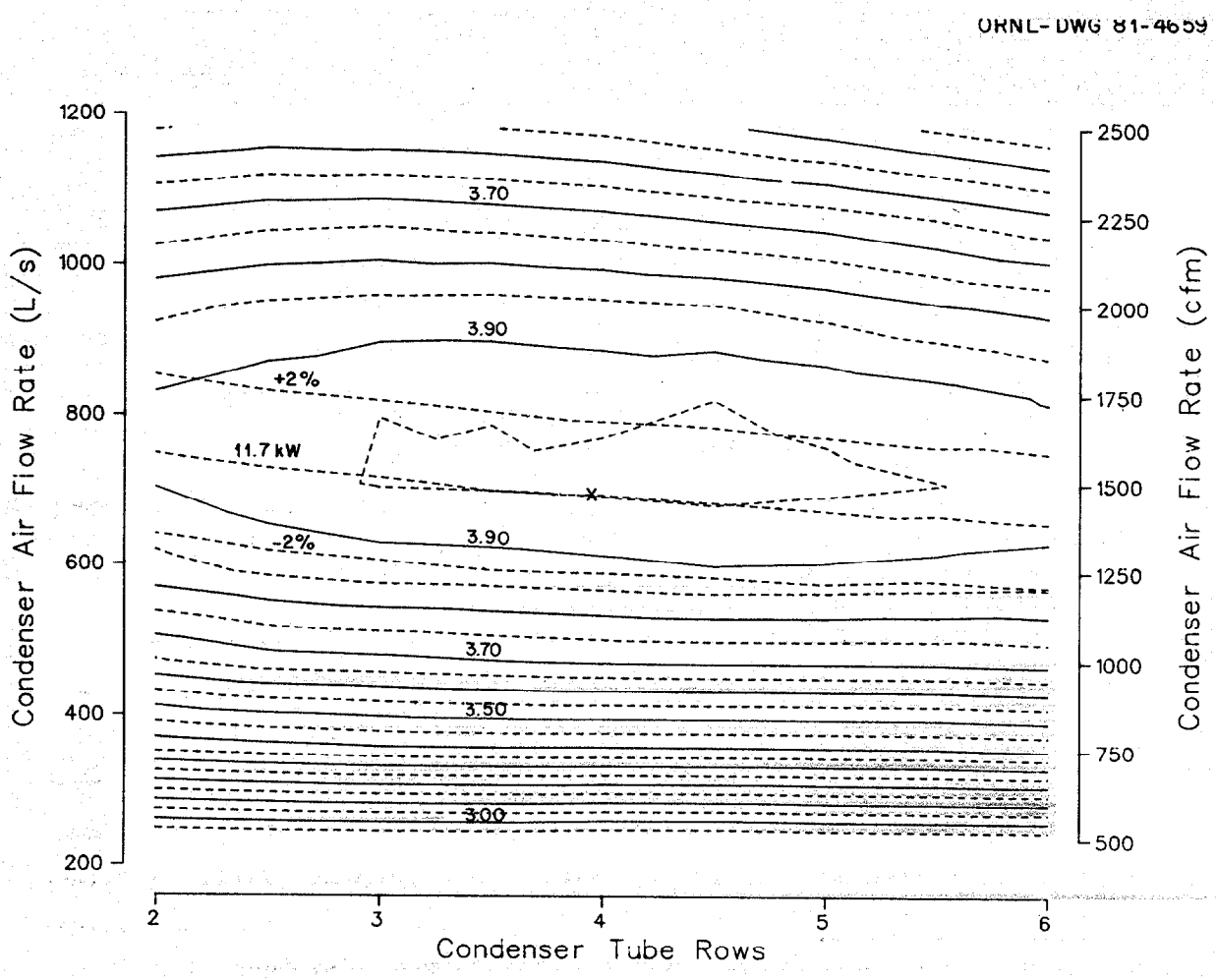


Fig. 5.7. Sensitivity of COP and heating capacity to condenser air flow rate and number of tube rows at $T_{amb}$ = 8.3°C (47°F) — system 10.

transfer coefficient associated with the smaller number of tube rows and larger face areas is closely compensated for by reductions in fan power. For larger numbers of rows, the increased fan power is almost balanced by the increase in air-side heat transfer coefficient.

Since the COP is fairly insensitive to the number of condenser (indoor) tube rows, the larger frontal areas found by the optimizer could be reduced and more rows added to better accommodate the limited space available for the indoor cabinet.

*Evaporator.* In Fig. 5.8, COP is plotted as a function of evaporator air flow rate and number of evaporator tube rows; as in the previous plot, the evaporator frontal area was adjusted to maintain fixed total area while the tube rows were varied. The COP contours for the evaporator

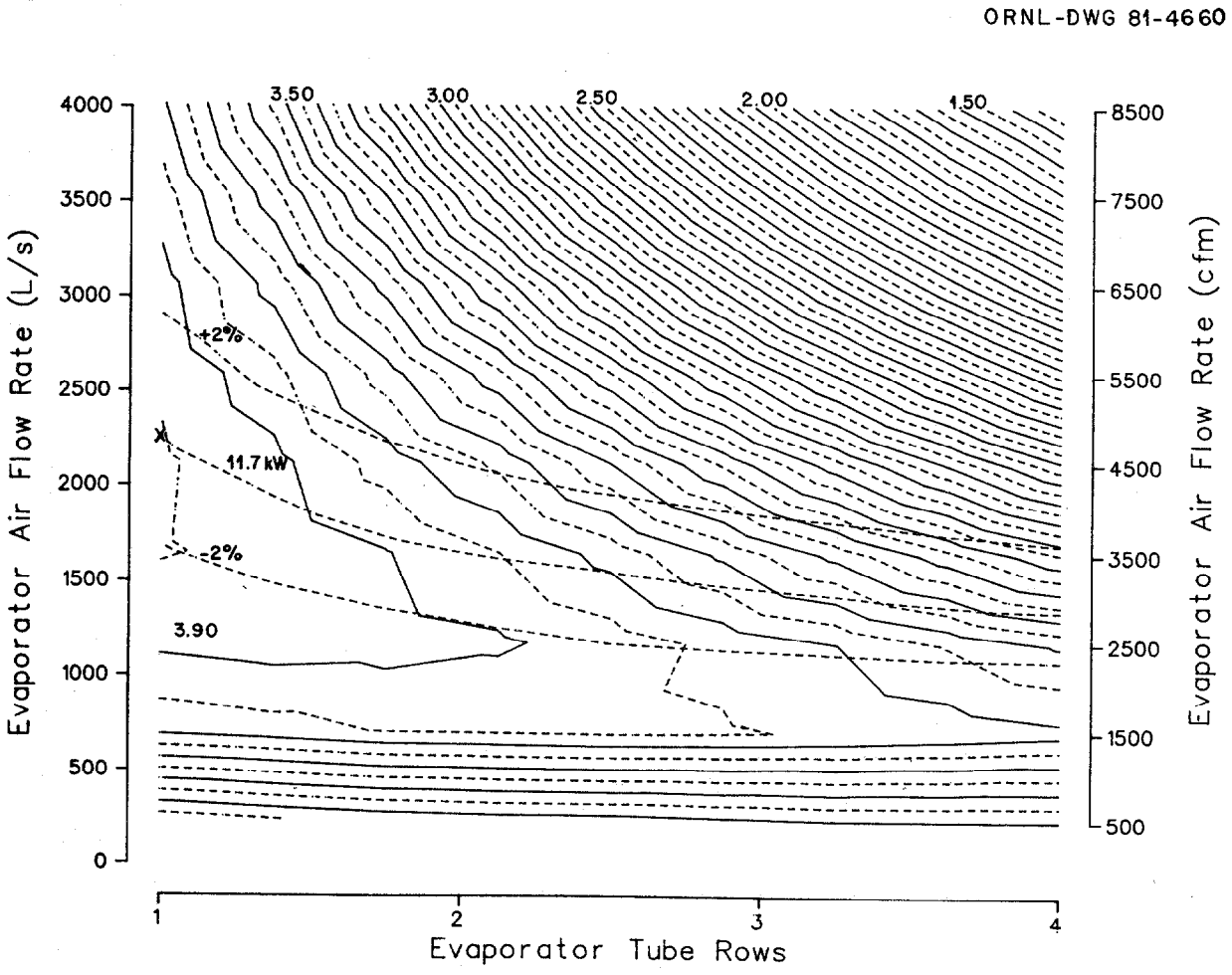


Fig. 5.8. Sensitivity of COP and heating capacity to evaporator air flow rate and number of tube rows at $T_{amb}$ = 8.3°C (47°F) — system 10.

approach a peak as the number of tube rows approaches one. In this case, because the majority of the air-side pressure drop occurs across the evaporator coil, a one-row coil with large frontal area allows for a significant reduction in coil $\Delta P$, and thus outdoor fan power, which more than compensates for the associated drop in air-side heat transfer coefficient.

### 5.2.4 Evaporator and condenser refrigerant circuits

Variation of the COP with the number of parallel refrigerant circuits in the evaporator and the number of circuits in the condenser is shown in Fig. 5.9. The rapid decline in COP for the lower numbers of circuits

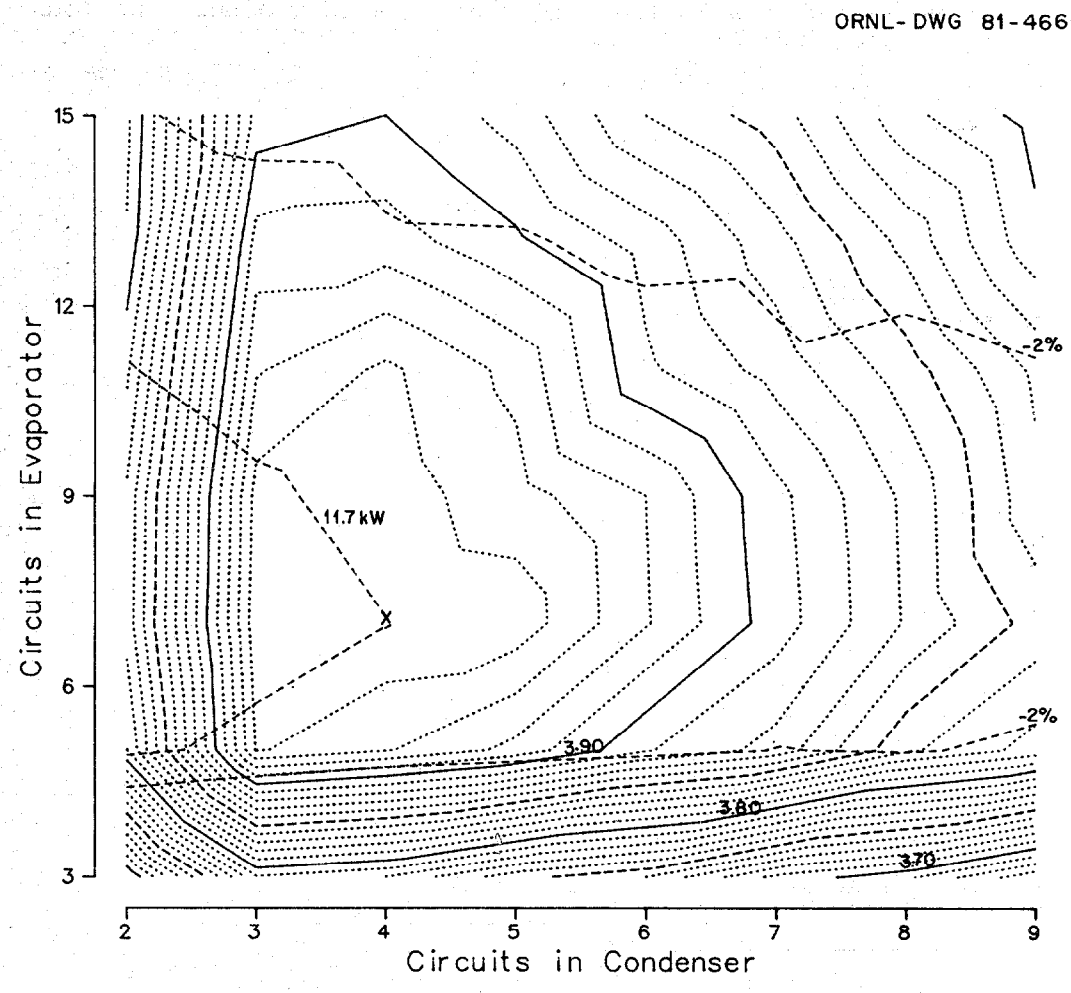


Fig. 5.9. Sensitivity of COP and heating capacity to the number of parallel refrigerant circuits at $T_{amb}$ = 8.3°C (47°F) — system 10.

reflects the effects of increased refrigerant pressure drops. Thus there is a critical minimum number of circuits (in this case five evaporator circuits and three condenser circuits) below which performance degrades rapidly. In Figs. 5.10 and 5.11, the related pressure drops in the condenser and evaporator are shown as functions of the number of circuits. Note that for the system considered, a pressure drop of 103 kPa (15 psi) is acceptable for the condenser; this corresponds to three parallel circuits. For the evaporator, the pressure drop should be kept smaller than 48 kPa (7 psi), for which five or more circuits are required. With higher numbers of circuits, performance rises quickly to a peak followed by a more gradual reduction in COP. The slow decline in COP with more circuits is due to the drop in refrigerant-side heat transfer coefficient as the mass flow in each individual circuit is reduced. Obviously, some

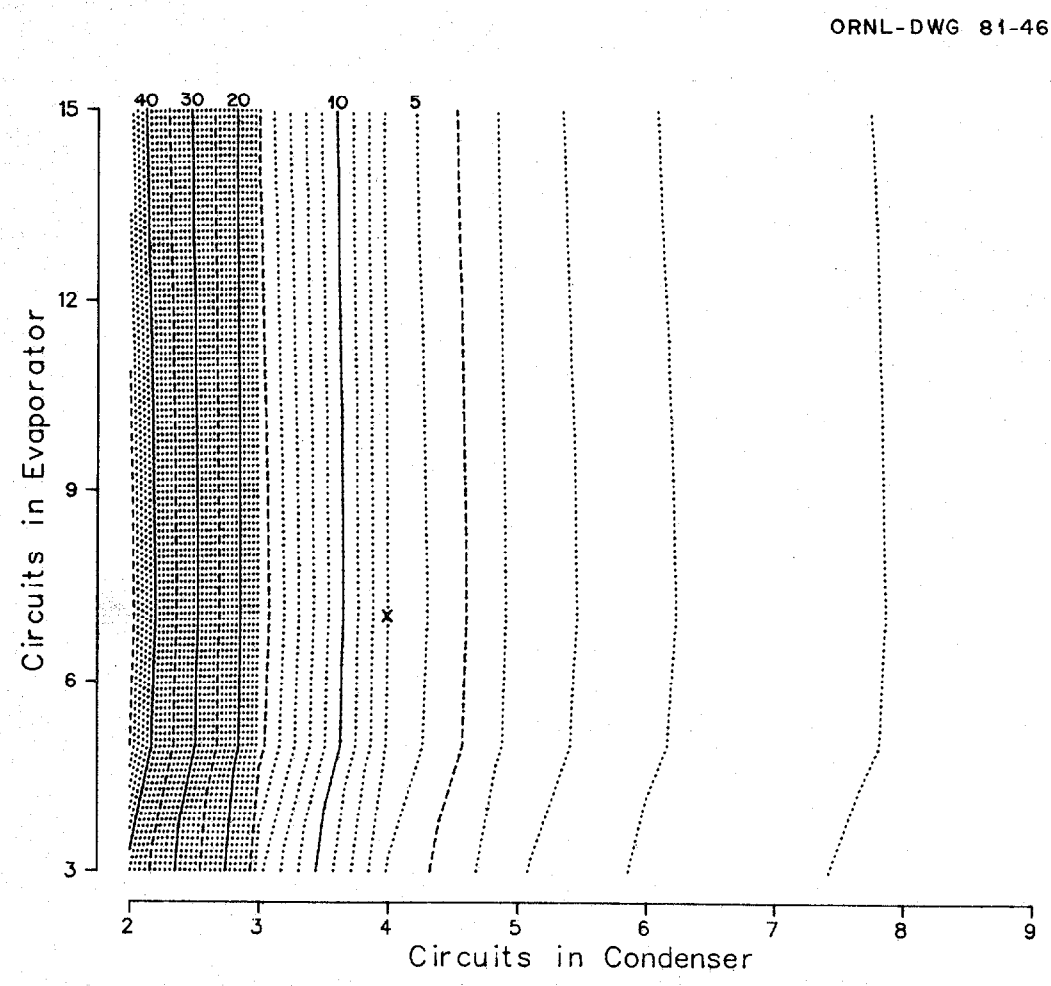


Fig. 5.10. Sensitivity of condenser pressure drop (psi) to the number of parallel refrigerant circuits at $T_{amb}$ = 8.3°C (47°F) — system 10 (conversion factor from psi to kPa = 6.895).

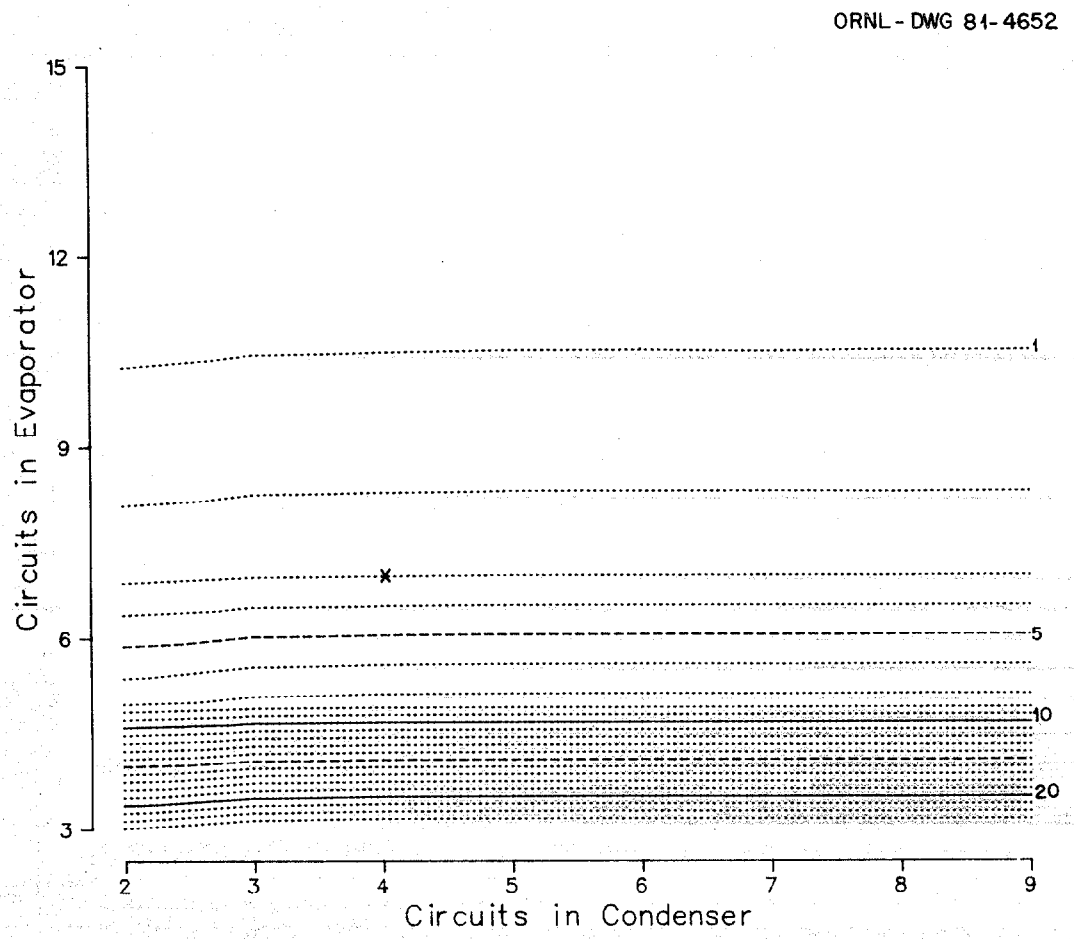


Fig. 5.11. Sensitivity of evaporator pressure drop (psi) to the number of parallel refrigerant circuits at $T_{amb}$ = 8.3°C (47°F) — system 10 (conversion factor from psi to kPa = 6.895).

compromise will be required here for good operation in the cooling mode where the functions of the coils are switched. Specifically, more than four indoor coil circuits would probably be needed in system 10 for optimum cooling performance (i.e., when the indoor coil becomes the evaporator). However, because increasing the number of circuits in the indoor coil only gradually reduces the COP, heating COP would not suffer much from this compromise.

### 5.2.5 Condenser air flow rate and ratio of condenser to total heat exchanger area

The ratio of condenser (indoor) to total heat exchanger area is of interest in regard to both the physical size of the indoor unit and

maintenance of sufficiently low evaporator temperatures in the cooling mode for proper dehumidification. The level of evaporating temperature in the cooling mode is also dependent on the indoor air flow rate. A sensitivity plot of these two parameters in the heating mode can be used to show the design flexibility of the heating COP should air flow or indoor size compromises be required in the cooling mode.

To maintain a constant value for total heat exchanger area, when the indoor-to-total-area ratio was changed, the evaporator (outdoor) area was adjusted accordingly. Because the number of tube rows in each coil was held constant, the desired area ratios were achieved by simply adjusting the frontal areas. The outdoor air flow rate was held constant.

As shown in Fig. 5.12, the optimum area ratio lies between 0.50 and 0.55. However, with proper adjustment of the condenser air flow rates,

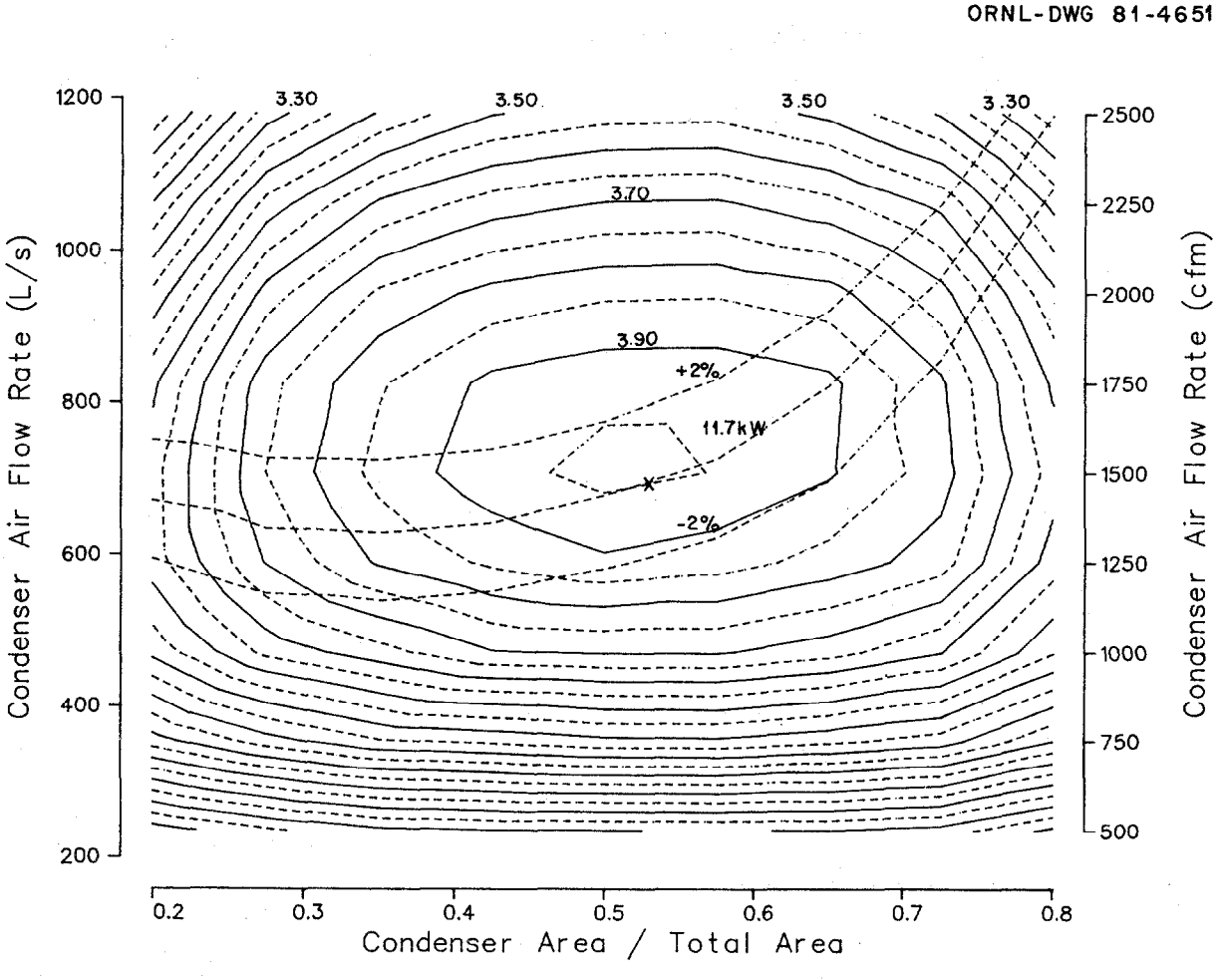


Fig. 5.12. Sensitivity of COP and heating capacity to condenser air flow rate and area ratio at $T_{amb}$ = 8.3°C (47°F) — system 10.

the design capacity (11.7 kW or 40,000 Btu/h) can be maintained over a condenser to total area ratio of 0.37 to 0.67 with a maximum COP loss of 2.5%. The region of interest for proper humidity control in the cooling mode is where the ratios are between 0.37 and 0.55. This is because the smaller indoor coil surface area and the accompanying lower indoor air flow rates will result in a lower evaporator temperature in the cooling mode and, thus, more moisture removal from the air. For systems with larger total available heat exchanger area, this ratio becomes an important design question for a reversible heat pump.

## 5.3 Trade-offs Between Compressor Displacement and Air Flow Rates

### 5.3.1 Analysis for two heat pump systems

The sensitivity of COP to changes in compressor displacement is not conveniently displayed with two-dimensional sensitivity plots such as those shown in the preceding sections. Too many parameters must be simultaneously considered because displacement is strongly coupled to both the evaporator and condenser air flow rates through the capacity constraint.

To examine the effect of variation of the compressor displacement, a series of sensitivity plots similar to that in Fig. 5.1 was made. Each plot showed the sensitivity of COP to both air flow rates; a different plot was required for each value of compressor displacement examined. From each plot, the combination of air flow rates was chosen which gave maximum COP and the desired heating capacity of 11.7 kW (40,000 Btu/h).

Figures 5.13 and 5.14 show the results of this analysis for systems 10 and 2, respectively, for which COP and the associated optimum air flow rates are plotted vs compressor displacement. Note that in each figure the higher compressor displacements require lower air flow rates for the maximum COP consistent with the capacity constraint. The curve of COP vs displacement in each figure has a rather broad peak instead of a sharply defined maximum. Also the peak of Fig. 5.14 is much broader than that in Fig. 5.13. Clearly the flexibility is greater for system 2 which has been only partially optimized. But even with the sharper peak

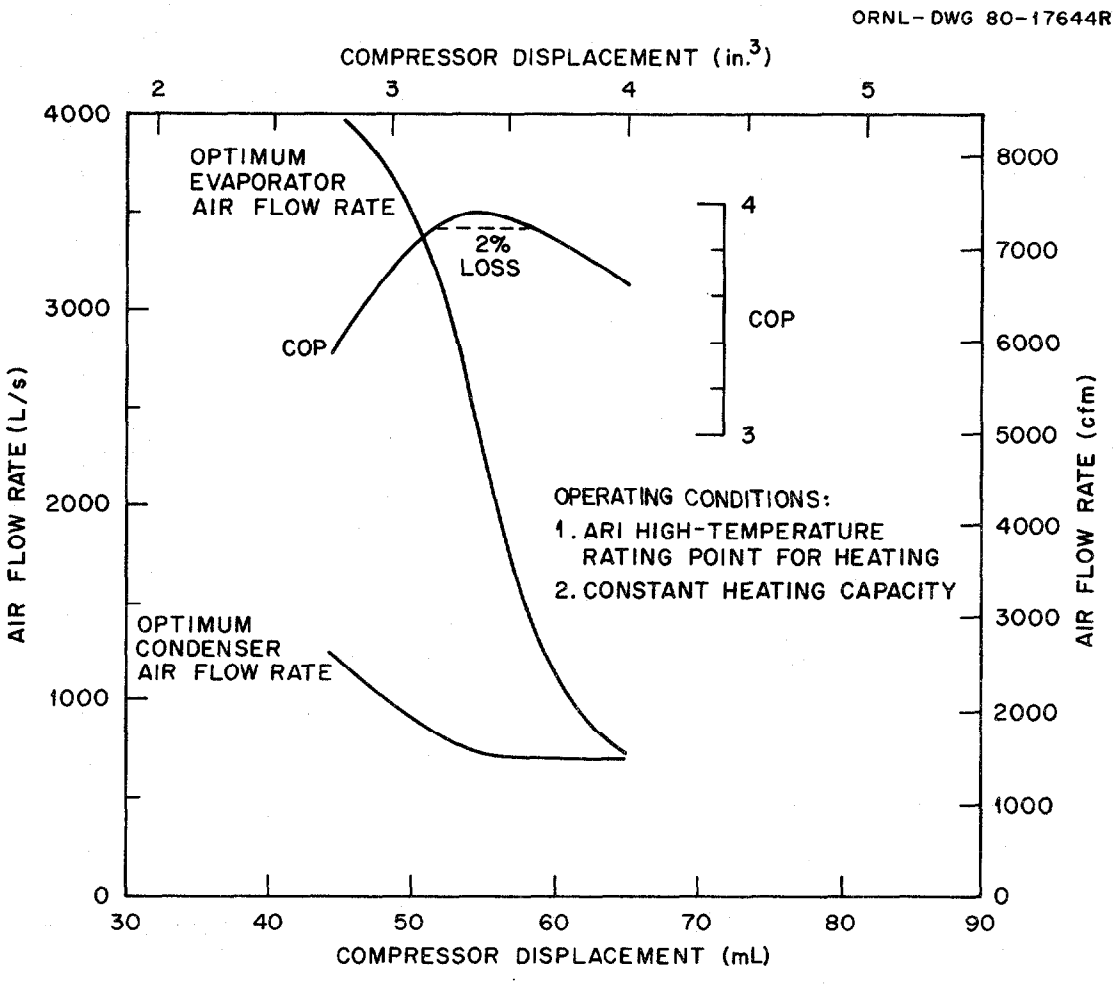


Fig. 5.13. Optimum COP and air flow rates as functions of compressor displacement — system 10.

shown in Fig. 5.13 for the improved system 10, variations of ±10% in compressor displacement are possible with only a 2% loss in COP. The evaporator air flow rate for the lower values of displacement do, however, become quite high.

A sampling of the sensitivity plots used in generating Fig. 5.14 is shown and discussed in Appendix D.

### 5.3.2 Trends of displacement for improved systems

As noted in the preceding discussion, the peak of the COP vs displacement curve is not as wide for the system with more improvements. The location of the peak is shifted also, toward smaller displacement

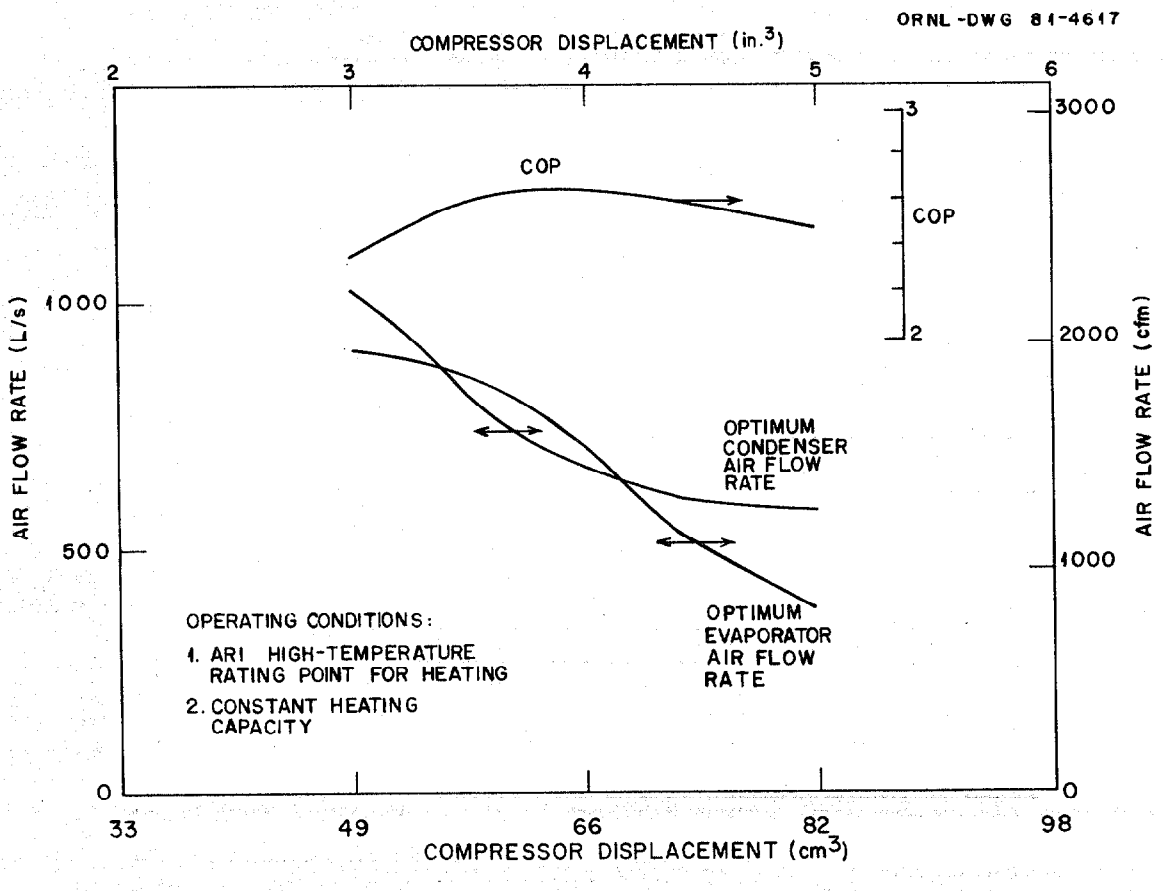


Fig. 5.14. Optimum COP and air flow rates as functions of compressor displacement — system 2.

values. In Fig. 5.15, a series of COP vs displacement curves are shown starting with the curve for system 2 and ending with the curve for system 10. The three intermediate curves are for systems 4, 5, and 7; the displacement and COP of the base case are also shown. Each successive curve shows the cumulative effect of one additional type of system improvement on the width of the COP plateau and on the optimum values of COP and displacement. Note that as the systems are improved, the widths of the plateaus become narrower. This implies that there is less flexibility in the improved systems and that good design techniques are more critical. However, in all the systems considered, there is some design flexibility with regard to the "optimum" displacements and associated air flow rates. This flexibility would be even broader if the area ratio and the other design variables were reoptimized for each value of displacement.

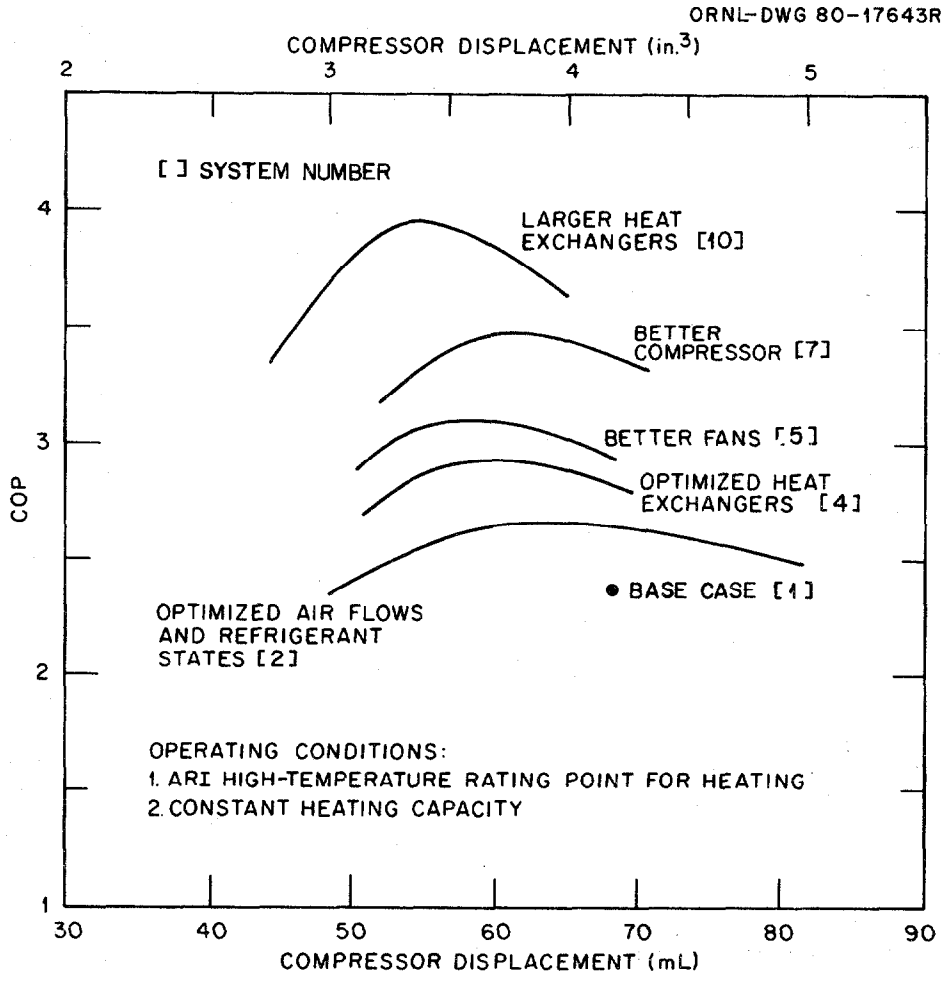


Fig. 5.15. Optimum COP vs compressor displacement for a series of cumulative improvements from the base case system.

Knowledge of this type of flexibility should prove useful in (1) designing for proper humidity control in the cooling mode, (2) maintaining acceptable noise levels and indoor air supply temperatures, and (3) choosing between discrete compressor displacement sizes commercially available.

The optimum values of displacement move to progressively smaller values in systems 2, 4, and 5. For system 7, however, an increase in displacement is required to accompany the compressor efficiency improvement to maintain the same heating capacity because less energy is added to the refrigerant by the more efficient compressor. This increase is followed by a substantial decrease for system 10 due to the increase in heat exchanger size.

These trends in compressor displacement with system improvements were noted earlier in Sect. 4 in the discussion of the optimization results. However, they were not apparent from the *initial* optimization results because the optimizer had difficulty pinpointing the precise optimum values of displacement and air flow rates. The problem in pinpointing the optimum is caused, we feel, by the high sensitivity of capacity and air flow rates to displacement. Near the optimum configuration, a small change in displacement requires a large change in air flow rates to follow the line of constant capacity. The optimization program had difficulty moving in the desired direction in reasonable computational time. Thus the curves in Fig. 5.15 were used to study the general displacement trends and to fine tune the initial optimization results. The system parameters given in Table 4.1 were the result of combined use of the optimization program and sensitivity plots. As further experience is gained in the setup and operation of the optimizer, the sensitivity plots will be used primarily for analysis of flexibilities about the optimum rather than as a supplemental tool for obtaining the optimums.

## 5.4 General Comments Regarding Sensitivity Plots

The sensitivity plots proved to be a useful design tool in conjunction with the optimizing program. Through this type of analysis, it was found that, based on heating-mode requirements alone, there is not one "best" system configuration but rather a family of near-optimum configurations for each level of total heat exchanger area, compressor efficiency, and fan efficiencies. The sensitivity plots should prove useful in the analysis of optimum cooling-mode performance by visually showing the effects of constraints relating to proper humidity control. With sensitivity plots available about the optimums for both the heating and cooling modes, the system designer would be better able to evaluate necessary system design compromises and perhaps reduce the family of solutions found here to a few "best" designs.

# 6. ANALYSIS OF FACTORS LIMITING FURTHER APPROACH TO IDEAL PERFORMANCE

## 6.1 Introduction

The results of Sect. 4 indicate that significant improvements in current heat pump performance are possible through system optimization and the use of more efficient compressors, fans, and heat exchangers. However, as shown in Fig. 6.1, the wide gap between currently achieved efficiency and that calculated for the ideal cycle (a Carnot cycle between the given source and sink temperatures) is only partially bridged even by

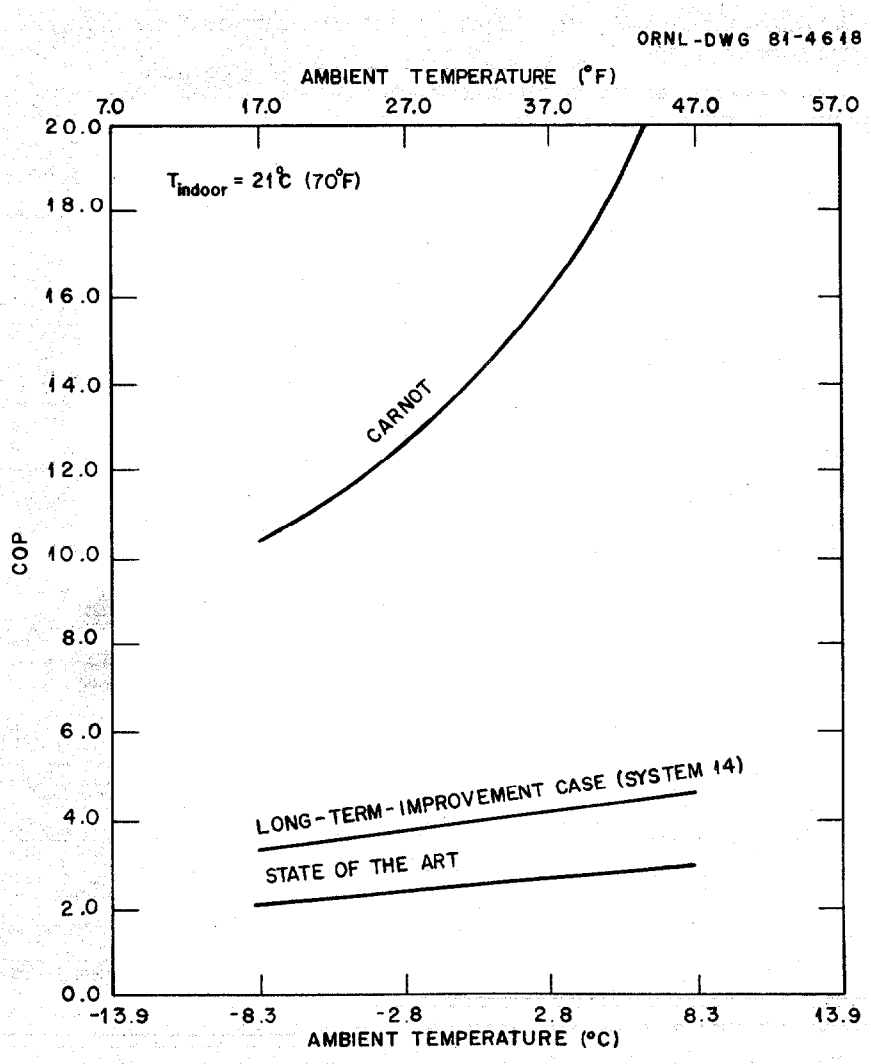


Fig. 6.1. SOA and long-term improved performance of conventional air-to-air heat pumps as compared to Carnot performance.

the long-term-improvement case. With the use of suitably modified ideal-cycle calculations, the remaining region was examined to see how the gap might be further reduced.

## 6.2 Limiting Factors

The inefficiencies of the conventional, single-speed, air-source heat pump can be separated, for purposes of discussion, into seven limiting factors:

1. inefficiencies inherent to the ideal conventional vapor-compression cycle,
2. the increase in heating capacity with ambient temperature, that is, the load-opposing nature of single-speed systems,
3. finite air flow rates,
4. finite heat exchanger size,
5. achievable overall compressor efficiencies ($\eta_{cm}$),
6. compressor shell heat loss, and
7. fan power requirements and overall fan inefficiencies.

## 6.3 Qualitative Effects

Factor 1 refers to the throttling losses and losses due to superheat of the compressor discharge gas; both are inherent irreversibilities of the vapor compression cycle.

Factors 2 and 3, when considered together, determine the magnitude of the air temperature changes ($\Delta T$'s) across the heat exchangers. Larger air $\Delta T$'s widen the effective source-to-sink temperature difference (and thus the pressure ratio) seen by the compressor and thereby increase the compressor power consumption. Similarly, the combination of factors 2 and 4 determines the magnitude of the refrigerant-to-air approach $\Delta T$'s for each heat exchanger. These additional $\Delta T$'s further widen the effective source-to-sink temperature difference and result in a further increase in compressor power consumption. At temperatures above the system balance point, the air and refrigerant-to-air $\Delta T$'s are larger than necessary for a given heat exchanger size since the heat pump

output exceeds the house requirements. Below the balance point, the heat exchangers are less heavily loaded (have smaller $\Delta T$'s) due to the reduced heating capacity; this unloading provides a closer approach to ideal performance for the heat pump alone, but poorer *system* performance because the reduced heat pump capacity must be supplemented with resistance heat.

The theoretical compressor power consumption determined by factors 1-4 is further increased by the reciprocal of factor 5 — the overall compressor efficiency. Additional losses result when part of the required compressor power is lost from the compressor shell rather than given to the refrigerant — factor 6.

Finally, forced movement of air through the heat exchangers and the indoor duct system requires parasitic power for the fans; the ideal fan power requirements are significantly increased above the ideal due to fan and fan motor inefficiencies.

## 6.4 Quantitative Effects

In Fig. 6.2., the successive effects of the various departures from Carnot efficiency are shown for the long-term improvement case. It should be noted that the width of the regions between successive curves (and thus the effect of a specific factor on percent COP reductions) depends to some extent on the order in which the factors are included. Thus Fig. 6.2 should not be used to form a ranking of the losses due to various factors; an analysis based on the second law of thermodynamics should be used to rank such factors.[16,17] The quantitative information to be gained from Fig. 6.2 is rather the levels of efficiency that could be obtained if the losses due to specific factors were somehow reduced.

Curve A in Fig. 6.2 represents the optimized results for the long-term improvement case as given earlier in Sect. 4. For curve B, the heat lost from the compressor shell has been added to the condenser output. In calculating curve C, the fan power requirements were set to zero. The heat exchanger size is effectively infinite in Curve D, that is, zero refrigerant to air $\Delta T$'s were assumed. The efficiency rises to the values shown by curve E if the air $\Delta T$'s are also reduced to zero (effectively

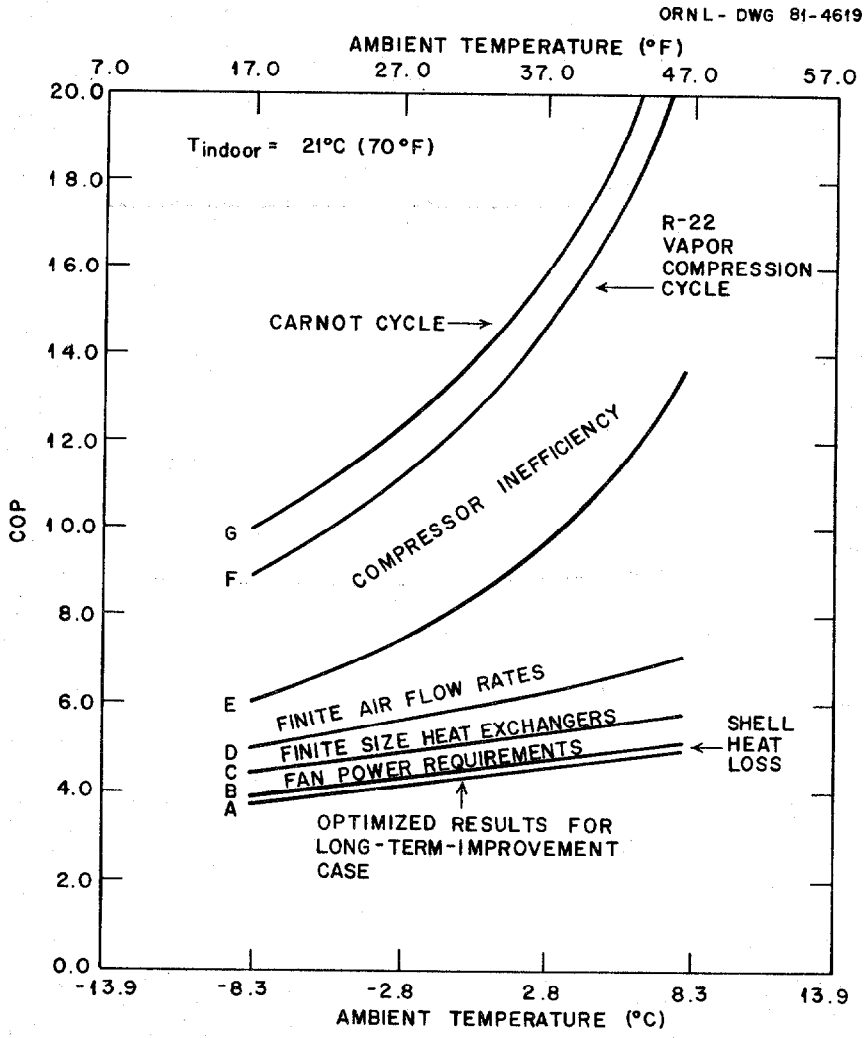


Fig. 6.2. Comparison of optimized results for long-term improvement with various levels of ideal performance.

requiring infinite flow rates for air). Curves F and G represent the efficiencies of the ideal R-22 vapor compression cycle and the Carnot cycle, respectively.

For the assumed overall compressor efficiency of 64%, curve E represents the limiting performance of R-22 vapor-compression cycles. The region between curves A and E represents the maximum range of improvement possible for R-22 vapor-compression cycles for a given compressor efficiency. The following section presents some possible means for narrowing this gap.

## 6.5 Further Improvements to Conventional Air-Source Heat Pump Systems

Improvements to air-source heat pump design beyond that suggested by the optimization study might include means for further reducing fan power consumption and compressor shell heat losses as well as further increases in heat exchanger area (or efficiency) and air flow rates. The limitations of such improvements are briefly examined.

*Fan power consumption.* As discussed in Appendix B, the values of outdoor fan power resulting from the system optimizations are below 100 W. Thus any further reduction in outdoor fan power would have a minimal effect on heat pump performance. Reductions in indoor fan power consumption through better design of ducts, filters, and the indoor cabinet (resulting in lower pressure drops) could yield some further improvement in heat pump COP, but possibly at the expense of good air distribution throughout the house.

*Compressor shell heat losses.* Thermal insulation of the shell could be beneficial if high suction-gas superheat can be avoided; excessive discharge temperatures and a requirement for larger compressor size could otherwise result. Placement of the compressor in the warmer indoor air is beneficial in the heating season, but detrimental when cooling is required. A more attractive alternative, routing of the heat lost from the compressor shell directly to the condenser in either mode, would overcome the objections to both of the other schemes.

*Further increases in heat exchanger area.* The regions between curves C and D in Figs. 6.2 and 6.3 (which shows the same information as Fig. 6.2 but for the short-term improvement case) are indicative of the gains in COP due to increases from finite to infinite heat exchanger areas. Region C-D in Fig. 6.2 is only about 25% narrower than that in Fig. 6.3 although curve C in the former is for 0.84 $m^2/kW$, twice as big as the 0.42 $m^2/kW$ represented in the latter. Thus further increases in heat exchanger area (and even the increase from 0.42 to 0.84 $m^2/kW$) are seen to be subject to rapidly diminishing returns. Also, the use of larger heat exchangers makes control of the refrigerant charge inventory more difficult; such control is important for compressor protection against refrigerant slugging.

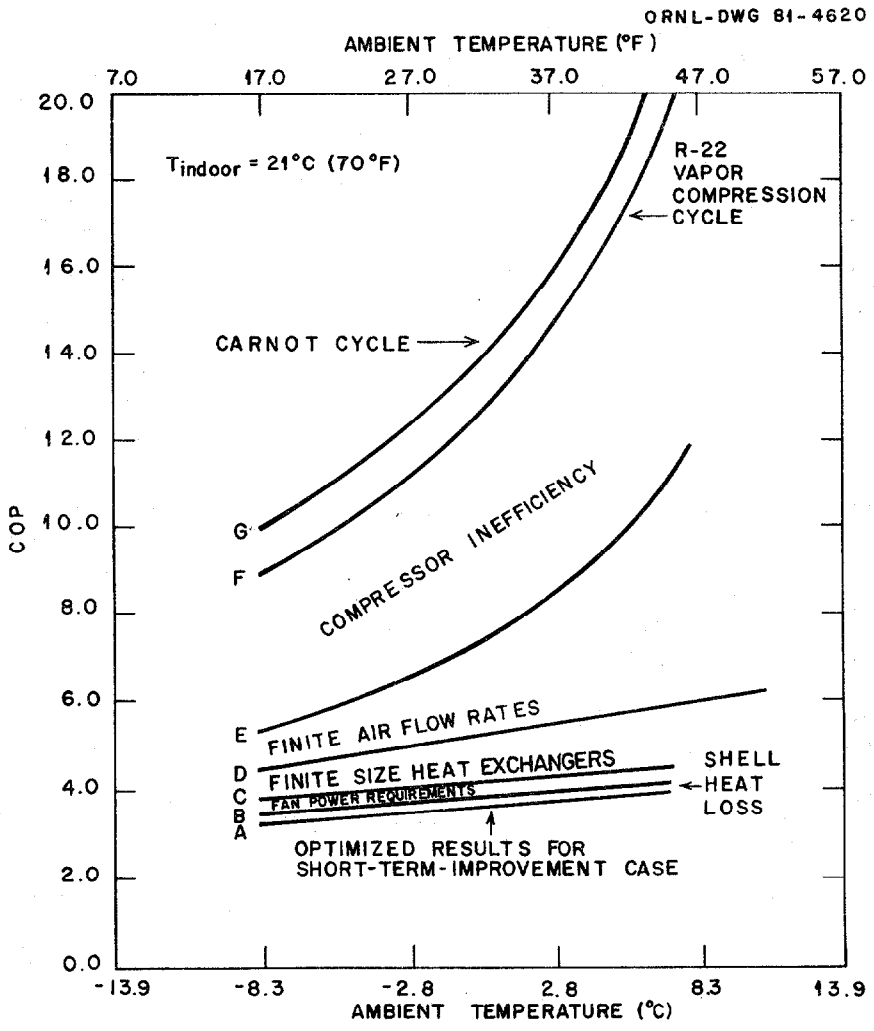


Fig. 6.3. Comparison of optimized results for short-term improvement with various levels of ideal performance.

*Further increases in air flow rates.* Increases in the air flow rates from those found by the optimizer would probably result in excessive noise production and unacceptably low indoor air supply temperatures.

## 6.6 Improvements Through System Concept Modifications

More promising approaches to higher COPs in air-source heat pumps than those predicted by the optimizer for conventional systems involve modified heat pump concepts. Three promising concepts are:

- capacity modulation
- multi-stage vapor compression
- use of nonazeotropic refrigerant mixtures.

All three concepts would serve to narrow the regions C-D and D-E in Figs. 6.2 and 6.3, the regions associated with losses due to the use of finite heat exchanger areas and air flow rates.

*Capacity modulation.* Conventional single-speed heat pumps have higher heating capacity (and consequently higher heat exchanger loading) than necessary at the warmer ambient temperatures of the heating range. Capacity modulation that allows the heat pump output to match the heating load more closely would reduce the heat exchanger loading at high ambients and thus provide enhanced efficiency at those temperatures. Some modulation schemes would also allow a reduction in the system balance point for heating mode as compared to the single-speed system. These systems would have greater low-temperature capacity but would experience higher heat exchanger loading than the single-speed heat pumps; the resulting decrease in *heat pump* efficiency would, however, be more than offset from the *system* viewpoint by reduced use of supplemental resistance heating. Losses due to on-off cycling would be reduced at all ambient temperatures above the system balance point of the comparable single-speed case. It is not clear, at this time, how net frosting-defrosting losses would be affected by capacity modulation since on-off cycling in single-speed systems results in some "natural" defrosting.

*Multi-stage vapor-compression.* These systems employ parallel compressors and refrigerant circuiting but have the heat exchangers arranged so that the air flows serially through them. Stoever,[18] Sandfort,[19] and Threlkeld[20] have described such two-stage vapor-compression cycles. The basic idea does not involve capacity modulation but rather allows one compressor system to operate at reduced pressure ratios while the other system operates at the usual conditions. This concept could, however, be combined with capacity modulation by using two different compressor sizes to achieve three discrete capacity choices. In such a system, the benefit of heat exchanger staging would be to boost the COP at low ambients in the heating mode and at high ambients in the cooling mode. In a nonmodulating system, the two parallel compressors would always run simultaneously and the staging benefits would apply to all ambient conditions.

*Nonazeotropic refrigerant mixtures.* Refrigerant mixtures could be used in otherwise conventional (single-stage, single-speed) heat pump designs.[21-23] They would take advantage of the resultant nonisothermal condensation and evaporation and should thereby reduce compressor power and size requirements. The use of one or more receivers in the refrigerant circuit to alter the active mixture composition could also result in some capacity modulation to assist or replace other capacity modulation schemes.[24-26]

Alternative heat pump concepts offer possibilities for efficiency improvement beyond that predicted in this study for the single-speed conventional heat pump. A future report is planned that will explore these possibilities for heat pumps employing continuous capacity modulation.

## REFERENCES


1. R. D. Ellison and F. A. Creswick, *A Computer Simulation of Steady-State Performance of Air-to-Air Heat Pumps*, ORNL/CON-16 (March 1978).

2. R. Cohen, "Research at the Ray W. Herrick Laboratories Related to Heat Pumps and Space Conditioning Systems," p. 20 in *Heat Pump and Space Conditioning Systems for the 1990's*, Proceedings of an International Symposium sponsored by Carrier Research Division, February 1979.

3. Air-Conditioning and Refrigeration Institute, *Standard for Air-Source Unitary Heat Pump Equipment*, ARI 240-77 (1977).

4. H. S. Kirschbaum and S. E. Veyo, *An Investigation of Methods to Improve Heat Pump Performance and Reliability in a Northern Climate*, Vols. I-III, Electric Power Research Institute, EPRI EM-319 (January 1977).

5. C. J. Blundell, "Optimizing Heat Exchangers for Air-to-Air Space-Heating Heat Pumps in the United Kingdom," *Energy Res.* I, 69-94 (1977).

6. R. W. Shaffer and W. D. Lee, "Energy Consumption in Hermetic Refrigerator Compressors," *Proceedings of the 1976 Purdue Compressor Technology Conference*, Ray W. Herrick Laboratories, West Lafayette, Indiana, July 6-9, 1976.

7. F. C. McQuiston and J. D. Parker, *Heating, Ventilating, and Air Conditioning Analysis and Design*, pp. 529-34, Wiley, New York, 1977.

8. C. C. Hiller and L. R. Glicksman, *Improving Heat Pump Performance via Compressor Capacity Control — Analysis and Test*, Report No. 24525-96, Heat Transfer Laboratory, Massachusetts Institute of Technology (1976).

9. R. D. Ellison et al., "Heat Pump Modeling: A Progress Report," *Proceedings of the Fourth Annual Heat Pump Technology Conference*, Oklahoma State University, Stillwater, Apr. 9-10, 1979.

10. H. S. Kirschbaum et al., op cit, Vol. III, p. B1-8.

11. A. A. Domingorena, *Performance Evaluation of a Low-First-Cost, Three-Ton, Air-to-Air Heat Pump in the Heating Mode,* ORNL/CON-18 (October 1978).

12. Air Conditioning and Refrigeration Institute, *Standard for Positive Displacement Refrigerant Compressors, Compressor Units and Condensing Units,* ARI 520-78 (1978).

13. Numerical Algorithms Group, *NAG Fortran Library, Mark 7,* Atomic Energy Establishment, Harwell, England, 1978.

14. W. F. Stoecker, *Design of Thermal Systems,* pp. 126-27, McGraw-Hill, New York, 1971.

15. H. S. Kirschbaum et al., op cit, Vol. I, p. 2.2-76.

16. R. Swers et al., "Thermodynamic Analysis of Compression Refrigeration Systems," *ASHRAE Trans.* 78(1), 143-52 (1972).

17. G. M. Reistad, "Availability Analysis of the Heating Process and a Heat-Pump System," *ASHRAE Symposium Bulletin,* LO-73-4 (1973).

18. H. J. Stoever, "Improved Inverted Refrigeration Cycle for Summer and Winter Air Conditioning," *Heat./Piping/Air Cond.* 4, 412-15 (June 1932).

19. J. F. Sandfort, "Standards of Performance for Heat Pump Cycles," *Midwest Power Conference — Proceedings,* Vol. 12, pp. 371-78 (1950).

20. J. L. Threlkeld, "A Thermodynamic Study of Vapor-Compression Heat Pump Cycles," *Refrig. Eng.* 61 (11), 1202-06ff (November 1953).

21. H. Kruse and R. Jakobs, "The Significance of the Non-azeotropic Binary Refrigerants When Used in Heat Pumps and Refrigeration Plants," *Klima-Kälte Ing.* 5(7-8), 253-60 (July-August 1977).

22. W. F. Stoecker, *Improving the Energy Effectiveness of Domestic Refrigerators by the Application of Refrigerant Mixtures,* ORNL/Sub-78/55463/1 (1978).

23. H. S. Kirschbaum et al., op cit, Vol. I, p. 2.2-108.

24. H. S. Kirschbaum et al., op cit, Vol. III, pp. B3-18.

25. W. D. Cooper and H. J. Borchardt, "The Use of Refrigerant Mixtures in Air-to-Air Heat Pumps," *XV International Congress of Refrigeration*, Venice, Italy, Paper E1-60 (September 1979).

26. H. B. Vakil, *Vapor Compression Cycle Device with Multi-Component Working Fluid Mixture and Method of Modulating Its Capacity*, General Electric Company, Schenectady, New York, U.S. Patent No. 4,179,898 (July 31, 1978).

# Appendix A

## A CAPACITY SCALING PROCEDURE

It was noted in Sect. 3.2.3 that for properly formulated system constraints, the optimum COPs for improved systems are independent of heating capacity. The form chosen in that section for capacity-related constraints is consistent with the scaling procedure described below, which was chosen as a compromise between simplicity and practicality. This discussion is to illustrate the concept rather than to recommend a specific scheme for all capacity ranges. Other scaling procedures can be used with the system configurations listed in Sect. 4.1 but new capacity-related constraints consistent with the procedure must be defined.

### A.1 Requirements for Capacity Scaling

The basic requirements for capacity scaling can be shown by reference to the COP equation for heating applications; that is,

$$COP = \frac{\dot{Q}_c + \dot{W}_{cf}}{\dot{W}_{cm} + \dot{W}_{cf} + \dot{W}_{ef}} , \qquad (A.1)$$

where $\dot{Q}$ and $\dot{W}$ denote heat transfer and work rates and the subscripts are defined as

c = condenser
cf = condenser (indoor) fan
cm = compressor
ef = evaporator (outdoor) fan

The heating capacity $\dot{Q}_H$ is given by the sum of $\dot{Q}_c$ and $\dot{W}_{cf}$. To maintain a constant COP for different values of $\dot{Q}_H$, the numerator and denominator in Eq. (A.1) must change by the same proportion.

## A.2 Expansion of the Terms in Eq. (A.1)

To show how system parameters can be changed to maintain a constant ratio of heat output to work input as heat output is varied, each component of Eq. (A.1) can be expanded as follows (as modeled in the ORNL Heat Pump Model):

*Numerator.* First, total heat output is given by

$$\dot{Q}_H = \dot{Q}_c + \dot{W}_{cf} = [\dot{Q}_a \rho_a c_{pa} \Delta T_a]_c \ , \qquad \text{(A.2)}$$

($[\dot{Q}_a \rho_a c_{pa} \Delta T_a]_c$: air-side energy gain)

where the condenser capacity, $\dot{Q}_c$, is

$$\dot{Q}_c = \dot{m}_r [\Delta h_r]_c = \sum_{i=1}^{3} [\varepsilon_i (C_{min})_i (T_{max} - T_{min})_i]_c \qquad \text{(A.3)}$$

($\dot{m}_r [\Delta h_r]_c$: refrigerant-side energy loss; $[\varepsilon_i (C_{min})_i (T_{max} - T_{min})_i]_c$: refrigerant-to-air heat transfer)

and the condenser fan power, $\dot{W}_{cf}$, is

$$\dot{W}_{cf} = \dot{Q}_{ac} \cdot [B_1 (\dot{Q}_a)^{B_2} + B_3 (\dot{Q}_a)^{B_4} + B_5 (\dot{Q}_a / A_f)^{B_6} (NR)^{B_7}]_c / \eta_{cf} \ . \qquad \text{(A.4)}$$

($B_1 (\dot{Q}_a)^{B_2}$: duct system $\Delta P$; $B_3 (\dot{Q}_a)^{B_4}$: cabinet and filter $\Delta P$; $B_5 (\dot{Q}_a / A_f)^{B_6} (NR)^{B_7}$: indoor coil $\Delta P$)

*Denominator.* Compressor power can be written as

$$\dot{W}_{cm} = \dot{m}_r [\Delta h_{r,isen}]_{cm} / \eta_{cm} = \dot{Q}_c - \dot{Q}_e + B_6 \dot{W}_{cm} \ , \qquad \text{(A.5)}$$

($\dot{m}_r [\Delta h_{r,isen}]_{cm} / \eta_{cm}$: compressor power input; $\dot{Q}_c - \dot{Q}_e$: energy gained by refrigerant; $B_6 \dot{W}_{cm}$: shell heat loss)

where the evaporator capacity, $\dot{Q}_e$, is

$$\dot{Q}_e = \dot{m}_r[\Delta h_r]_e = \sum_{i=1}^{2} [\varepsilon_i (C_{min})_i (T_{max} - T_{min})_i]_e \qquad (A.6)$$

refrigerant-side energy gain; air-to-refrigerant heat transfer

$$= [\dot{Q}_a \rho_a c_{pa} \Delta T_a]_e \ .$$

air-side energy loss

The last work input term is the evaporator fan power; that is,

$$\dot{W}_{ef} = \dot{Q}_{ae}[B_8(\dot{Q}_a/A_f)^{B_9} \cdot (NR)^{B_{10}}]_e/\eta_{ef} \ . \qquad (A.7)$$

outdoor coil and cabinet $\Delta P$

The notation is as follows:

- $\dot{Q}$ = volumetric air-flow rate,
- $\rho$ = density,
- $\dot{m}$ = mass flow rate,
- $c_p$ = specific heat at constant pressure,
- $C_{min}$ = minimum capacity rate ($\dot{m} \cdot c_p$) of the two flow streams — refrigerant or air,
- $\varepsilon$ = heat exchanger effectiveness,
- $\eta$ = component efficiency — compressor or fan,
- $\Delta T$ = temperature change,
- $\Delta P$ = pressure drop,
- $\Delta h$ = specific enthalpy change,
- $A_f$ = frontal area, and
- NR = number of tube rows.

The subscripts not earlier defined are

- r = refrigerant,
- a = air,
- e = evaporator,
- i = index that denotes heat exchanger regions in which the refrigerant state is superheated, two-phase, or subcooled when i = 1, 2, or 3, respectively,

isen = isentropic (constant entropy) process from compressor shell inlet to outlet,

max = maximum temperature of refrigerant or air, and

min = minimum temperature of refrigerant or air.

The terms $B_1$ through $B_{10}$ are constants.

*Thermodynamic States and Thermophysical Properties.* In general, when nominal capacity is scaled, the thermodynamic states of the refrigerant and the two air streams are held constant. Under these conditions, all $\Delta h$, $\Delta T$, $(T_{max} - T_{min})_i$ and $\rho$ values must remain constant along with refrigerant and air-side pressure drops. The thermophysical properties, such as $c_p$, are also invariant.

With these terms fixed in Eqs. (A.2) through (A.7), the remaining system parameters must be handled in such a manner as to maintain constant COP through Eq. (A.1) without violating any of the preceding assumptions.

## A.3 Scaling Method

As noted earlier in this appendix, there are a number of ways to accomplish scaling. A scaling method follows which is compatible with the choice of constraints made in Sect. 3.

Seven of the ten optimization parameters can be scaled linearly with heating capacity.

These are the compressor displacement and, for each heat exchanger, frontal area ($A_f$), volumetric air-flow rate ($\dot{Q}_a$), and number of refrigerant circuits. Thus the optimum values of these seven parameters in Table 4.1 can be divided by the chosen nominal capacity and expressed on the basis of per unit nominal capacity similar to the way the capacity-related constraints were handled in Sect. 3.2.3.

The remaining three optimization parameters, condenser subcooling and number of tube rows (NR) in each heat exchanger, are held fixed during scaling.

By scaling frontal areas and air flow rates in the same way, the air velocity across the heat exchangers remains constant. With fixed

heat exchanger geometry, this results in constant air-side heat transfer coefficients and coil pressure drops. If simultaneously on the refrigerant side the number of circuits and the refrigerant flow rate (through compressor displacement) are scaled proportionally, the refrigerant velocity in each channel and thus the refrigerant-side heat transfer coefficients and pressure drops remain constant. Note that the total number of return bends is required to vary linearly along with the changes in area and number of circuits (as noted in the constraint formulations in Sect. 3.2.3) to maintain a constant number of return bends per circuit. With this requirement, a doubling of the heating capacity would require a doubling of the height of the heat exchanger. Alternatively, to maintain a coil of constant aspect ratio, the number of refrigerant circuits and/or the diameter of the heat exchanger tubes would have to be scaled nonlinearly with capacity.

By varying air and refrigerant flow rates by the same proportion, the energy balances from the air to the refrigerant [Eqs. (A.2), (A.3), and (A.5)] can be maintained provided the $\varepsilon$ values remain fixed. Since $\varepsilon = F(C_{min}/C_{max}, UA/C_{min})$ and since U (the overall heat transfer conductance), $C_{min}/C_{max}$, and $A/C_{min}$ values are constant, the $\varepsilon$'s remain constant as the capacity size is scaled.

As the evaporator and condenser heat flow rates are scaled, Eq. (A.5) shows that the compressor input power changes proportionally. Equation (A.7) shows that the evaporator fan power, $W_{ef}$, increases in proportion to $\dot{Q}_{ae}$ since $NR_e$ and $(\dot{Q}_a/A_f)_e$ are held constant. In a similar fashion, the indoor coil component of $\dot{W}_{cf}$ [Eq. (A.4)] varies in proportion to $\dot{Q}_{ac}$. For the remaining components of Eq. (A.4), if the cross-sectional area of ducts, cabinet, and filter are scaled linearly, their contributions to $\dot{W}_{cf}$ will vary approximately in proportion to $\dot{Q}_{ac}$. This approximation is adequate for scaling the configurations given in Table 4.1 to other capacity sizes typical of residential application.

Finally, the refrigerant pressure drops in the interconnecting refrigerant lines can be held approximately constant by linear scaling of the internal cross-sectional areas.

## Appendix B

## DETAILED SYSTEM OPERATING CONDITIONS

In Table 4.1, the system configurations and overall performance results were given for 14 systems. In Tables B.1, B.2, and B.3, further computed system operating conditions are provided. These data were extracted from the output of heat pump model runs at 8.3°C (47°F) and -8.3°C (17°F) ambients.

In Table B.1, compressor, fan, and refrigerant data are given for the 8.3°C ambient condition. The headings $\eta_{vol}$ and $\dot{m}_r$ refer to volumetric efficiency (based on compressor shell inlet conditions) and refrigerant mass flow rate, respectively. These two quantities are related by the equation

$$\dot{m}_r = \eta_{vol} \cdot \rho_{shell\ inlet} \cdot N \cdot D \ , \qquad (B.1)$$

where

$\rho_{shell\ inlet}$ = refrigerant density at compressor shell inlet,

N = motor speed,

D = compressor displacement.

The actual overall compressor efficiency $\eta_{cm}$, as given in Table B.1, is lower than $\eta_{cm(max)}$ by the fraction $\eta_{super}$ [from Eq. (3.5)] since at the 8.3°C ambient, $\eta_{motor}/\eta_{motor(max)}$ has been assumed equal to unity.

The values of $\eta_{vol}$, $\dot{m}_r$, and $\eta_{cm}$ given in Table B.1 can be used in conjunction with the values of compressor displacement given in Table 4.1 to make compressor substitutions. For compressors that have equivalent values of $\eta_{cm}$ and shell heat loss, $\dot{Q}$ shell, but differing values of $\eta_{vol}$, the required displacement given in Table 4.1 can be adjusted to maintain the same refrigerant flow rate. Such substitutions can be made without affecting the calculated values of COP or heating capacity. Thus, compressors that have different amounts of suction gas heat transfer inside the compressor shell and/or different values of effective clearance volume ratio from the values assumed in this study will require different values

Table B.1. Additional operating conditions for the base case and optimized systems at 8.3°C (47°F) ambient[a]

| System No. | System identification[b] | | | | Compressor[c] (Motor speed = 3450 rpm) | | | | | Fan power | | R-22 temperatures[d] | | | | | R-22 pressure drop[e] | |
|---|---|---|---|---|---|---|---|---|---|---|---|---|---|---|---|---|---|---|
| | $A_{tot}$ ($ft^2/ton_{nom}$) | $\eta_{cm}$ (max) | Overall fan η's | | $\eta_{cm}$ | $\eta_{vol}$ | $\dot{m}_r$ | Shell heat loss | Motor input power | | | Cond. in | Sat., cond. in | Cond. out | Sat., evap. out | Suction port | | |
| | | | Cond. | Evap. | | | | | | Cond. | Evap. | | | | | | Cond. | Evap. |
| | | (%) | | | (%) | | (lbm/h) | (Btu/h) | | (Btu/h) | | (°F) | | | | | (psi) | |
| | | | | | | | | Base case | | | | | | | | | | |
| 1 | 8 | 48 | 17 | 14 | 46.2 | 64.3 | 363.2 | 3234 | 14380 | 1171 | 1281 | 254.7 | 130.1 | 79.6 | 25.9 | 59.0 | 2.07 | 7.17 |
| | | | | | | | | Limited optimizations with base case heat exchangers | | | | | | | | | | |
| 2 | 8 | 48 | 17 | 14 | 46.8 | 75.5 | 405.6 | 2651 | 11780 | 2685 | 613 | 189.2 | 105.7 | 95.1 | 27.0 | 39.6 | 4.70 | 9.36 |
| 3 | 8 | 48 | 34 | 28 | 46.8 | 76.3 | 413.7 | 2643 | 11750 | 1739 | 439 | 189.3 | 104.5 | 93.9 | 27.5 | 39.9 | 4.93 | 9.58 |
| | | | | | | | | Full optimizations | | | | | | | | | | |
| 4 | 8 | 48 | 17 | 14 | 46.9 | 76.5 | 395.7 | 2510 | 11160 | 2185 | 362 | 185.5 | 104.3 | 81.9 | 27.7 | 40.0 | 18.4 | 2.37 |
| 5 | 8 | 48 | 34 | 28 | 46.8 | 76.9 | 397.7 | 2495 | 11090 | 1491 | 212 | 183.7 | 103.2 | 78.9 | 27.6 | 39.8 | 18.2 | 2.37 |
| 6 | 8 | 56 | 17 | 14 | 54.8 | 75.0 | 403.0 | 1809 | 10050 | 1800 | 293 | 179.5 | 106.4 | 82.1 | 27.0 | 37.5 | 18.4 | 2.47 |
| 7 | 8 | 56 | 34 | 28 | 54.8 | 76.3 | 415.1 | 1792 | 9957 | 1310 | 245 | 174.6 | 103.9 | 82.8 | 27.7 | 37.9 | 20.6 | 2.58 |
| 8 | 8 | 64 | 34 | 28 | 62.9 | 75.1 | 422.8 | 1608 | 8933 | 1245 | 442 | 164.2 | 105.5 | 80.0 | 28.2 | 37.6 | 20.5 | 2.62 |
| 9 | 16 | 48 | 34 | 28 | 47.0 | 81.7 | 407.9 | 2129 | 9464 | 1317 | 237 | 165.2 | 97.3 | 77.3 | 33.6 | 44.1 | 13.6 | 2.78 |
| 10 | 16 | 56 | 34 | 28 | 54.9 | 80.1 | 431.0 | 1626 | 9033 | 903 | 177 | 161.9 | 99.5 | 84.2 | 32.2 | 41.4 | 7.01 | 2.97 |
| 11 | 16 | 64 | 34 | 28 | 63.2 | 79.7 | 441.5 | 1444 | 8020 | 1000 | 123 | 149.9 | 98.6 | 85.0 | 31.9 | 40.4 | 7.28 | 3.35 |
| 12 | 32 | 48 | 34 | 28 | 47.2 | 84.8 | 423.0 | 1899 | 8438 | 1409 | 278 | 152.7 | 93.6 | 75.7 | 38.2 | 47.6 | 7.65 | 3.61 |
| 13 | 32 | 56 | 34 | 28 | 55.3 | 83.8 | 426.4 | 1369 | 7603 | 996 | 177 | 149.2 | 95.4 | 79.4 | 37.4 | 45.6 | 7.79 | 3.59 |
| 14 | 32 | 64 | 34 | 28 | 63.2 | 82.8 | 435.4 | 1252 | 6957 | 989 | 169 | 141.6 | 95.9 | 76.8 | 36.6 | 44.3 | 5.11 | 3.53 |

[a] $T_{amb}$ = 8.3°C (47°F); ambient relative humidity = 70%; $T_{indoor}$ = 21°C (70°F).

[b] To convert from $ft^2/ton_{nom}$ to $m^2/kW_{nom}$, multiply by 0.0264.

[c] To convert from lbm/h to g/s, multiply by 0.126; from Btu/h to W, multiply by 0.293.

[d] $T_{°C} = (T_{°F} - 32)/1.8$.

[e] To convert from psi to kPa, multiply by 6.89.

Table B.2. Additional operating conditions for the base case and optimized systems at -8.3°C (17°F) ambient[a]

| System No. | Compressor[b] | | | | | | | R-22 temperatures[c] | | | | | R-22 pressure drop[d] | |
|---|---|---|---|---|---|---|---|---|---|---|---|---|---|---|
| | $\eta_{cm}$ | $\eta_{motor}$ | $\eta_{vol}$ | Motor speed (rpm) | $\dot{m}_r$ (lbm/h) | Shell heat loss | Input power | Cond. in | Sat., cond. in | Cond. out | Sat., evap. out | Suction port | Cond. | Evap. |
| | (%) | | | | | (Btu/h) | | (°F) | | | | | (psi) | |
| 1 | 45.2 | 77.8 | 60.0 | 3494 | 239.5 | 2359 | 10034 | 227.1 | 107.8 | 77.3 | 4.36 | 22.2 | 1.38 | 5.02 |
| 2 | 45.9 | 78.1 | 66.3 | 3488 | 231.6 | 1993 | 8583 | 202.8 | 94.4 | 84.7 | 3.38 | 19.5 | 1.88 | 4.90 |
| 3 | 45.9 | 78.2 | 67.1 | 3490 | 237.2 | 2006 | 8660 | 200.7 | 93.7 | 84.1 | 3.98 | 19.9 | 1.97 | 5.05 |
| 4 | 46.0 | 78.2 | 67.6 | 3486 | 228.3 | 1903 | 8212 | 198.1 | 92.4 | 73.7 | 4.03 | 20.9 | 7.14 | 1.26 |
| 5 | 46.0 | 78.2 | 67.7 | 3489 | 229.8 | 1905 | 8241 | 197.9 | 92.5 | 72.0 | 4.26 | 21.4 | 6.75 | 1.26 |
| 6 | 53.9 | 83.3 | 65.4 | 3489 | 231.5 | 1366 | 7261 | 187.1 | 94.0 | 73.3 | 3.51 | 20.4 | 7.02 | 1.30 |
| 7 | 54.0 | 83.4 | 67.0 | 3487 | 240.3 | 1367 | 7295 | 182.5 | 91.8 | 74.7 | 4.18 | 21.2 | 8.16 | 1.38 |
| 8 | 62.0 | 83.4 | 64.1 | 3490 | 242.3 | 1232 | 6586 | 170.5 | 94.3 | 72.5 | 4.04 | 21.0 | 7.55 | 1.39 |
| 9 | 46.3 | 78.5 | 72.4 | 3482 | 234.1 | 1698 | 7418 | 182.2 | 88.1 | 71.0 | 8.87 | 26.0 | 4.88 | 1.48 |
| 10 | 54.4 | 83.6 | 71.4 | 3485 | 248.9 | 1279 | 6906 | 172.5 | 89.1 | 74.9 | 7.82 | 19.7 | 2.76 | 1.58 |
| 11 | 62.3 | 83.6 | 69.5 | 3486 | 253.6 | 1134 | 6119 | 157.0 | 88.4 | 76.2 | 7.64 | 24.7 | 2.87 | 1.77 |
| 12 | 46.4 | 78.7 | 75.4 | 3476 | 235.1 | 1578 | 6947 | 174.3 | 86.4 | 70.3 | 11.7 | 24.8 | 2.37 | 1.87 |
| 13 | 54.6 | 83.8 | 75.0 | 3480 | 239.6 | 1111 | 6057 | 162.5 | 85.7 | 71.6 | 11.1 | 22.1 | 2.84 | 1.87 |
| 14 | 62.4 | 83.8 | 72.6 | 3481 | 241.2 | 1015 | 5532 | 153.7 | 88.5 | 70.4 | 10.7 | 21.0 | 1.54 | 1.80 |

[a] $T_{amb}$ = -8.3°C (17°F); ambient relative humidity = 70%; $T_{indoor}$ = 21°C (70°F).

[b] To convert from lbm/h to g/s, multiply by 0.126; from Btu/h to W, mulitply by 0.293.

[c] $T_{°C} = (T_{°F} - 32)/1.8$.

[d] To convert from psi to kPa, multiply by 6.89.

Table B.3. Heat exchanger performance data for selected systems[a]

| System No. | Evaporator | | | | | | | | | | | | |
|---|---|---|---|---|---|---|---|---|---|---|---|---|---|
| | Two-phase region | | | | | | Superheated region | | | | | | |
| | $\dot{Q}_f$ | F | $(UA)_{air}$ (Btu/h·°F) | $(UA)_{ref}$ (Btu/h·°F) | $(UA)_{tot}$ (Btu/h·°F) | ε | $\dot{Q}_f$ | F | $(UA)_{air}$ (Btu/h·°F) | $(UA)_{ref}$ (Btu/h·°F) | $(UA)_{tot}$ (Btu/h·°F) | ε | $\varepsilon_{tot}$ |
| 1 | 0.956 | 0.734 | 3250 | 6530 | 2170 | 0.680 | 0.044 | 0.266 | 1180 | 284 | 228 | 0.961 | 0.690 |
| 2 | 0.992 | 0.984 | 3830 | 10000 | 2770 | 0.760 | 0.008 | 0.016 | 61.6 | 18.7 | 14.4 | 0.341 | 0.753 |
| 4 | 0.992 | 0.974 | 2730 | 5580 | 1830 | 0.393 | 0.008 | 0.026 | 71.7 | 16.5 | 13.4 | 0.172 | 0.388 |
| 5 | 0.992 | 0.974 | 2810 | 5509 | 1862 | 0.380 | 0.008 | 0.026 | 75.2 | 16.9 | 13.8 | 0.176 | 0.377 |
| 7 | 0.992 | 0.974 | 2890 | 5789 | 1928 | 0.374 | 0.008 | 0.026 | 77.0 | 17.5 | 14.3 | 0.174 | 0.371 |
| 10 | 0.993 | 0.978 | 4400 | 9120 | 2970 | 0.429 | 0.007 | 0.022 | 97.4 | 23.8 | 19.1 | 0.213 | 0.426 |
| 14 | 0.993 | 0.979 | 7244 | 14270 | 4805 | 0.463 | 0.007 | 0.021 | 154 | 38.7 | 30.9 | 0.310 | 0.462 |

| Condenser | | | | | | | | | | | | | | | | | | |
|---|---|---|---|---|---|---|---|---|---|---|---|---|---|---|---|---|---|---|
| Superheated region | | | | | | Two-phase region | | | | | | Subcooled region | | | | | | |
| $\dot{Q}_f$ | F | $(UA)_{ref}$ (Btu/h·°F) | $(UA)_{air}$ (Btu/h·°F) | $(UA)_{tot}$ (Btu/h·°F) | ε | $\dot{Q}_f$ | F | $(UA)_{air}$ (Btu/h·°F) | $(UA)_{ref}$ (Btu/h·°F) | $(UA)_{tot}$ (Btu/h·°F) | ε | $\dot{Q}_f$ | F | $(UA)_{air}$ (Btu/h·°F) | $(UA)_{ref}$ (Btu/h·°F) | $(UA)_{tot}$ (Btu/h·°F) | ε | $\varepsilon_{tot}$ |
| 0.0 | 0.0 | | | | | 0.852 | 0.621 | 1520 | 2580 | 956 | 0.696 | 0.148 | 0.379 | 928 | 358 | 258 | 0.840 | 0.714 |
| 0.0 | 0.0 | | | | | 0.969 | 0.935 | 2620 | 4550 | 1660 | 0.643 | 0.031 | 0.065 | 182 | 66.0 | 48.4 | 0.303 | 0.622 |
| 0.065 | 0.028 | 89.2 | 56.5 | 34.6 | 0.456 | 0.883 | 0.852 | 2720 | 7480 | 1990 | 0.753 | 0.052 | 0.120 | 382 | 226 | 142 | 0.578 | 0.712 |
| 0.061 | 0.026 | 87.2 | 52.6 | 32.8 | 0.427 | 0.881 | 0.828 | 2778 | 7339 | 2015 | 0.730 | 0.052 | 0.146 | 488 | 275 | 176 | 0.670 | 0.696 |
| 0.046 | 0.021 | 69.0 | 44.2 | 26.9 | 0.456 | 0.908 | 0.875 | 2873 | 8019 | 2115 | 0.743 | 0.046 | 0.104 | 341 | 204 | 128 | 0.523 | 0.701 |
| 0.003 | 0.002 | 10.5 | 4.83 | 3.31 | 0.363 | 0.953 | 0.915 | 4820 | 10300 | 3280 | 0.891 | 0.044 | 0.083 | 437 | 188 | 132 | 0.477 | 0.855 |
| 0.0 | 0.0 | | | | | 0.941 | 0.884 | 7026 | 15830 | 4867 | 0.959 | 0.059 | 0.116 | 918 | 404 | 280 | 0.718 | 0.940 |

[a] $T_{amb}$ = 8.3°C (47°F); ambient relative humidity = 70%; $T_{indoor}$ = 21°C (70°F). To convert from Btu/h·°F to W/°C, multiply by 0.527.

of compressor displacement but will yield the same system COP's and capacities provided that $\eta_{cm}$ and $\dot{Q}_{shell}$ are the same.

The required motor shaft power as tabulated in Table 4.1 and discussed in Appendix C is related to the compressor-motor input power given in Table B.1 by

$$\text{motor shaft power} = \text{input power} \cdot \eta_{motor} , \qquad (B.2)$$

The next columns in Table B.1 are the condenser (indoor coil) and evaporator (outdoor coil) fan power consumptions.

Condenser fan power consumption increases from the base case values for all optimized systems that have the same indoor overall fan efficiency as the base case; this is because of the increase in indoor air flow rate for the optimized systems. The increase in the indoor air flow rate results in substantial reductions in compressor power which offsets the increases in indoor fan power. For the optimized systems at the higher levels of overall fan efficiency, the indoor air flow rates remain close to the levels for the optimized systems with the lower fan efficiencies; therefore, the indoor fan powers are reduced by about half from that of the other optimized systems due to the doubling of the overall fan efficiencies.

Evaporator fan power consumption is significantly smaller than that of the base case system for all of the fully optimized systems. This occurs because, for the outdoor unit, the total air-side pressure drop is directly proportional to the pressure drop across the outdoor coil (in contrast to the indoor unit where the coil pressure drop is only about 20% of the total pressure drop); with large-frontal-area, one-row outdoor coils, the air-side pressure drop is substantially reduced from the base case values even though the outdoor air flow rates are substantially higher. These outdoor configurations of high air flow rate and low static pressure drop result in fan specific speeds that are a factor of 2 to 3 higher than those currently available from single propeller or axial fans. The use of four to six fans of typical speed (820 rpm) in parallel or two or three fans of slower speed in parallel would be necessary to achieve the assumed overall fan efficiencies. However, both of these solutions

are likely to be impractical from other engineering considerations (such as proper air distribution over the coil and starting fan blades with such small motors) and with respect to costs. In this case, the optimum solution for fixed outdoor fan efficiency resulted in impractical fan requirements. Preliminary calculations suggest that with a two- or 3-row outdoor coil, proportionally smaller frontal areas, and a reduction in the outdoor air flow rates, the required fan specific speeds could be reduced to achieve the assumed overall fan efficiencies with one or two fans working against larger pressure drops. Outdoor fan power consumption should be on the order of 100 to 200 W depending upon the level of fan efficiency assumed. It is estimated that the effect of such a change in the outdoor configuration would reduce the value of optimum COP less than 5% for the short-term improvement case (system 10) and less than 10% for the long-term improvement case (system 14). In future studies, curves of static efficiency vs specific speed for propeller and axial fans should be built into the heat pump model; the optimum outdoor coil configuration will thus be constrained by specifying the fan requirements in more detail.

The remaining columns in Table B.1 are for the calculated refrigerant temperatures and pressure drops. Using this information, the refrigerant states at important points throughout the cycle can be studied.

In Table B.2, similar operating data are given for an ambient temperature of -8.3°C (17°F). Two new entries, $\eta_{motor}$ and motor speed, have been added and the fan powers have been deleted (since these are the same as in Table B.1). The values of $\eta_{motor}$ and motor speed are given for the -8.3°C ambient condition since these parameters are affected by the part-load performance of the compressor motor.

In both Tables B.1 and B.2, a major trend to note is the decrease in the difference between saturation temperatures in the evaporator and condenser as the total available heat exchanger area $A_{tot}$ is increased. This decrease results in smaller pressure ratios and thereby lower compressor power consumption.

Table B.3 is a continuation of Table B.1 in which detailed heat exchanger performance is tabulated for selected systems operating at the 8.3°C (47°F) ambient condition. The heading definitions are as follows:

$\dot{Q}_f$ = fraction of total $\dot{Q}$ transferred in a specific refrigerant region.

F = fraction of total heat exchanger area occupied by superheated, two-phase, or subcooled refrigerant regions.

(UA) = effective conductance, that is,

$$(UA)_{air} = h_{air} \cdot A_{air\text{-}side} \cdot \eta_s \cdot F \ , \tag{B.3}$$

where

$h_{air}$ = heat transfer coefficient on air-side,

$A_{air\text{-}side}$ = total surface area on air-side,*

$\eta_s$ = overall surface efficiency;

$$(UA)_{ref} = h_{ref} \cdot A_{ref\text{-}side} \cdot F \ , \tag{B.4}$$

where

$h_{ref}$ = heat transfer coefficient on refrigerant-side,

$A_{ref\text{-}side}$ = total surface area on refrigerant side;*

$$(UA)_{tot} = \left[\frac{1}{(UA)_{air}} + \frac{1}{(UA)_{ref}}\right]^{-1} . \tag{B.5}$$

$\varepsilon$ = heat exchanger effectiveness.

$\varepsilon_{tot}$ = overall heat exchanger effectiveness given by

$$\varepsilon_{tot} = \left[\left(\frac{Q_f}{\varepsilon}\right)_{\substack{\text{superheat}\\ \text{region}}} + \left(\frac{Q_f}{\varepsilon}\right)_{\substack{\text{two-phase}\\ \text{region}}} + \left(\frac{Q_f}{\varepsilon}\right)_{\substack{\text{subcooled}\\ \text{region}}}\right]^{-1} .$$

---

*For the heat exchanger geometry assumed in Sect. 3.2.1, the areas $A_{air\text{-}side}$ and $A_{ref\text{-}side}$ are related to the frontal areas and numbers of tube rows in Table 4.1 by

$$A_{air\text{-}side} = 22.1 \cdot \text{frontal area} \cdot \text{number of tube rows}, \tag{B.6}$$

$$A_{ref\text{-}side} = 1.06 \cdot \text{frontal area} \cdot \text{number of tube rows}, \tag{B.7}$$

Equations (B.3) through (B.7) can be used to compare the (UA) results given in Table B.3 with values obtained for a different heat exchanger of equal total available surface area ($A_{air\text{-}side}$). The tube wall resistance has been assumed negligible.

For the superheated refrigerant region in the condenser, all of the cases considered in Table B.3 have smaller $\dot{Q}_f$ values than would be expected from the superheat content of the entering refrigerant (from Table B.1). This occurs because, in the model, the superheat region is defined to be only where the tube wall temperature is above the saturation temperature. When the wall temperature is below saturation, condensation occurs at the wall even though the bulk of the refrigerant is still superheated. Thus, the part of, the superheat energy transfer where condensation is occuring at the wall is included as part of the two-phase region.

The tabulated results in Table B.3 show the following trends:

1. In the two-phase regions, $(UA)_{air}$ is typically about 50% of $(UA)_{ref}$.
2. In the single-phase regions, $(UA)_{air}$ is three to five times larger than $(UA)_{ref}$.
3. For optimized systems with larger heat exchangers, $(UA)_{tot}$ in the two-phase regions (the dominant region in each heat exchanger) has increased. However, the values of $\varepsilon_{tot}$ do not necessarily follow this trend; in fact, the values of $\varepsilon_{tot}$ for the larger evaporators (in systems 10 and 14) are lower than $\varepsilon_{tot}$ for systems 1 and 2. This indicates that heat exchanger effectiveness alone is not a good measure of better system design.

Appendix C

## ANALYSIS OF COMPRESSOR MOTOR REQUIREMENTS

In the optimization procedure described in Sect. 3, the assumption was made that the compressor motor would operate at nominal "rated" load (i.e., rated torque) when the heat pump was operating at an 8.3°C (47°F) ambient temperature. Typical curves of motor efficiency and speed vs percent rated load* (as shown in Fig. C.1) were then used to compute motor performance at "part-load" conditions, that is, for ambient temperatures less than the 8.3°C rating point.

The assumption regarding the selection of rated load requires further analysis to ensure that a compressor motor can be selected which will perform as assumed in the heating mode and further provide the torque needed for the more extreme loads in the cooling mode. If not, a motor with a larger rated load (torque) would be needed and the motor efficiency values originally calculated for the lower ambient, heating mode conditions could possibly have to be lowered. This is because a larger motor would be operating at a smaller percent of rated load for such conditions. As is seen from Fig. C.1, the motor efficiency begins to drop off significantly for loads below about 65% of rated load.

System 10, the short-term improvement case, was chosen for the motor sizing analysis. The first six lines in the body of Table C.1 show the results of the analysis for a range of heating and cooling operating conditions (as specified by ARI Standard 240-77† for system 10. The operating conditions (temperatures and relative humidity) on the first two lines are the ARI low- and high-temperature rating points for heating. The conditions on the third line are the ARI required maximum

---

*J. H. Johnson, "Hermetic Motor Efficiency, *Proceedings of the Conference on Improving Efficiency and Components in HVAC Equipment and Components for Residential and Small Commercial Buildings*, Purdue University, October 1974.

†Air-Conditioning and Refrigeration Institute, *Standard for Air-Source Unitary Heat Pump Equipment*, ARI 240-77 (1977).

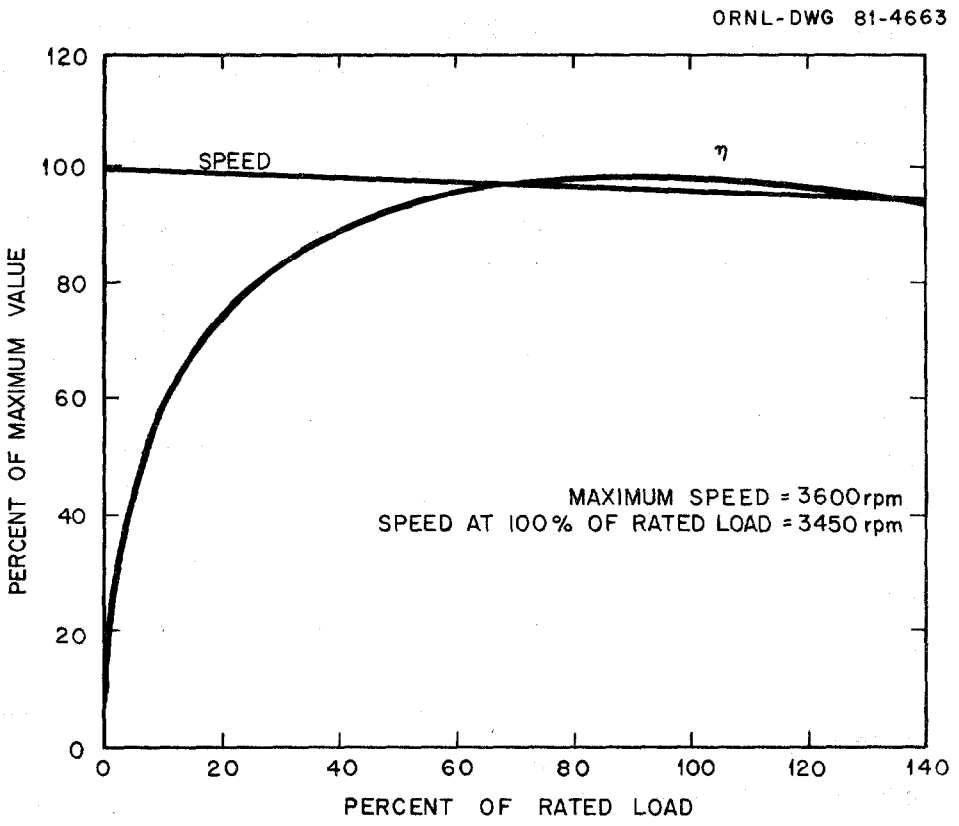


Fig. C.1. Compressor motor efficiency characteristics.

operating conditions for heating. The next two lines are for low* and high temperature rating conditions for cooling followed by the required maximum cooling operating conditions.

The last six lines cover the same range of cooling conditions for reduced indoor air-flow rates as noted. Because it is common for the indoor fan to have two- or three-speed capability, these additional indoor flow rates were included to study their effect on maximum compressor motor load requirements. The reduced indoor air flow rates in the cooling mode offer a means for obtaining better humidity control.

For all twelve runs, values of motor speed, shaft power, torque, capacity (heating or cooling), and COP were tabulated as calculated by the heat pump model. For the cooling runs, the predicted ratios of

*D. A. Didion, "New Testing and Rating Procedures for Seasonal Performance of Heat Pumps," *ASHRAE J.* 21, 9 (September 1979).

Table C.1. Compressor motor load analysis — system 10; motor sized for 100% rated torque = 6.2 N·m (72.8 oz·ft) at 3450 rpm; that is, 100% rated shaft power = 2.23 kW (2.99 hp)

| $T_{amb}$ | | $T_{indoor}$ | | Relative humidity | Motor speed | Shaft motor | | Torque | | Percent rated torque | Percent rated shaft power | Sensible-to-total ratio | Capacity | | COP | EER |
|---|---|---|---|---|---|---|---|---|---|---|---|---|---|---|---|---|
| °C | °F | °C | °F | (%) | (rpm) | kW | hp | N·m | oz·ft | | | | kW | kBtu/h | | |
| | | | | | | Heating mode[a] | | | | | | | | | | |
| -8.3 | 17 | 21.1 | 70 | 70[b] | 3485 | 1.69 | 2.27 | 4.6 | 54.7 | 75 | 76 | | 7.3 | 25.0 | 3.13 | |
| 8.3 | 47 | 21.1 | 70 | 70[b] | 3450 | 2.23 | 2.99 | 6.2 | 72.8 | 100 | 100 | | 11.7 | 40.0 | 3.96 | |
| 23.9 | 75 | 26.7 | 80 | 58[b] | 3401 | 2.94 | 3.94 | 8.3 | 97.3 | 134 | 132 | | 16.1 | 55.0 | 4.10 | |
| | | | | | | Cooling mode[a] | | | | | | | | | | |
| 27.8 | 82 | 26.7 | 80 | 51[c] | 3427 | 2.56 | 3.43 | 7.1 | 84.1 | 116 | 115 | 0.82 | 12.2 | 41.7 | 3.55 | 12.1 |
| 35.0 | 95 | 26.7 | 80 | 51[c] | 3403 | 2.92 | 3.92 | 8.2 | 96.8 | 133 | 131 | 0.86 | 11.2 | 38.3 | 2.85 | 9.73 |
| 46.1 | 115 | 35.0 | 95 | 31[c] | 3358 | 3.59 | 4.81 | 10.2 | 120.4 | 165 | 161 | 1.00 | 11.5 | 39.2 | 2.33 | 7.95 |
| | | | | | | Cooling mode[d] | | | | | | | | | | |
| 28 | 82 | 27 | 80 | 51[c] | 3428 | 2.54 | 3.41 | 7.1 | 83.6 | 115 | 114 | 0.72 | 12.0 | 40.8 | 3.68 | 12.6 |
| 35 | 95 | 27 | 80 | 51[c] | 3405 | 2.88 | 3.86 | 8.1 | 95.3 | 131 | 129 | 0.76 | 11.0 | 37.5 | 2.94 | 10.0 |
| 46 | 115 | 35 | 95 | 31[c] | 3365 | 3.48 | 4.67 | 9.9 | 116.6 | 160 | 156 | 1.00 | 10.8 | 37.0 | 2.34 | 7.99 |
| | | | | | | Cooling mode[e] | | | | | | | | | | |
| 28 | 82 | 27 | 80 | 51[c] | 3430 | 2.51 | 3.37 | 7.0 | 82.6 | 114 | 113 | 0.64 | 11.6 | 39.7 | 3.69 | 12.6 |
| 35 | 95 | 27 | 80 | 51[c] | 3408 | 2.83 | 3.80 | 8.0 | 93.7 | 129 | 127 | 0.68 | 10.8 | 36.7 | 2.98 | 10.2 |
| 46 | 115 | 35 | 95 | 31[c] | 3371 | 3.39 | 4.55 | 9.6 | 113.4 | 156 | 152 | 1.00 | 10.2 | 34.8 | 2.30 | 7.85 |

[a] Indoor air flow rate = 708 L/s (1500 cfm).

[b] Outdoor relative humidity.

[c] Indoor relative humidity.

[d] Indoor air flow rate = 566 L/s (1200 cfm).

[e] Indoor air flow rate = 472 L/s (1000 cfm).

sensible to total heat transfer are also given. The entries in Table C.1 for percent of nominal torque and power were calculated from

$$\%\ \text{nominal torque at } T_{amb} = \frac{\text{torque at } T_{amb} \cdot 100\%}{\text{torque at 100\% rated load}}, \qquad (C.1)$$

$$\%\ \text{nominal shaft power at } T_{amb} =$$

$$\frac{\text{shaft power at } T_{amb} \cdot 100\%}{\text{shaft power at 100\% rated load}} . \qquad (C.2)$$

Note that torque is related to shaft power by

$$\text{torque (N·m)} = \frac{\text{shaft power (W)}}{\text{motor speed (rpm)}} \cdot \frac{60}{2\pi},$$

or

$$\text{torque (oz·ft)} = \frac{\text{shaft power (hp)}}{\text{motor speed (rpm)}} \cdot \frac{33{,}000 \cdot 16}{2\pi} . \qquad (C.3)$$

Also note that shaft power at 100% rated load is not the same as the motor horsepower rating.

For the present discussion, the entries of primary interest in Table C.1 are those for percent nominal torque. This value varies from a minimum of 75% at the low ambient heating condition to a maximum of 165% for the maximum cooling load operating condition with the indoor fan running at high speed. At the medium and low fan speeds the maximum torque required is reduced to 160 and 156% respectively.

From a survey of compressor motor curves for typical heat pump applications and discussions with a hermetic motor manufacturer, it was concluded that maximum operating load (or torque) should not exceed 150% of rated load. While maximum breakdown torque (the point at which the motor stalls) of such motors at 3000 rpm and 25°C can exceed 200% of rated torque, considerations of reduced voltage conditions and actual

motor-operating temperatures lead to the lower figure of 150% of rated torque. This limit is slightly exceeded by the values calculated for system 10 at maximum cooling load conditions. To stay within the assumed limit, the rated torque (related to motor size) must be increased.

In Table C.2, the 100% value of rated torque was increased to 6.8 N·m (80 oz·ft) from the value of 6.2 N·m (72.8 oz·ft) used in Table C.1. Assuming motor speed to remain at 3450 rpm at 100% rated load, the required shaft power at 100% rated load would proportionally increase from 2.23 kW (2.99 hp) to 2.45 kW (3.29 hp) [from Eq. (C.3)]. With the

Table C.2. Range of percent rated torque required of a properly sized compressor motor — system 10

Motor sized for 100% rated torque = 6.8 N·m (80 oz·ft) at 3450 rpm, that is, 100% rated shaft power = 2.45 kW (3.29 hp)

| $T_{amb}$ °C (°F) | $T_{indoor}$ °C (°F) | Percent rated torque |
|---|---|---|
| | *Heating mode*[a] | |
| -8.3 (17) | 21.1 (70) | 68 |
| 8.3 (47) | 21.1 (70) | 91 |
| 23.9 (75) | 26.7 (80) | 122 |
| | *Cooling mode*[a] | |
| 27.8 (82) | 26.7 (80) | 105 |
| 35.0 (95) | 26.7 (80) | 121 |
| 46.1 (115) | 35.0 (95) | 150 |
| | *Cooling mode*[b] | |
| 27.8 (82) | 26.7 (80) | 105 |
| 35.0 (95) | 26.7 (80) | 119 |
| 46.1 (115) | 35.0 (95) | 146 |
| | *Cooling mode*[c] | |
| 27.8 (82) | 26.7 (80) | 103 |
| 35.0 (95) | 26.7 (80) | 117 |
| 46.1 (115) | 35.0 (95) | 142 |

[a] Indoor air flow rate 708 L/s (1500 cfm).

[b] Indoor air flow rate 566 L/s (1200 cfm).

[c] Indoor air flow rate 472 L/s (1000 cfm).

larger rated torque, the new range of operating torques is from 68 to 150% for an indoor air flow rate of 708 L/s (1500 cfm). For the lower indoor air-flow rates of 566 and 472 L/s (1200 and 1000 cfm), in the cooling mode, the maximum required operating torque is 146 and 142%. (Note that all these calculations assume that the required compressor displacement would be reduced slightly to account for the increase in motor speed which results from operating at lower percent rated torque values.) Therefore, with a slightly larger motor, the maximum required conditions can be met without significant change in the motor efficiency at the low-temperature rating point in the heating mode. It should further be noted that cooling mode performance has not been optimized; with optimization, the maximum torque requirements could possibly be further reduced and no increases in motor "size" required.

Therefore, it is concluded that while the motor "sizing" technique used in obtaining the results of Table 4.1 may result in 100% rated torque and shaft power values that are slightly too small, adjustment of these values would have only a minor effect on the performance levels calculated at the -8.3°C (17°F) ambients. However, in considering the family of solutions obtained by trading compressor displacement with air flow rates (in Sect. 5.3.2), attention should be given to the possible effects on the range of required compressor motor loads.

Appendix D

## THE SENSITIVITY OF COP AND HEATING CAPACITY TO AIR FLOW RATES FOR A SERIES OF COMPRESSOR DISPLACEMENTS — SYSTEM 2

The sensitivity plots shown and discussed herein represent a sampling of the plots used in generating Fig. 5.14 of Sect. 5.3.1. The purpose of this discussion is to provide further insight regarding the trade-offs between compressor displacement and air flow rates.

In Figs. D.1 through D.3, the compressor displacements are 71.0, 61.5, and 54.1 mL (4.33, 3.75, and 3.30 $in.^3$), respectively. Otherwise,

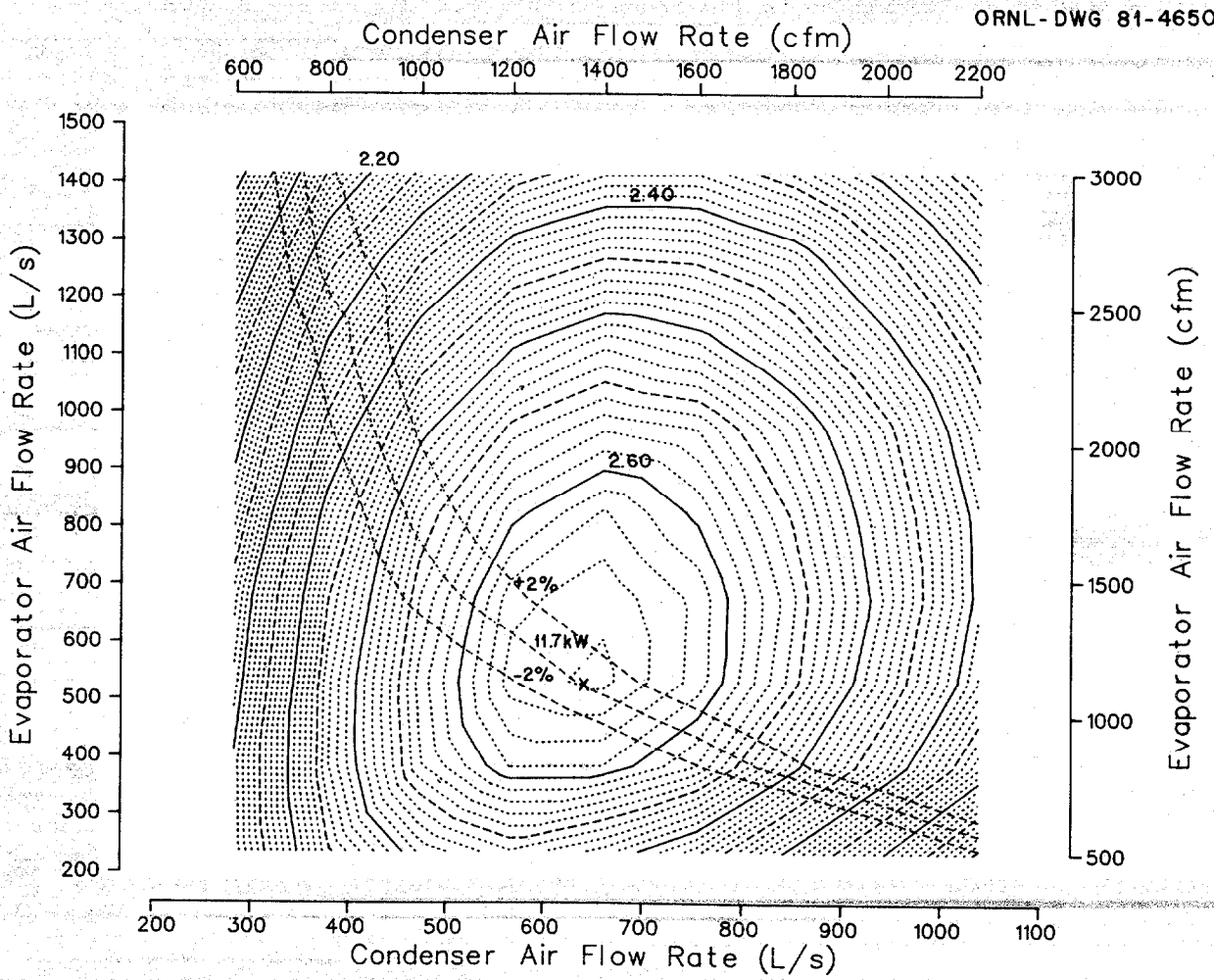


Fig. D.1. Sensitivity of COP and heating capacity to air flow rates at $T_{amb}$ = 8.3°C (47°F) — system 2 with compressor displacement of 71.0 mL (4.33 $in.^3$).

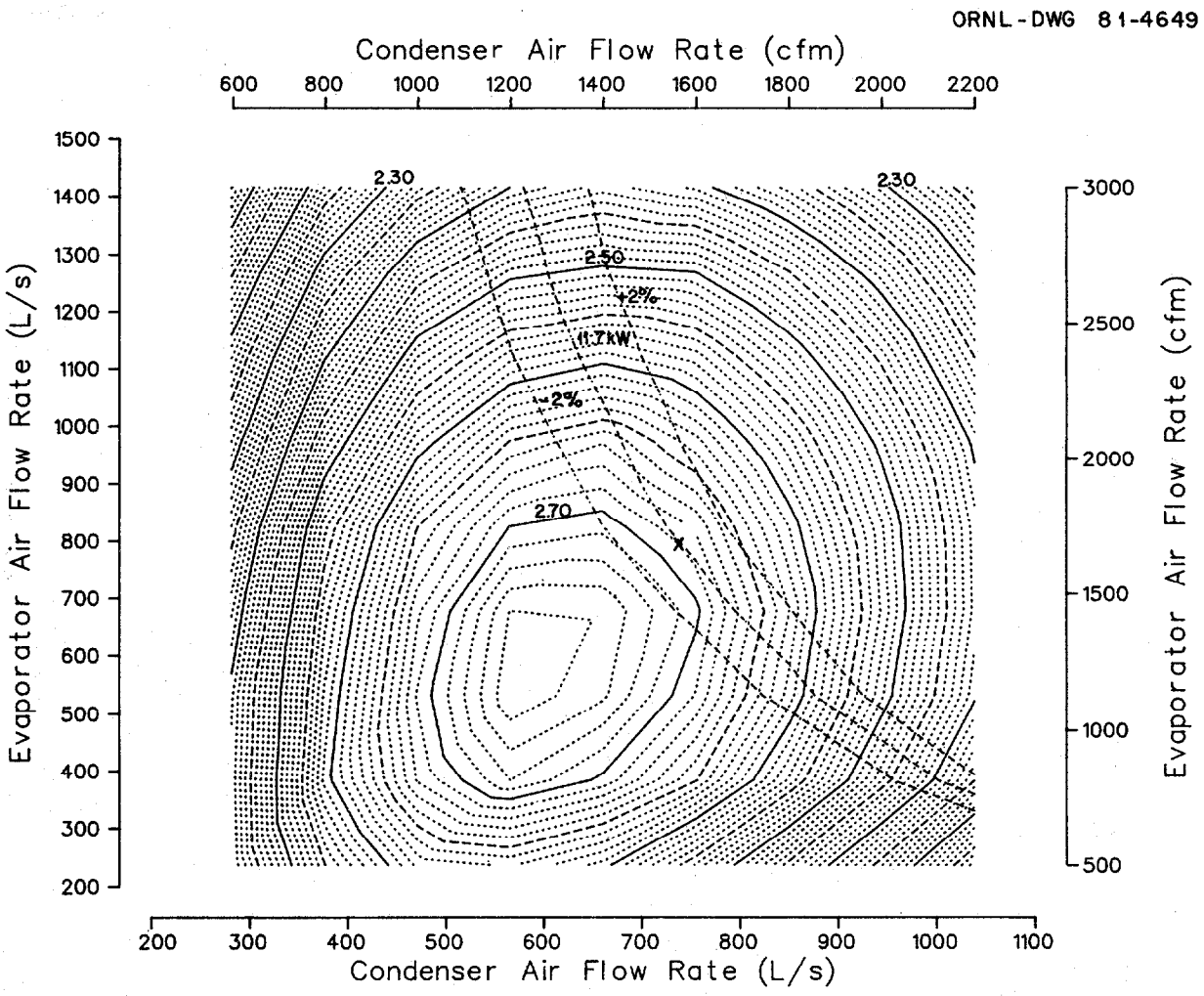


Fig. D.2. Sensitivity of COP and heating capacity to air flow rates at $T_{amb}$ = 8.3°C (47°F) — system 2 with compressor displacement of 61.5 mL (3.75 $in.^3$).

all three plots represent the same system configuration (system 2) over a common range of condenser and evaporator air flow rates.

As the compressor displacement is decreased in successive plots, the peak COP, ignoring capacity constraints, increases. When the capacity constraint is considered, the best COP that lies along the 11.7-kW (40,000-Btu/h) capacity line moves from the peak of the COP contours in Fig. D.1 to contours that are further removed from the peaks in Figs. D.2 and D.3 but that are not necessarily of lower COP value. The movement off of the peak contour as displacement is decreased does not result in lower values of the optimum constrained COP (e.g., Fig. D.2) until the rate of fall from the peak due to the capacity constraint exceeds the

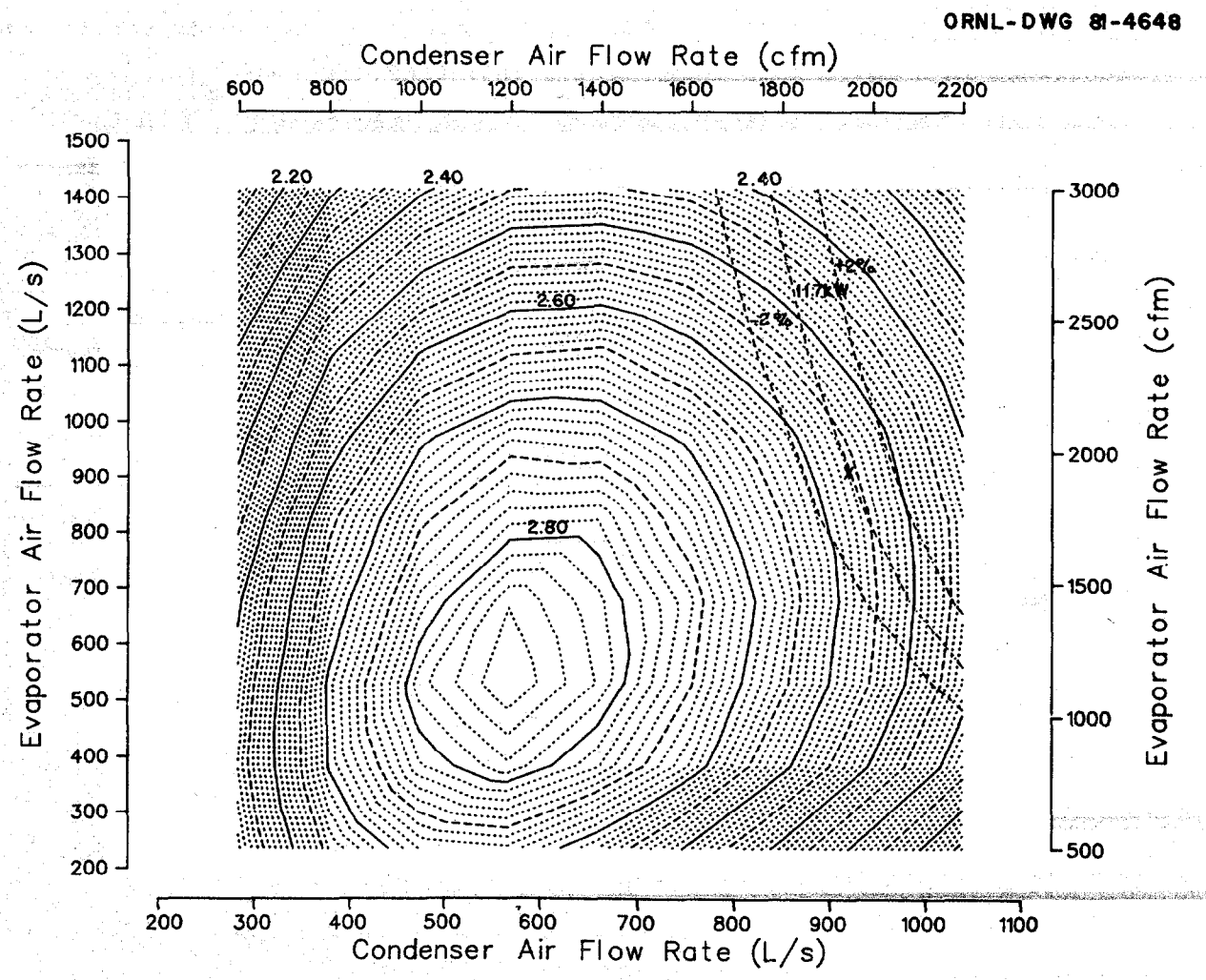


Fig. D.3. Sensitivity of COP and heating capacity to air flow rates at $T_{amb}$ = 8.3°C (47°F) — system 2 with compressor displacement of 54.1 mL (3.30 $in.^3$).

rate of rise in the value of the peak COP contour (e.g., Fig. D.3). In fact, the best constrained COP in the three figures occurs in Fig. D.2 where the nominal capacity line does not cross the point of maximum unconstrained COP (in contrast to Fig. 5.1 of system 10). Also, displacements higher than that in Fig. D.1 must result in lower constrained COPs as well because the peak COP will further decrease and the capacity constraint will move the constrained COP even lower.

These graphical observations can be explained in physical terms as follows. The unconstrained COP will increase as displacement is decreased because the associated heating capacity drops and the heat exchangers become more lightly loaded (smaller refrigerant-to-air $\Delta T$'s and smaller

air $\Delta T$'s, that is, a smaller condenser to evaporator temperature difference), resulting in a lower compression ratio and, thus, reduced compressor power requirements. However, to meet the required capacity with the smaller displacements, the air flow requirements continue to increase until the point at which increasing fan powers outweigh decreasing compressor power. Thus, there is a range of compressor displacements for each particular system in which the increases in fan power consumption can be traded for decreases in compressor power with minimal effect of the COP.

Figures. D.1 through D.3 also further illustrate the mathematical criterion for maximum constrained COP given in Sect. 5.2.1; that is, the configuration that produced the best constrained COP in each of the three figures occurs at the point where the required capacity line is tangent to a surface of constant COP.

## INTERNAL DISTRIBUTION

1. R. K. Adams
2. S. I. Auerback
3. M. R. Baker
4. R. S. Carlsmith
5. F. C. Chen
6. W. L. Cooper
7. F. A. Creswick
8. R. C. DeVault
9. C. R. Eichelberger
10. R. D. Ellison
11. W. Fulkerson
12. R. E. Goodson, Consultant
13. W. L. Jackson
14. R. A. Just
15. G. Kamp
16. T. R. LaPorte, Consultant
17. C. G. Lawson
18. L. McCold
19. H. A. McLain
20. J. W. Michel
21. D. R. Miller
22. W. R. Mixon
23. L. I. Moss, Consultant
24. M. R. Patterson
25. A. M. Perry
26. G. D Pine
27. R. C. Robertson
28. G. Samuels
29. G. G. Slaughter
30. T. W. Thomas
31-32. Central Research Library
33. Laboratory Records (RC)
34-36. Laboratory Records Dept.
37. ORNL Patent Office

## EXTERNAL DISTRIBUTION

38. C. A. Allen, Energy Information Administration
39. E. K. Bastress, Energy Conversion and Utilization Technology Division
40. Congressional Information Service
41. J. J. Cuttica, Energy Conversion Equipment Branch
42. A. A. Domingorena, Carrier Corporation
43. G. D. Duffy, Air Conditioning News
44. Edison Electric Institute
45. R. J. Fiskum, Department of Energy
46. J. H. Gibbons, Office of Technology Assessment
47. D. E. Grether, Friedrich Air Conditioning and Refrigeration
48. G. C. Groff, Carrier Corporation
49. R. J. Hemphill, Gas Research Institute
50. Larry Hobart, American Public Power Association
51. Tina Hobson, Department of Energy
52. H. Jaster, General Electric Corporation
53. P. L. Johnson, Oak Ridge Associated Universities
54. F. R. Kalhammer, Electric Power Research Institute
55. T. Kapus, Department of Energy
56. R. W. King, Copeland Corporation
57. Arvo Lannus, Electric Power Research Institute
58. D. C. Lim, Department of Energy
59. H. P. Luckett, Popular Science
60. Jim McCallum, Air Conditioning and Refrigeration Business
61. J. P. Millhone, Department of Energy
62. F. H. Morse, Department of Energy
63. National Energy Information Center

64. T. Ratchford, House of Representatives
65. Bill Riley, Heil Quaker Corporation
66. J. Rizzuto, New York State Energy Research and Development Authority
67. J. H. Rothenburg, Department of Housing and Urban Development
68. J. D. Ryan, Department of Energy
69. L. A. Sarkes, American Gas Association
70. M. L. Savitz, Department of Energy
71. J. L. Schulze, General Electric Company
72. D. E. Sherpereel, Whirlpool Corporation
73. J. A. Smith, Department of Energy
74. E. W. Spannhake, White Consolidated Industries, Inc.
75. W. D. Syniuta, Advanced Mechanical Technology, Inc.
76. C. C. Theil, Jr., National Science Foundation
77. S. S. Waddle, Department of Energy
78. D. J. Walukas, Foster-Miller Associates
79. Office of the Assistant Manager for Energy Research and Development, U.S. Department of Energy
80-107. Technical Information Center, Department of Energy
108-507. Efficiency and Renewables Research Section Library, Building 9102-2, Conference Room

*U.S. GOVERNMENT PRINTING OFFICE: 1981-740-062/284